

Chemical Insights from Carbon 1s Photoelectron Spectroscopy and Theoretical Modeling

VELAUG MYRSETH OLTEDAL



Thesis for the Degree of Doctor Scientiarum
Department of Chemistry
University of Bergen

· 2007 ·

ISBN: 978-82-308-0418-6
Bergen, Norway 2007

Printed by Allkopi Ph: +47 55 54 49 40

To Leif and my family

Bergen
24. May 2007

There once was a girl named Irene
Who lived on distilled kerosene
But she started absorbin'
A new hydrocarbon
And since then has never benzene.

— *author unknown*

Preface

This thesis, submitted for the degree of Doctor Scientiarum at the University of Bergen, consists of a summary and five papers. The work has mainly been carried out at the Department of Chemistry, University of Bergen, Norway, over the period 2001-2007. I was provided with a scholarship from the Research Council of Norway to perform the research for this thesis. My advisors have been Leif J. Sæthre and Knut J. Børve.

Throughout this period, I have been fortunate to be able to travel abroad many times on various occasions. All the experiments were performed at MAX-lab in Lund, Sweden, and at the Advanced Light Source (ALS) in Berkeley, California. I participated in the data acquisition a total of eight times at MAX-lab and three times at the ALS. In January 2003, I had the opportunity to participate in data acquisition at the synchrotron ASTRID in Aarhus, Denmark, with the group of Jens Onsgaard. The results from ASTRID are not included in this thesis.

I have had the privilege of working with Prof. T. Darrah Thomas at Oregon State University in Corvallis, OR. During 2000, 2002 and 2004, I spend one month each time in Corvallis, analyzing data and writing papers. Our group in Bergen also cooperates extensively with the group of Svante Svensson and Olle Björneholm in Uppsala, Sweden, and I have visited the Uppsala group on several occasions.

In June 2002, I presented a poster at the 19th International Conference of X-ray and Inner-shell Processes in Rome, Italy. I have also presented posters at several of the Annual Meetings of the Association for Synchrotron Radiation Users at MAX-lab, in Lund, Sweden. In 2006, I had the opportunity to give oral presentations both at the NordForsk Network Meeting in Bergen, and also at the 19th Annual Meeting of the Association for Synchrotron Radiation Users at MAX-lab, in Lund.

During this period, I have attended other workshops, meetings and research schools of various kinds. Among these are the Annual Norwegian Synchrotron User Meetings in 2002 and 2007, in Norway, and CAMM (Centre for Advanced Molecular Materials) winterschool 2004, in Uppsala.

Acknowledgments

First of all, I warmly thank my advisors, Prof. Leif J. Sæthre and Prof. Knut J. Børve. Obviously, your contributions in completing this thesis have been indispensable. Leif, thank you for your never-ending patience and encouragement through the last years. You always have time, when we knock on your door. Your wide experience in photoelectron spectroscopy has been a great inspiration to me. Knut, you are always present in mind, in discussions and when supervising. Your enthusiasm and knowledge, about everything, has made research exciting to me.

I have had the great pleasure of joining international collaborations during the present work. During my stays in Corvallis, I felt very welcomed and made good friends. Darrah and Barbara, I am indebted to you for your great hospitality every time I have been in Corvallis, and especially in March 2004 when I experienced a difficult time. Thank you, Darrah, for all the time you have spend helping me and explaining various aspects of electron spectroscopy and theory. Al and Mary, thanks for your friendship and care. Thank you Tom, for explaining various topics with an amazing patience. Edwin, thanks for joining our beamtimes and making them more enjoyable. To all the people in Uppsala—you have really contributed in making the last years exciting and worth while. I want to especially mention Svante, for your never-failing enthusiasm (that's an understatement) and for teaching me schottis. Karo, for fun times and for your friendship. I wish to thank Jens, Lone and Trine in Aarhus, for a good time at ASTRID in 2003.

I will also use the opportunity to thank all my fellow colleges and friends at the Department of Chemistry, for making these years a fun and challenging time. Especially Maria, Mahmoud, Alf, Jarle, Mathias, Elaine, Manuel, and Giovanni, for providing a supportive and cheerful atmosphere at work and for the many coffee breaks. I also want to thank the administrative staff at our department, for all help and support through these years.

I am pleased to thank the staff at MAX-lab and the ALS for assistance and help during our beamtimes. In particular, I want to thank Margit Bässler and Maxim Tchapyguine at MAX-lab, and John Bozek and David Kilcoyne at the

ALS.

My special thanks go to my husband, Leif. I would not have made this without you. Your love, encouragement and patience, especially in the last weeks, has been invaluable. And Simon— you are my sunshine! I deeply thank my family, for listening to my frustrations, for babysitting, and for endless support in many ways. I thank my good friends, Trude and Jorunn, for many consoling talks.

I acknowledge a scholarship from the Research Council of Norway (NFR), as well as grant of computer time through the Norwegian High Performance Computing Consortium NOTUR.

Abstract

Inner-shell ionization energies provide local probes of the charge distribution in molecules and of the ability of a molecule to accept charge at specific sites. As such, core-ionization energies are related to and may provide insight into other chemical properties that depend on the same ability. X-ray photoelectron spectroscopy (XPS) is the preferred tool for exploring core-ionization energies. In the present work, synchrotron radiation was used to acquire photoelectron spectra of several carbon-containing molecules in the gas phase. Carbon 1s ionization energies are of special interest because of the vital role of organic molecules in life processes. A prerequisite for obtaining accurate ionization energies is access to reliable methods for calibration of the energies. This work has been concerned with establishing procedures for very accurate calibration of C1s ionization energies.

With today's instrumentation, it is possible to obtain high-resolution photoelectron spectra that reveal details of the fine structure which have not been observed previously. The fine structure may be very complex, due to contributions associated with the inequivalent carbons in a molecule, as well as vibronic structure. To assign such a spectrum and obtain chemical shifts, one is dependent on theory to prepare lineshape models for each carbon in the molecule. In this thesis, several approaches for modeling vibronic progression in XPS measurements of hydrocarbons were tested. A relatively simple model for taking into account effects of vibronic coupling in the spectra was developed. This model is expected to work well also for larger, more complex systems. With this tool, it is possible to assign photoelectron spectra and obtain chemical shifts for the different carbons in a molecule with high accuracy. It is now believed that vibronic structure arising from core-ionization of hydrocarbons is well understood. This knowledge has been applied to various molecular systems of chemical interest. It is shown that core-ionization energies may provide insight into chemical properties such as proton affinity and reactivity, and how these properties are influenced by a methyl substituent. Experience from gas-phase XPS is also found to be of considerable use in assignment of adsorbed-state photoelectron spectra.

Contents

List of papers	xi
1 Introduction	1
2 X-ray photoelectron spectroscopy	5
2.1 Synchrotron radiation	5
2.2 The beamline	7
2.3 Experimental details	7
3 Theoretical methods and procedures	11
3.1 Electronic-structure calculations	12
3.1.1 The Hartree-Fock approximation and the Møller-Plesset methods	12
3.1.2 Density functional theory	13
3.1.3 Basis set	14
3.1.4 Hole-state calculations	15
3.2 Franck-Condon analysis	15
3.2.1 Normal-mode calculations	15
3.2.2 Aspects of vibronic coupling	18
3.3 Chemical shifts	20
3.4 Proton-affinity calculations	21
3.5 Computational details	21
4 Lineshape functions and data analysis	23
4.1 Post-Collision Interactions	23
4.2 Other broadening parameters	24
4.3 Curve fitting	25
5 Summary of main results	27
5.1 Methods for calibration	27
5.1.1 Calibration of electron spectrometers	28

5.1.2	Accurate adiabatic and vertical ionization energies	28
5.2	The C1s photoelectron spectra of cyclic hydrocarbons	30
5.2.1	Benzene	30
5.2.2	Effects of incomplete localization of the core hole	31
5.2.3	Six-membered cyclic hydrocarbons	33
5.2.4	Methyl-substituted benzenes	36
5.3	Ionization energies and other chemical properties	36
5.3.1	Proton affinities, activation energies, and core-ionization energies	38
5.3.2	Additivity of substituent effects	40
5.4	Molecular reference spectra for adsorption studies	43
6	Conclusions	47
7	Suggestions for further work	51
	Bibliography	53

List of papers

This thesis is based on the following five papers, which will be referred to in the text by their Roman numerals.

Paper I Adiabatic and vertical carbon 1s ionization energies in representative small molecules.

V. Myrseth, J. D. Bozek, E. Kukk, L. J. Sæthre, and T. D. Thomas.

Journal of Electron Spectroscopy and Related Phenomena, 2002, **122**, 57–63.

Paper II Xenon N_{4,5}OO Auger spectrum—a useful calibration source.

T. X. Carroll, J. D. Bozek, E. Kukk, V. Myrseth, L. J. Sæthre, T. D. Thomas, and K. Wiesner.

Journal of Electron Spectroscopy and Related Phenomena, 2002, **125**, 127–132.

Paper III Vibrational structure and vibronic coupling in the carbon 1s photoelectron spectra of benzene and deuterobenzene.

V. Myrseth, K. J. Børve, K. Wiesner, M. Bäessler, S. Svensson, and L. J. Sæthre.

Physical Chemistry Chemical Physics, 2002, **4**, 5937–5943.

Paper IV Carbon 1s photoelectron spectroscopy of six-membered cyclic hydrocarbons.

V. M. Oltedal, K. J. Børve, L. J. Sæthre, T. D. Thomas, J. D. Bozek, and E. Kukk.

Physical Chemistry Chemical Physics, 2004, **6**, 4254–4259.

Paper V The substituent effect of the methyl group. Carbon 1s ionization energies, proton affinities, and reactivities of the methylbenzenes.

V. Myrseth, L. J. Sæthre, K. J. Børve, and T. D. Thomas.

Journal of Organic Chemistry, 2007, **72**, 5715–5723.

The following paper is one to which I contributed but is not included in the thesis. It may provide a useful reference.

- Line shape and lifetime in argon 2p electron spectroscopy.

T. X. Carroll, J. D. Bozek, E. Kukk, V. Myrseth, L. J. Sæthre, and T. D. Thomas.

Journal of Electron Spectroscopy and Related Phenomena, 2001, **120**, 67–76.

Chapter 1

Introduction

When atoms are joined together to form molecules, they share electrons. However, it is only the outer electrons that are shared. The innermost or core electrons are kept by each individual atom. At the same time, the energy by which the core electrons are tied to the nuclei is influenced by the surroundings. We call this energy binding or ionization energy. Depending on the surrounding atoms, core electrons of the same type of atom have different binding energies. These differences are called chemical shifts. Thus, if one is able to determine chemical shifts within a molecule, one can get information about chemical properties at specific sites in that molecule. Such chemical properties are for instance proton affinity, acidity, and electrophilic reactivity, which all involve adding charge to a molecule. Accordingly, core-electron binding energies serve as local probes of the charge distribution in a molecule, and of the ability of a molecule to accept or donate charge at a particular site.

X-ray photoelectron spectroscopy, XPS, is an excellent tool for exploring core-electron binding energies. This technique takes advantage of the photoelectric effect, discovered by Heinrich Hertz in 1887.¹ In a simplified picture, an incoming photon expels an electron from its orbit in the atom or molecule. The photon energy in excess of the binding energy of the electron, is transferred as kinetic energy, E_K , to the electron. This gives us the photoelectric law, first formulated by Einstein.² In this, E_K can be expressed as:

$$E_K = h\nu - E_B$$

where E_B represents the binding energy and $h\nu$ the energy of the photon. To measure photoelectron spectra, one needs a source of photons and a way to measure the kinetic energy of the outgoing photoelectron. Then one can find the binding energy, or ionization energy, from the equation above.

The use of core-electron spectroscopy in chemistry is often referred to as ESCA (electron spectroscopy for chemical analysis). The field of ESCA was

founded in the 1960s, when spectrometers for measuring electron energies were developed.³ Since then, both experimental and theoretical techniques and equipment have developed enormously. In ESCA, carbon 1s ionization energies have been of special interest because of the rich and important chemistry of carbon-containing compounds. However, until recently carbon 1s photoelectron spectra have been hampered by lack of resolution. Carbon atoms with quite distinct chemical properties may have 1s ionization energies that are very similar, leading to overlapping of peaks in the photoelectron spectra. In addition, vibrational excitation often accompanies core ionization and adds complexity to the spectra. The development of third-generation synchrotron facilities, together with high-resolution electron spectrometers, have made a striking difference in this situation. With today's instrumentation, it is possible to resolve fine structure in core-level photoelectron spectra of many molecules.

In order to assign the various peaks in a high-resolution photoelectron spectrum, one is dependent on quantum chemical computations. Theoretical tools exist that make it possible to prepare lineshape models for each inequivalent atom in a molecule. By fitting the theoretical lineshapes to the experimental spectrum, one can obtain accurate experimental core-ionization energies for each atom. The theoretical analysis may include determining effects of both vibrational excitation and vibronic coupling on the photoelectron spectra. Vibronic coupling may occur particularly in molecules containing equivalent carbon atoms. The equivalent atoms will have core-energy levels with nearly the same energy. These energy levels can couple via the nuclear motion, leading to a splitting of the vibrational lines in the photoelectron spectrum. Besides providing information on the structure and bonding of the ionized state, these effects are interesting in their own right.

The main aim of this thesis has been to extract accurate carbon 1s ionization energies for several molecules in the gas phase using high-resolution synchrotron radiation and advanced theoretical methods. Shifts in 1s ionization energies are found to correlate with other chemical properties and may provide insight into various chemical processes. The thesis is based on five scientific papers, as listed on page xi. They will be referred to in the text by their Roman numerals. Following is a brief outline of the main results from each paper.

Despite the high resolution of the synchrotron light, the accuracy with which the photon energy is known is not high. As a consequence, in XPS it is necessary to include an internal standard for which the ionization energy is well known. Paper I provides very accurate adiabatic and vertical carbon 1s ionization energies for nine small molecules. The ionization energies for these compounds span most of the range of known carbon 1s energies and can be used as reference energies for calibration of other molecules. In Paper II, a method for calibrat-

ing electron spectrometers is presented. This method provides a higher level of accuracy for such calibrations than what has been presented in the literature before.

Benzene can be regarded the prototype of aromatic molecules. Paper III presents a detailed study of the vibrational structure in photoelectron spectra of benzene and deuterio-benzene. The effects of vibronic coupling on the spectra were examined using several models at different levels of complexity. In particular, one relatively simple model was found to give results comparable to results from the most elaborate model. The simpler model is expected to work well in predicting effects of vibronic coupling in photoelectron spectra of larger, more complex systems.

C1s photoelectron spectra were measured for a series of six-membered cyclic hydrocarbons, ranging from the saturated cyclohexane molecule, through the unsaturated cyclohexene, to 1,3- and 1,4-cyclohexadiene. The results are presented in Paper IV. Together with benzene, these molecules show the evolution of chemical effects with increasing number of double bonds. We are able to assign unambiguously the various features of each spectrum to the corresponding carbon atoms in the molecules. This provides C1s ionization energies for each individual atom. Theoretically predicted chemical shifts are shown to reproduce the experimental shifts.

Paper IV also presents how experience from gas-phase XPS can be applied in studies of adsorption of unsaturated hydrocarbons on silicon surfaces. It appears that there exists a general misunderstanding in the published literature concerning the assignment of saturated and unsaturated hydrocarbons in XPS spectra of the surface layer. We contend that high-resolution gas phase spectra might contribute to the assignment of the physisorbed species.

Substituent effects in aromatic compounds have been subject to extensive studies since early in the last century. Core-ionization energies, which reflect the ability of a molecule to accept charge at a specific site, might shed new light on this subject. Paper V is a study of the substituent effect of the methyl group in a series of methyl-substituted benzenes. For the first time, one is able to assign 1s ionization energies to each inequivalent carbon atom in these molecules. We find correlations between the ionization energies and the energy changes for other chemical processes that also involve addition of charge at specific sites. Deviations from these correlations provide insight into the effect of conjugation for the methyl substituent.

In this summary, the acquisition of experimental data and calculation of theoretical lineshape models will be described, as well as various aspects relating to interpretation of the data. The following chapter gives an outline of the experimental instrumentation and procedures. In chapter 3, theoretical methods

and procedures are presented. Chapter 4 describes the curve-fitting procedure and other aspects of the data analysis. Concluding remarks and suggestions for further work are given in chapters 5 and 6, respectively. In the final section, the five scientific papers that form the basis of this thesis are presented.

Chapter 2

X-ray photoelectron spectroscopy

The experiments were performed both at the MAX II storage ring at MAX-lab⁴ in Lund, Sweden, and at the Advanced Light Source (ALS)⁵ in Berkeley, California, over the period 1999-2005. Both MAX II and the ALS are third-generation synchrotrons. The main principles of synchrotron instrumentation are similar for the two facilities, and the experimental setup will be illustrated with reference to MAX II. The two main components of a synchrotron facility are the storage ring and the beamlines. In the storage ring, exceptionally bright light is produced, which is then directed down beamlines, eventually hitting the target atoms or molecules in the end station (experimental chamber). In XPS, core electrons are ejected from the sample and their energy measured. The next two sections will give more details on the synchrotron facility at MAX-lab and beamline I411,^{6,7} used in many of the experiments in this thesis. More details on beamline 10.0.1 at the ALS can be found in ref. 8.

2.1 Synchrotron radiation

In a synchrotron, relativistic electrons are injected into the storage ring (usually by a linear accelerator) and accelerated to nearly the speed of light. Figure 2.1 shows an overview of the injector and the MAX II storage ring at MAX-lab. At MAX II,⁴ electrons are stored with an energy of 1.5 GeV. The beam current is 200 mA, and the lifetime of the beam is more than 10 hours. The storage ring has a circumference of 90 m, with ten straight sections inserted. Magnetic lenses keep the electrons on the desired trajectory. Each time an electron is accelerated (undergoes a change of direction) by a bending magnet, electromagnetic radiation is emitted. At MAX II, synchrotron radiation is produced in two other ways as well; by undulators and by wigglers that are inserted in the straight sections. Only undulators will be described here. Undulators are periodic mag-

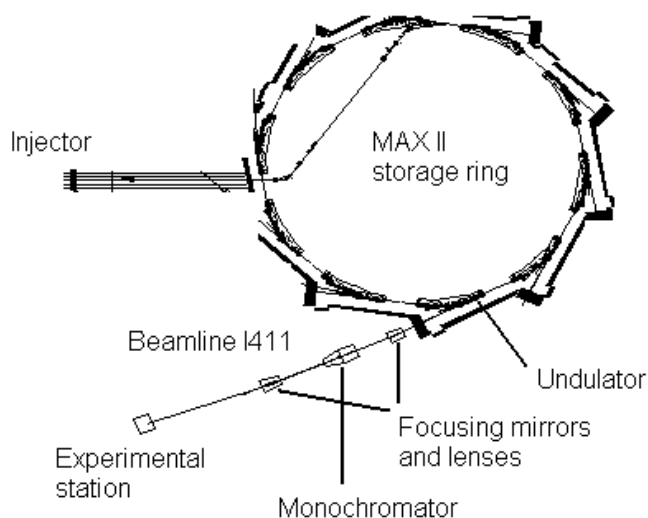


Figure 2.1: Schematic drawing of the MAX II storage ring and beamline I411 at MAX-lab. The figure is reproduced from refs. 4 and 9, with permission.

netic structures that comprise a linear array of dipole magnets with alternating polarity. When the electrons pass through the undulator, they start moving in harmonic oscillations. By adjusting the gap between the poles, one can achieve coherent interference patterns between the radiation emitted by the same electron at the different turns. One can also change from one harmonic to another, thereby changing the energy of the outgoing beam. Tuneability of the photon energy is among the most important properties of synchrotron light. Another important property is the high brilliance of the photon beam from undulators and wigglers. Brilliance is defined as flux of photons per unit source area and per unit solid angle of emission. In other words, the ideal light source could be characterized by high intensity from a very small source in only one direction and with only one wavelength. Though still not ideal, synchrotron radiation is 100 million times brighter than conventional X-ray sources.

The undulator used for beamline I411 is a permanent magnet hybrid undulator with a 60 mm period and a total length of 2.65 m. The usable energy range of the undulator is 50–1500 eV. Most experiments have been performed with a photon energy of 330 eV, corresponding to an undulator gap of 30.76 mm using the third harmonic.

2.2 The beamline

From the undulator, the photon beam is directed down the beamline by different optical elements. The most important parts of beamline I411 are illustrated in Figure 2.1. Beamline I411^{6,7} has differential pumping which keeps an ultra high vacuum (UHV) in the beamline. The photons are monochromatized by an SX-700 plane grating monochromator.^{10,11} Conventional X-ray sources used quartz-crystal monochromators, which had a resolution limited to about 0.25 eV.¹² With today's monochromators, combined with synchrotron radiation, it is possible to get a bandwidth much smaller than the natural linewidth (about 0.1 eV for carbon), and still have enough intensity for photoelectron spectroscopy. The monochromatized light is further focused, both vertically and horizontally, by a toroidal mirror toward the sample focus point at the end station. The end station (or experimental chamber) has the capability of handling both solid, cluster, liquid and gas-phase samples. Only gas-phase experiments were performed in this work. The end station consists of an analyzer chamber and a hemispherical electron-energy analyzer, Scienta SES-200.¹³⁻¹⁵ Figure 2.2 shows a schematic drawing of the Scienta. The sample gas is let into the analyzer chamber, where photoionization takes place. In the Scienta, the photoelectrons first pass through an electron lens, which retards or accelerates the electrons to a certain pass energy. The pass energy is the energy of an electron that will travel in a circular path at the mean radius of the analyzer. Since the analyzer is operating at a fixed pass energy during the acquisition of a spectrum, the chosen energy interval has to be scanned by accelerating or retarding the photoelectrons in the electron lens. The electrons then pass between two hemispherical electrodes, and electrons with different kinetic energy will go in orbits with slightly different radii. Finally, the electrons arrive at the multichannel detector, which functions as an electron multiplier. The multiplied electron signal is detected as flashes on a phosphorous screen by a CCD camera, and these flashes are counted by computer software. In this way, a spectrum is generated, plotted as intensity versus kinetic or binding energy. All measurements were made with the analyzer perpendicular to the beam direction and at an angle of 54.7 degrees to the polarization direction of the light (the "magic" angle³).

2.3 Experimental details

All samples were obtained commercially and used without extensive purification. Most of the samples purchased were in liquid form. Liquid samples were transferred to a test tube and connected to the gas inlet system. To get rid of air and volatile impurities in the liquids, a freeze-pump-thaw cycle was used

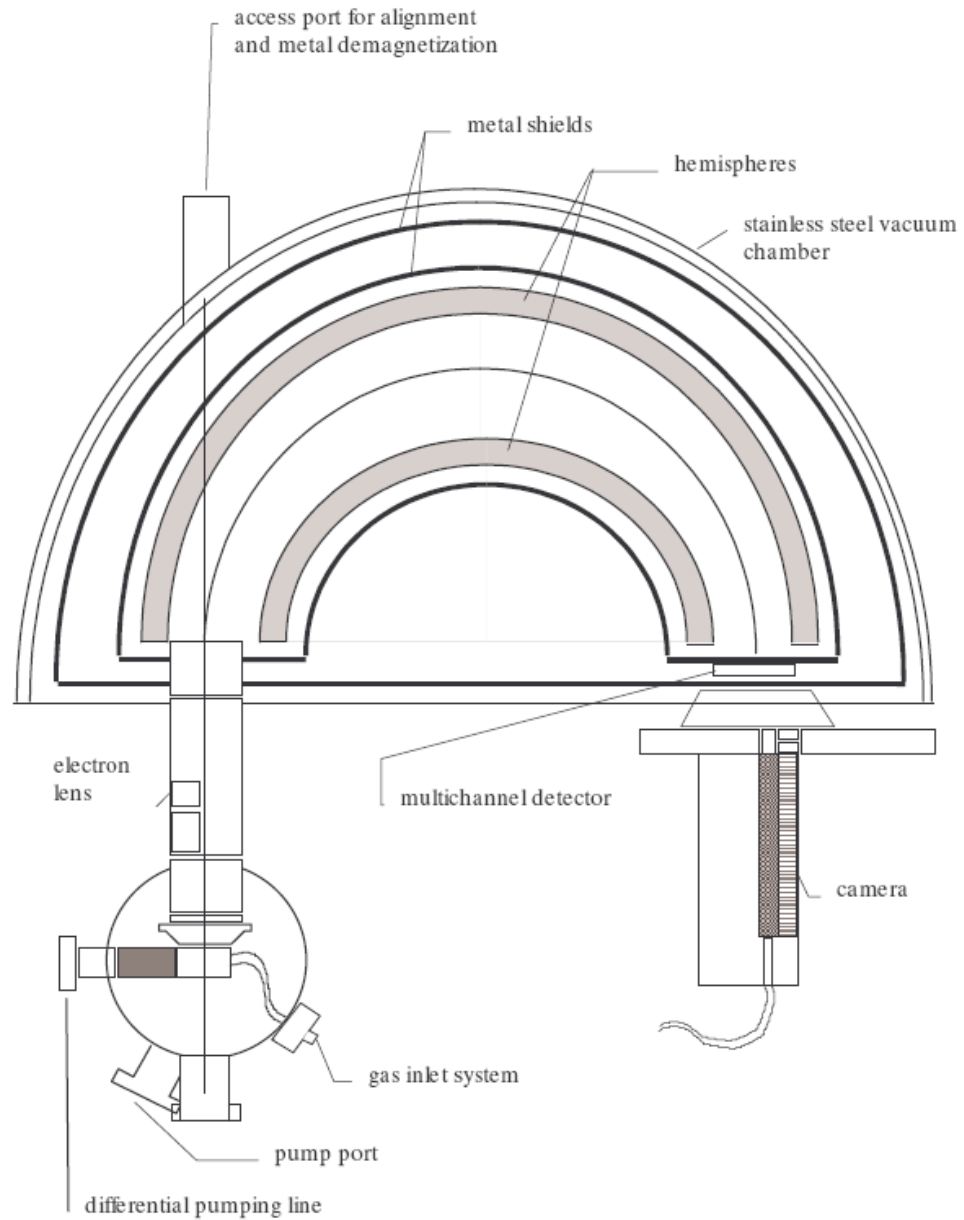


Figure 2.2: Schematic drawing of the Scienta SES-200.

and then repeated once, for each sample. The vapor pressures of the liquids at room temperature were sufficient to get a high enough gas pressure in the analyzer chamber, without further heating. As for the gaseous samples, the gas bottle was directly connected to the gas inlet system.

The typical pass energy in our experiments was 20 eV. The gas pressure in the analyzer chamber was held around $4 \cdot 10^{-6}$ atm. It needs to be adjusted slightly for each compound to optimize the intensity. All aromatic compounds, except one, were measured at MAX-lab (Papers III and V). 1,2,4,5-tetramethylbenzene, together with cyclohexane, cyclohexene, 1,3- and 1,4-cyclohexadiene (Paper IV) were measured at the ALS. All compounds from Paper I were also measured at the ALS. The xenon measurements were done both at MAX-lab and at the ALS, as specified in Paper II.

Chapter 3

Theoretical methods and procedures

Once the photoelectron spectrum has been acquired, one wants to assign the spectrum and interpret the data. The spectra are often complex, typically consisting of several overlapping peaks associated with inequivalent carbons in the molecule. In addition, each peak may have fine structure arising from vibrational excitation of the molecule upon core ionization. In order to deconvolute such a spectrum, one can use theoretical calculations to model the vibrational lineshapes associated with each carbon. From the assignment of the spectrum, one obtains absolute and relative experimental ionization energies for each carbon in the molecule. The difference in ionization energy between two atoms is called the chemical shift. Relative ionization energies are also obtained from electronic structure calculations, and one can compare experimental and theoretical chemical shifts.

This chapter gives a qualitative description of the theoretical methods used in the thesis and provides computational details. Rather than providing a detailed account of the theory, the intention of this chapter is to give a qualitative description from a user's point of view. For further information on the theoretical methods, see refs. 16 and 17.

Core-ionization energies reflect the ability of a molecule to accept positive charge at a specific site. Therefore, one would expect core-ionization energies to relate closely to other chemical quantities that depend on this ability, such as proton affinities (the negative of enthalpies of protonation). Since experimental proton affinities are often not available for individual sites in a molecule, we have used theoretical calculations to predict proton affinities for individual carbons in methyl-substituted benzenes. The theoretical method used in this respect is also described here.

3.1 Electronic-structure calculations

In order to prepare theoretical lineshape models for the inequivalent carbons in a molecule, one needs accurate geometries, energies, normal modes and vibrational frequencies for the neutral as well as for the core-ionized molecule. This section gives a short overview of the theoretical methods and other aspects related to computations in this thesis. Details of, and references for, the theoretical calculations are given in section 3.5 on page 21.

3.1.1 The Hartree-Fock approximation and the Møller-Plesset methods

The starting point for most quantum mechanical calculations today is the time-independent Schrödinger equation:

$$\hat{H}\Psi = E\Psi$$

\hat{H} is called the Hamilton operator, and describes the total energy, E , of the system (atom or molecule). Ψ is the wavefunction which contains information about all the properties of the system that can be determined experimentally, for instance kinetic energy or charge distribution. Exact solutions of the Schrödinger equation are not practically feasible for any but the simplest systems, like the hydrogen atom. For quantum mechanical computations of larger systems, one has to apply a number of approximations. To this end, many different approaches and methods have been developed, characterized by their level of accuracy. Here, only the methods applied in this thesis will be described.

The computations in this thesis employ *first-principle* methods. In this context, a *first-principle* method is one that is based solely on the laws of quantum mechanics and the values of a small number of physical constants, like the speed of light and Planck's constant. I.e., no experimental data concerning the atoms or molecules are used to deduce values for the integrals that appear when finding approximate solutions to the Schrödinger equation.¹⁸ The simplest *first-principle* method is termed the Hartree-Fock (HF) approximation. In HF theory, one finds solutions to the one-electron Schrödinger equation, called orbitals. An orbital is a one-electron function that describes an electron in the average field of the nucleus and all the other electrons. In HF, electron correlation is neglected, i.e. one assumes that electrons move independently of each other. This means that the many-electron wavefunction, termed molecular orbital, can be represented as an anti-symmetrized product of one-electron wavefunctions (atomic orbitals).

One way to incorporate electron correlation is to treat the correlation as a perturbation to the HF system.¹⁾ The perturbation method introduced by Møller and Plesset¹⁹ (MPn) has become very popular and includes orbitals that are unoccupied in the Hartree-Fock state into the wavefunctions. This allows excitation of electrons to the unoccupied orbitals, thereby giving the electrons more freedom to move around and avoid each other. MP2 is the simplest of MPn methods and includes excitation of only two electrons at a time. Møller-Plesset theory includes also third- and fourth-order levels denoted MP3 and MP4, respectively. Both HF and MPn methods compute approximate solutions to the Schrödinger equation using a series of rigorous mathematical approximations.¹⁶

When selecting an appropriate electronic-structure model, the most important considerations are the level of confidence required in the results and the computational costs. The major fault inherent in the HF method is the neglect of electron correlation. Even though the HF method can provide a qualitatively correct description for most molecules, it does not predict bond lengths and energies with the accuracy required for our purposes. The MP2 method performs much better in this respect for the systems we have studied.²⁰ Naturally, the computational cost for MP2 is higher than for HF. The cost for a HF calculation scales as N^4 , where N is the number of basis functions. MP2 scales as N^5 , MP3 as N^6 and MP4 as N^7 .²¹ HF and MP2 were both used for computing proton affinities in this thesis.

3.1.2 Density functional theory

Another *first-principle* method, used in most of this work, is Density Functional Theory (DFT).¹⁷ In DFT, electron correlation is taken into account by including what is called the exchange-correlation functional. A functional is a function whose argument is also a function. The exchange-correlation functional can include terms accounting for both exchange energy²⁾ and electron correlation. DFT methods do not involve finding wavefunctions. Rather, DFT optimizes the electron density, ρ . The computational cost for a DFT calculation scales as N^3 , which is lower than both HF and MP2. For an "average" problem, DFT is the most cost-effective method to achieve a given level of accuracy.²¹

DFT methods differ in which functional is used for the exchange functional and which is used for the correlation functional. In addition to pure DFT methods, hybrid methods also exist in which the exchange functional is a linear com-

¹⁾In other words, one uses perturbation theory with the Hartree-Fock operator as the unperturbed hamiltonian.

²⁾Exchange energy is represented as a correction to the classical Coulomb repulsion term, resulting from the indistinguishability of electrons.

combination of the Hartree-Fock exchange and a DFT exchange functional. In this thesis, Becke's three parameter hybrid method using the Lee, Yang, and Parr (LYP)²² correlation (B3LYP)²³ was used. B3LYP's overall performance is remarkably good for main-group elements, and its predictions of molecular properties, like bond lengths and proton affinities, are competitive with much more advanced methods. Since B3LYP involves the HF exchange functional, the computational cost for B3LYP scales as HF, N^4 . B3LYP was found to be a suitable compromise between level of accuracy and computational costs for our purposes.²⁰ Further details on B3LYP can be found in refs. 17 and 24.

3.1.3 Basis set

A basis set is the set of mathematical functions from which the wavefunction or orbital is constructed.²¹ The basis set needs to be specified in an electronic structure calculation. It consists of a certain number of atomic orbitals or basis functions. Atomic orbitals can be approximated by contracted Gaussian functions, which are linear combinations, with fixed coefficients, of primitive Gaussian functions. The primitive Gaussian functions are of the form $P(x, y, z)e^{-\alpha x^2}$, where $P(x, y, z)$ is any polynomial in the cartesian coordinates x, y, z , and α is the orbital coefficient. An atomic orbital can be represented by more than one basis function, or contracted Gaussian function, leading to a more flexible basis set. Depending on the number of basis functions for each atomic orbital, the basis sets are called double-, triple-, quadruple-zeta, etc. Molecular orbitals are in turn represented as linear combinations of atomic orbitals, known as the LCAO approximation. In addition, one can add what is called polarization functions which are Gaussian functions corresponding to one quantum number of higher angular momentum than the atomic valence orbitals. Polarization functions add flexibility within the basis set, allowing for more accurate description of chemical bonds. Another common addition to basis sets is diffuse functions. These are Gaussian functions that more accurately describe the parts of atomic orbitals that are distant from the nuclei. The computations in this thesis have used a triple-zeta basis set, meaning that each valence atomic orbital is represented by three contracted Gaussian functions. The basis set was augmented by one set of polarization functions for each atom; a d-set for carbon and a p-set for hydrogen. Generally, a larger basis set provides a more accurate description of the molecular orbitals, but the computational cost is higher.

3.1.4 Hole-state calculations

Electronic-structure calculations for a molecule with a core hole are less than straight forward. Using the variational principle, one wants to acquire as low energies as possible for the calculated orbitals.²¹ In many cases, this would mean relaxing a valence electron to fill the core hole, and the core hole would disappear. Hole-state calculations can be performed,^{25,26} but for most systems they are not practically feasible. A much used approximation is the equivalent-cores method, in which the core-ionized atom with a nuclear charge of Z is replaced by a valence-ionized atom having a closed-shell core and nuclear charge of $Z+1$. In the case of core-ionized carbon, carbon is replaced by the isovalent N^+ . The equivalent-cores approximation contains inherent errors, since it cannot accurately describe the interaction of the valence electrons with the core.^{20,27,28} One shortcoming is that it does not always predict changes in bond lengths and angles correctly. Correct prediction of these parameters is important for the vibrational analysis (see section 3.2.1). As an improvement over the equivalent-cores approximation, one can model the effect of the core hole using an effective core potential (ECP). With an ECP, the core electrons and core hole are represented by potentials, rather than treated as actual particles, and the core hole will be localized to one atom. Although the ECP model suffers from some of the same problems as does the equivalent-cores approximation, bond lengths and angles obtained with ECP are more accurate. In this work, only ECP was used for modeling core holes.

3.2 Franck-Condon analysis

3.2.1 Normal-mode calculations

Removing a core electron is a quite dramatic event for a molecule. A simplified way to think of this process is as follows: when the photon comes in and expels an electron, the excess photon energy is transferred to the electron as kinetic energy. However, some of the photon energy might be kept by the molecule, and as a result the molecule will start to vibrate more vigorously. The photoelectron will then be detected with slightly less kinetic energy, and this shows up in the photoelectron spectrum as a progression of vibrational peaks. The more correct quantum mechanical description is based on the Franck-Condon principle (also known as the sudden approximation). This states that since electronic transitions are very fast compared with nuclear motions, an electronic transition is most likely to occur within a stationary nuclear framework. Once the transition has occurred, the nuclei will relax. The resulting state is called a

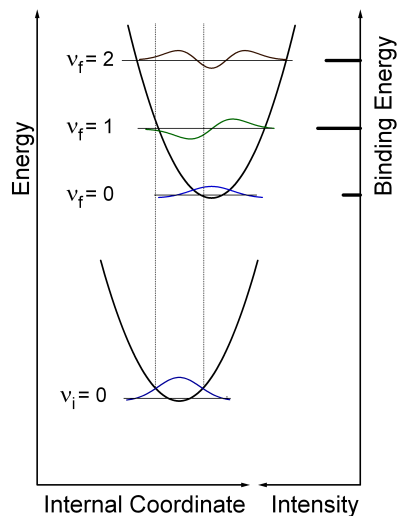


Figure 3.1: *Illustration of the Franck-Condon principle for a harmonic oscillator in a one-dimensional case. ν_i and ν_f refers to the vibrational quantum number for the initial and final electronic state, respectively. The figure is reproduced from ref. 9, with permission.*

Franck-Condon state, and the transition is called a vertical transition. The adiabatic transition is from $\nu_i=0$ (ν_i is the set of vibrational quantum numbers of the lower, initial electronic state) to $\nu_f=0$ of the upper, final electronic state. The probability of a transition is determined by the square of the overlap integral between the vibrational wavefunctions of the two states involved. The square of the overlap integrals are called Franck-Condon factors and determine the relative intensities of the different vibrational lines in a photoelectron spectrum. The Franck-Condon principle is illustrated in Figure 3.1 for a harmonic oscillator in a one-dimensional case. On the left hand side, the electronic potential energy is plotted as a function of an internal coordinate, for the ground and excited electronic states. The internal coordinate represents the nuclear displacement. In this figure, only transitions from the ground vibrational state are considered. For most molecules, this is the only vibrational state which is occupied at normal temperatures. The wavefunctions are plotted for each vibrational level, and the dotted lines show the overlapping region for the wavefunctions. Note that the wavefunctions are dimensionless and, hence, the left energy axis does not apply to them. From the figure, we see that the overlap between $\nu_i=0$ and $\nu_f=1$ has the greatest absolute value. This is illustrated to the right in the figure, where the Franck-Condon factors are shown for each transition.

The different characteristic ways in which a molecule can vibrate are called normal modes. The most important ones are stretching, bending, and torsional modes. To calculate Franck-Condon factors, one needs to know accurate geometries, normal modes and vibrational frequencies for the neutral and core-ionized molecules. This is provided in the output from the Gaussian^{29,30} calculations. Franck-Condon factors are calculated by the *g2fc* program,^{31,32} which reads the output files of Gaussian and computes changes in normal coordinates. It produces a vibrational profile, containing relative intensities and energies for the modes of interest, which can be used as input in fitting the experimental spectra. For polyatomic molecules, normal modes for the neutral molecule are not necessarily the same as for the core-ionized state, and this complicates calculation of Franck-Condon factors. A simplified, diagonal approach based on a one-to-one mapping between neutral- and ionized-state normal modes²⁸ was tested in papers III and IV. Compared to Franck-Condon factors computed in the full harmonic approximation including mode-mixing, only negligible errors were introduced in the simplified approach. As a result, the vibrational profiles used for fitting the spectra in the present work were based on the latter, simplified approach.

To illustrate some of the principles described here, one can use methane as a simple example. Methane is a totally symmetric molecule, and retains its symmetry throughout a core ionization. According to the Franck-Condon principle, the vibrationally excited states must also be totally symmetric. For non-totally symmetric states, the overlap between the vibrational wavefunctions for the ground and ionized state is zero. This means that, within the Franck-Condon approximation, only the symmetric C*-H stretching mode is excited in methane (C* denotes the core-ionized atom). The vibrational frequency for this mode is approximately 400 meV. Vibrational structure in an experimental spectrum of methane was first observed in 1974 by Gelius *et al.*³³ Later, the fine structure of the vibrational progression has been studied in close detail.^{20,34} However, recent investigations show that unexpected features are present in the C1s photoelectron spectrum of methane. One has found evidence of Fermi-resonance³⁵ and of recoil effects that lead to a violation of the Franck-Condon principle upon core-ionization of methane.³⁶ These effects will not be discussed here.

One of the most recent methane spectra, from Paper I, is shown in Figure 3.2. The spectrum is acquired with high-resolution synchrotron radiation, and displays a clearly resolved vibrational progression of the symmetric stretching mode. The tall peak at 290.7 eV is the adiabatic peak, with $\nu_f=0$ for the symmetric stretching mode. Then follows the first and second excited vibrational levels as peaks to higher ionization energy from the adiabatic peak. The peak from the third excited level is barely visible at 291.9 eV. The energy positions of

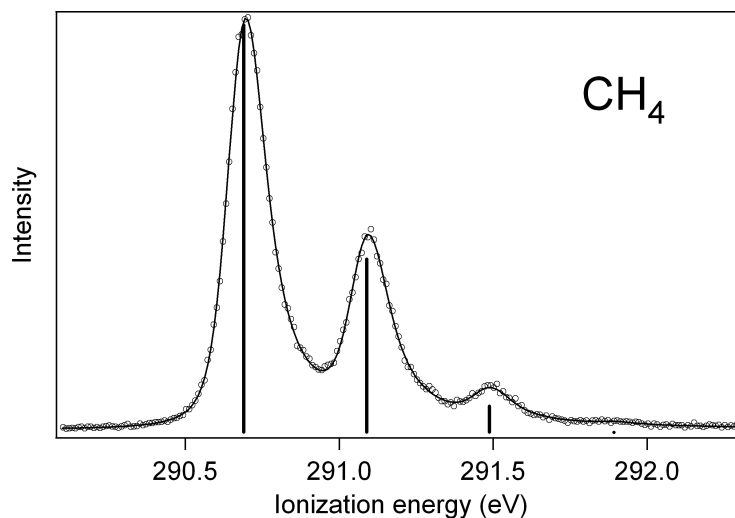


Figure 3.2: Carbon $1s$ photoelectron spectrum of methane (circles) shown together with a least squares fit to the data (solid line). The vibrational lines from the symmetric stretching mode are indicated as bars. The spectrum is adapted from Paper I.

each vibrational line are indicated by the bars, and the spacing between each line is approximately 400 meV as expected from the vibrational frequency of the symmetric stretching mode. This example illustrates in a simple way how vibrational motion of a molecule shows up in an XPS spectrum. One can note in the figure that the energy position of the first vibrational line does not coincide with the energy position of the peak maximum. The reason for this is that the peak maximum is slightly shifted by the Post-Collision Interaction (PCI) effect (see chapter 4.1).

For molecules in which more than one vibrational mode are excited, the photoelectron spectra are more complicated. There will be one vibrational progression for each excited mode. In addition, the different vibrational modes can combine into combination modes. The intensity of a combination mode is the product of the intensities for each individual mode, and the energy of a combination mode is the sum of the energies for each individual mode.

3.2.2 Aspects of vibronic coupling

After the Franck-Condon profile has been calculated, one has to consider whether vibronic coupling may alter the vibrational progression. Vibronic coupling may have an effect on photoelectron spectra when a molecule contains equivalent, adjacent carbons, or when non-equivalent carbons accidentally have

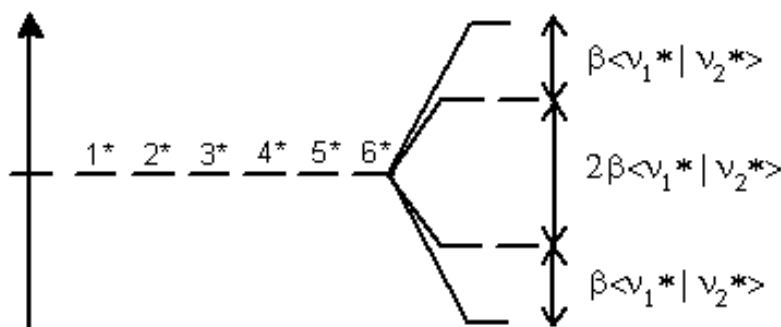


Figure 3.3: A schematic representation of how each six-fold degenerate diabatic vibronic level in $C1s$ -ionized benzene is split according to Equation 3.1. The figure is adapted from Paper III.

core levels with the same energy (degenerate energy levels).

The Born-Oppenheimer approximation states that, because of the great difference in masses of electrons and nuclei, the electron can respond almost instantaneously to movement of the nuclei. In this way, one can regard electronic and nuclear movement as independent of each other. This is called the adiabatic approximation and is valid in most cases, because the energy gaps between electronic states are usually large compared to typical vibrational spacings. In the adiabatic approximation, the core hole is considered delocalized over the equivalent atoms. However, if the electronic states are closely spaced, they can couple via the nuclear motion. This is particularly the case for molecules with equivalent atoms. Ionization of core electrons of equivalent atoms gives rise to several nearly degenerate electronic states that can couple via nontotally-symmetric vibrational modes. This is called vibronic coupling and signals a breakdown of the Born-Oppenheimer approximation. It can lead to a symmetry breaking in the molecule which results in localized core holes.

A slightly different approach is to start out from localized-hole (diabatic) electronic states. Any tendency toward delocalization of the core hole may be described as coupling of diabatic vibronic states. If the overlap between the diabatic degenerate core orbitals is sufficiently large, for instance when the carbon-carbon distance is short, a splitting between the electronically coupled vibronic states occur. This may be characterized as a case of incomplete or partial localization of the core hole. At the level of first-order degenerate perturbation theory, each diabatic vibrational level, ε_{ν} , is split according to Equation 3.1:

$$E_n = \varepsilon_{\nu} + x_n \beta \langle L, \nu | R, \nu \rangle \quad (3.1)$$

where E_n are the resulting vibronic levels, ν is the set of vibrational quantum

numbers for the ionized state, and β is the electronic coupling integral which is common to all vibrational levels.³⁷ $\langle L, \nu | R, \nu \rangle$ is the vibrational overlap integral between the vibrational wavefunctions when the core hole is localized on the left atom (L) and those when it is localized on the right atom (R). The vibrational overlap integral is specific to each (diabatic) vibrational state, ν . x_n is a number dependent on the symmetry and the type of molecule considered. For a diatomic molecule $x_n = -1, 1$. For the benzene molecule, $x_n = -2, -1, -1, 1, 1, 2$. The splitting of the diabatic vibronic energy levels in benzene is illustrated in Figure 3.3. The electronic coupling integral, β , depends strongly on the distance between the carbon atoms and is about 10 meV for adjacent singly-bonded carbons and about 30 meV for adjacent doubly-bonded carbons. It may be ignored for non-adjacent atoms. β can be calculated from the electronic wavefunctions. For hydrocarbons, the vibrational overlap integral is of order 0.5 for the adiabatic transition $\langle L, 0 | R, 0 \rangle$, and it tends to decrease as the degree of vibrational excitation increases.

In most cases when a molecule contains equivalent carbon atoms, the splitting of vibronic energy levels is small, and the carbon 1s ionized molecules can be described in the localized-hole approximation. However, the effect on the C1s photoelectron spectra may not be negligible. We find that, for equivalent adjacent carbon atoms, the fit to the spectra are improved when splitting the vibrational levels. Chapter 5 describes in what way splitting is included in the fits of the various molecules.

3.3 Chemical shifts

From the core-level photoelectron spectrum, one can acquire ionization energies, or core-electron binding energies, for each atom in the molecule. To a first approximation, the binding energies of the core levels are independent of chemical environment and, hence, can be used to identify the atomic species. However, there are small variations in the binding energies caused by the chemical surroundings, and the differences in binding energies are called chemical shifts. These shifts contain chemical-state information and can be compared with other chemical properties, like proton affinities or reaction rates. This has been done for carbon 1s shifts in a series of methyl-substituted benzenes in Paper V, and the results are presented in chapter 5.

Koopmans' theorem states that the negative of the one-electron orbital energy, ε , can be approximated with the ionization energy, I , of the electron from that orbital: $I \approx -\varepsilon$. ε is the orbital energy from HF theory; i.e. $-\varepsilon$ is the energy required to remove an electron from an orbital with the assumption that the remaining electrons do not adjust their positions. Koopmans' theorem im-

plies that chemical shifts can be estimated theoretically by taking differences in orbital energies. This theorem is only an approximation, since in reality, the remaining electrons do relax into a new distribution. A better approach is to estimate ionization energies, or shifts in these, from more realistic hole-state calculations, for instance B3LYP. By taking differences in total energy between the neutral and core-ionized species and relating these quantities to some reference molecule, one can predict theoretical shifts with quite satisfactory accuracy. Theoretical shifts in ionization energy can be compared with the experimental shifts, and in Papers IV and V, we find that the theoretical predictions systematically overestimate the observed shifts by 12%. This is a common feature of many such calculations;³⁸⁻⁴⁰ the trends are predicted correctly, but the slopes are either too high or too low, depending on the details of the basis sets and methods used. In any case, the theoretical calculations can be used to corroborate the assignments of measured ionization energies to specific carbon atoms in a 1s photoelectron spectrum.

3.4 Proton-affinity calculations

Since experimental proton affinities (the negative of enthalpies of protonation) are usually not known for all sites in a molecule, it is useful to be able to predict these theoretically. We have used the method proposed by Maksić *et al.*,^{41,42} which combines HF and MP2. In this method, all geometries are optimized by the HF/6-31G* model, and zero-point energies are taken from this calculation. Total energies are then computed in single-point MP2(fc)/6-31G** calculations using the HF geometries. This approach has been found to reproduce known experimental proton affinities for aromatic systems quite well and makes it possible to calculate enthalpies of protonation for large molecules with reasonable computer effort.

3.5 Computational details

The electronic-structure calculations were performed with the Gaussian set of programs.^{29,30} One starts each Gaussian calculation by making an input file, containing a "guess" geometric structure of the molecule together with specifications of the type of calculation, method, basis set and other details. At the end of the calculation, the output is written to a text file, containing molecular orbitals, geometries, energies and other molecular properties as requested in the input.

All computations, except those for proton affinities, employed the B3LYP

functional.²⁴ Carbon and hydrogen were described by Dunning's triple-zeta basis set,⁴³ TZ(Dunning), augmented by a single set of polarization functions.⁴⁴ Triple zeta means that there are three basis functions per valence atomic orbital. In this basis set, each core-atomic orbital is represented by two basis functions. For the core-ionized carbon atom, the corresponding nitrogen basis was used with all exponents scaled by a common factor of 0.9293, as obtained by minimizing the energy of core-ionized methane.⁴⁵

The core of the ionized carbon atoms was represented by the effective core potential (ECP) of Stevens *et al.*⁴⁶ scaled to account for only one electron in the 1s shell.²⁰

In the Gaussian calculation, the vibrational frequencies were computed within the harmonic oscillator approximation. The harmonic frequencies are expected to be higher than the observed frequencies. In keeping with earlier experience from other molecules,⁴⁷ we have, in the *g2fc* program,³¹ scaled all frequencies by a factor of 0.99 except for the symmetric C*-H stretching mode. In the latter case, the scaling factor was 0.95 for sp³ hybridized carbons and 0.96 for sp² carbons. A Morse potential was used for the symmetric C*-H stretching mode for sp³ carbons. In the case of benzene, the neutral-state frequencies are known from experiment, and the calculated frequencies for the ionized state were scaled by the ratio of observed-to-calculated frequencies for the neutral state. Calculations of Franck-Condon factors are extremely sensitive to changes in bond lengths and bond angles upon ionization. At the level of theory used in this thesis, the contraction of C*-H bond lengths is exaggerated by 0.2 pm for sp² carbons and 0.3 pm for sp³ carbons.^{20,47} The corresponding C*-H bond lengths have been lengthened accordingly, before the Franck-Condon factors were calculated.

Chapter 4

Lineshape functions and data analysis

After the photoelectron spectra have been acquired and the vibronic progression predicted by theory, there are a few steps left in the data analysis before the actual fitting procedure can be performed. There are several parameters, in addition to the vibronic progression, that influence the line shapes of the photoelectron spectra. These parameters will be discussed in this chapter, and the curve-fitting procedure will be presented in some detail.

4.1 Post-Collision Interactions

Inner-shell photoionization at energies close to the ionization threshold can result in certain types of correlation effects known as Post-Collision Interactions (PCI). After ionization from a core orbital, the molecule (or atom) is left in an unstable state and must expend the excess energy. This can be done in two ways; fluorescence decay or Auger decay. The two decay processes are illustrated schematically in Figure 4.1. In fluorescence decay, an electron from a valence orbital drops down into the core hole and the excess energy is emitted in the form of an X-ray (photon). Auger decay, on the other hand, involves a second electron called the Auger electron. When a valence electron fills the core hole, the excess energy is carried away by the highly energetic Auger electron. The Auger process dominates for the lighter elements, including carbon. If a photon energy close to the ionization threshold is used, the ejected photoelectrons have a quite low kinetic energy and will be overtaken by the Auger electrons at some point. Thus, there will be an exchange of energy between the two electrons, in favor of the Auger electron. In addition, after the overtake the photoelectron experiences an increased charge from the ionized molecule, +2 instead of +1. The

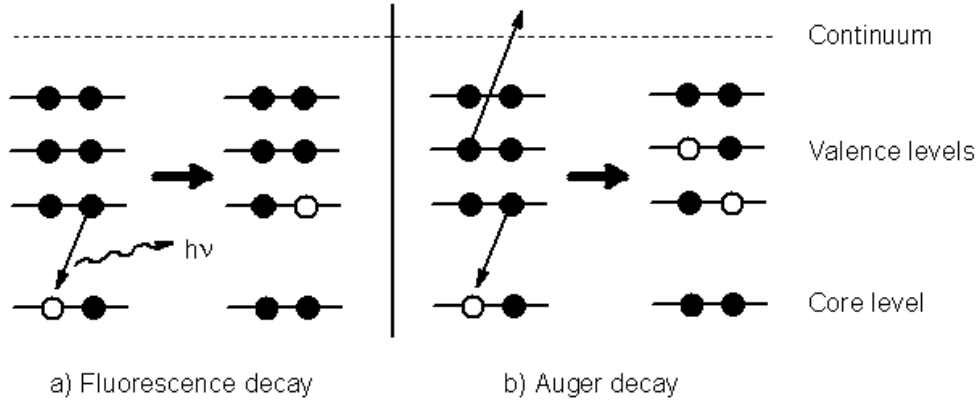


Figure 4.1: Schematic representation of two possible electronic decay mechanism for core-ionized species. a) Fluorescence decay, where a photon is emitted. b) Auger decay, where a valence electron is ejected when the core hole is filled.

result is a retardation of the photoelectron, which gives rise to an asymmetric lineshape of the photoelectron spectrum, with a tail to higher ionization energy (or lower kinetic energy). The PCI effect broadens the spectrum somewhat, and the peak maximum is slightly shifted in energy.⁴⁸ To model the PCI effect in our spectra, we have used Equation (12) of van der Straten *et al.*,⁴⁹ which is expected to be valid in the energy region we have studied. The PCI equation is dependent on the kinetic energies of the Auger and photoelectrons, A_e and k_e , respectively. This is expressed in the asymmetry parameter, $Asym$:

$$Asym = \frac{1}{\sqrt{2}} \left(\frac{1}{\sqrt{k_e}} - \frac{1}{\sqrt{A_e}} \right) \quad (4.1)$$

$Asym$ represents the asymmetric distortion of the photoelectron peak due to PCI. When fitting the photoelectron spectra, the asymmetry parameter is set according to Equation 4.1. Equation 4.1 is not valid for photon energies very close to threshold, but is well justified for our experiments.

4.2 Other broadening parameters

A core hole has a finite lifetime, τ , which is determined by the decay process. For Auger decay, the lifetime of the core hole is typically a few femto seconds (10^{-15} s). Any state that has a finite lifetime must be regarded as having an imprecise energy. The uncertainty in the energy shows up in the photoelectron

spectrum as a broadening given by:⁴⁸

$$\tau \cdot \Gamma_L \approx \hbar$$

where Γ_L is called the lifetime broadening. In the absence of contributions from instrumental broadening and PCI, Γ_L is the full width at half maximum (FWHM) of an atomic spectrum (for molecules, vibrational progression may broaden the spectrum). The lifetime broadening relation is similar to Heisenberg's uncertainty relationship, but has a different theoretical origin. It shows that the shorter the lifetime of a state, the less precise is its energy. For C1s lines, Γ_L is approximately 100 meV.^{48,50,51} The lifetime broadening has the shape of a Lorentzian curve.

A second broadening effect comes from the resolution of the different components of the instrumental setup. The photons have a given energy distribution, and the electron analyzer has a certain resolution. The experimental broadening, Γ_G , has the shape of a Gaussian function. In our experiments, the total experimental resolution for the C1s spectra ranged from 45 to 90 meV.

4.3 Curve fitting

The last step in the process of obtaining carbon 1s ionization energies from the experimental spectra is curve fitting. The curve-fitting procedure was performed using a least-squares optimization method, provided by E. Kukk.⁵² In this procedure, the Franck-Condon profile from the *g2fc* program³¹ is used as input. The Franck-Condon profile is contained in a text file (Igor wave), with relative energies and intensities for each vibronic line in two separate columns. It is to be noted that each inequivalent carbon in a molecule has its own unique Franck-Condon profile. In Igor, each vibronic line is convoluted with an analytical PCI-shape that contains the contributions from lifetime and instrumental broadening. Parameters to be set in the fit are absolute and/or relative energies and intensities, background, Lorentzian and Gaussian widths, and asymmetry for each inequivalent carbon. All parameters can be either fixed or free (determined by optimization). Typically, a good starting point for the optimization would be to set the relative energies for each profile according to predictions from theory. Intensities (or areas) are normally optimized in the fit, although in some cases it is necessary to fix the relative intensities between different carbons according to stoichiometric ratios. The background is set as constant, i.e. not sloping, and its value is optimized. Normally, the Lorentzian width is fixed to 100 meV, and the Gaussian width is fixed to the estimated experimental resolution. The asymmetry parameter is usually set according to Equation 4.1. During the least-squares optimization, the free parameters are adjusted iteratively until

the best possible match to the spectrum is obtained. χ^2 is the goodness-of-fit parameter. Ideally, χ^2 should be close to unity.

To sum up, in the curve-fitting routine the theoretically predicted profiles are optimized to fit the experimental spectrum. When calibration is included, this provides absolute and relative 1s ionization energies for each carbon in the molecule.

Curve fitting was performed using the scientific data-analysis program Igor Pro,⁵³ including the macro package SPANCF provided by E. Kukk.⁵²

Chapter 5

Summary of main results

5.1 Methods for calibration

All the experimental work in this thesis is based on measurements of inner-shell ionization energies by means of photoelectron spectroscopy. A requirement for such measurements to be useful is that they are accurate, and this involves access to convenient procedures for calibration of the energies. In the early days of electron spectroscopy, conventional X-ray sources were used in which the photon energies were accurately known. The limitation of using conventional X-ray sources is, however, the resolution. With this type of instrumentation, the measurement of carbon 1s ionization energies for molecules represents, in most cases, an average over the vibrational profile, or the vertical ionization energies. However, the availability of high-resolution electron spectrometers and light sources at third-generation synchrotrons has now made it possible to resolve the vibrational structure for a number of molecules. Thus, it is now possible to determine not only the vertical but also the adiabatic C1s ionization energies, and with much higher absolute accuracy than before. To do this, one needs knowledge about the electron spectrometer and how the kinetic energy scale of the spectrometer is related to the actual voltage supplied. A method for calibrating electron spectrometers is presented in Paper II.

With synchrotron radiation, however, the accuracy with which the photon energy is known is not high, and it is necessary to include an internal standard for which the ionization energy is well known. Paper I reports highly accurate measurements of carbon 1s ionization energies of nine representative molecules that provide potential calibration standards for future measurements. In addition, the ionization energies are of interest in their own right for the chemical information they contain and for comparison with theoretical calculations.

5.1.1 Calibration of electron spectrometers

Electron kinetic-energy spectra are typically obtained by measuring the counting rate of the electrons detected in the spectrometer as a function of a voltage applied to the spectrometer. Ideally the kinetic energy is linearly related to this voltage with unit slope. In Paper II we have investigated the quality of the electron analyzers used in the experimental work of this thesis. A useful standard for this purpose is the xenon $N_{4,5}OO$ Auger spectrum. The notation $N_{4,5}OO$ refers to a decay process in which the initial state, before the Auger decay, is a $4d_{3/2}^{-1}$ or $4d_{5/2}^{-1}$ state ($N_{4,5}$), and the final state is doubly ionized in 5s, p, d, or f (OO). The Auger spectra were acquired using two different Scienta SES-200 analyzers,^{8,14,15} with slits and pass energies chosen to give a resolution of 35-40 meV. The 4d photoelectron peaks were included in some of the measurements. The Auger spectrum has 19 prominent lines ranging in kinetic energy from 8 to 36 eV. The relative energies of some of these lines are known with high accuracy from optical measurements. The absolute energies can be determined by combining the optical energies with the 4d ionization energies. With this information, the energy scale can be calibrated.

By comparing our measured Auger energies with the reference energies, we found that the two sets of data agreed within a few meV. Regarding the relationship between the nominal voltage increments and the true voltage increments, we found that the nominal voltage had an accuracy of a few parts in 10^4 . As such, the slope is very close to one and there is no evidence of significant nonlinearity in the kinetic energy scale of the two electron analyzers studied. The kinetic energies reported in Paper II for the xenon $N_{4,5}OO$ Auger spectrum should provide a set of calibration points for this type of electron spectrometers at a level of accuracy that is higher than what has been available before.⁵⁴⁻⁵⁶ The absolute and relative uncertainties of the Auger energies were estimated to no higher than 11 and 3 meV, respectively.

5.1.2 Accurate adiabatic and vertical ionization energies

As the photon energy of synchrotron light is not known very accurately, one needs to calibrate the measured ionization energies by using an internal standard with well known ionization energy. In Paper I, the carbon 1s energies for nine compounds were measured with reference to the argon $2p_{3/2}$ line. The ionization energy of the $2p_{3/2}$ line is known with an accuracy of 0.02 eV.^{40,57,58} Since argon is monatomic, there is no vibrational excitation and fitting the spectrum is unambiguous. The other compounds measured were methane, ethane, ethene, ethyne, carbon monoxide, carbon dioxide, fluoromethane, trifluoromethane, and tetrafluoromethane. The carbon 1s ionization energies for these molecules

Table 5.1: *Adiabatic and vertical ionization energies (eV)*

Molecule	I_C (adiabatic)	I_C (vertical)
Methane	290.689	290.844
Ethane	290.545	290.714
Ethene	290.695	290.823
Ethyne	291.128(avg) ^a	291.249 ^a
Carbon monoxide	296.069	296.229
Carbon dioxide	297.664	297.699
Tetrafluoromethane	301.898	301.898
Fluoromethane	293.478	293.557
Trifluoromethane	299.143	299.159

^aUnweighted average for the $^2\Sigma_g$ and $^2\Sigma_u$ states

span most of the range of known carbon 1s energies, from about 291 to 302 eV. The experimental resolution was estimated to 88 meV. For each molecule, an argon spectrum was recorded simultaneously. This makes it possible to determine the difference between the kinetic energies accurately. Combining this with the known energy of the argon $2p_{3/2}$ line (taken to be 248.629 eV⁵⁸) gives the ionization energy, I_C , of each molecule:

$$I_C = 248.629 + \Delta_K + \Delta_R$$

where Δ_K is the difference in the measured kinetic energies (argon minus carbon) and Δ_R is the difference in the recoil energies imparted to the remaining ion. Δ_R is typically less than 1 meV. Values of the adiabatic carbon 1s ionization energies determined in this way are given in Table 5.1. Also shown in the table are vertical ionization energies. In Paper I, we compare our vertical energies with other previously reported values for the same molecules. The overall root-mean square difference is 0.05 eV, which shows that the agreement is quite good. Combining the uncertainty in the argon ionization energy with the differences between our ionization energies and other measurements leads to an overall uncertainty in the absolute ionization energies of 0.03 eV. The relative uncertainty between one ionization energy and another in our measurements is less than this, possibly as low as in the third decimal place. The ionization energies reported here provide a set of highly accurate carbon 1s energies that may be used for calibration in future measurements.

5.2 The C1s photoelectron spectra of cyclic hydrocarbons

A primary goal for this work was to obtain accurate C1s ionization energies for each inequivalent carbon in different unsaturated hydrocarbons. The 1s ionization energies are related to various chemical properties and are, therefore, a source of important chemical information. The experimental spectra can be very complex, even for small molecules, and in order to determine accurate ionization energies one needs reliable methods to deconvolute the spectra. This requires understanding of the electronic and vibrational structure, and in particular, effects of incomplete localization of the core hole for adjacent equivalent carbons. In Paper III, effects of incomplete localization of the core hole was studied in detail for the aromatic benzene and d-benzene molecules, and the results for benzene will be presented in section 5.2.2.

The C1s photoelectron spectra for two groups of molecules will be presented in this section. The benzene molecule may be regarded as part of both groups, the first one being six-membered cyclic hydrocarbons including cyclohexane, cyclohexene, and 1,3- and 1,4-cyclohexadiene (see Paper IV). This series of molecules represents an evolution from a saturated molecule through the unsaturated molecules to benzene, in which the π -electrons in the ring are completely delocalized. The other group is methyl-substituted benzenes, from toluene with only one methyl group to 1,2,4,5-tetramethylbenzene with four methyl substituents. The special stability associated with aromatic compounds is altered when introducing substituents on the ring. This group of molecules is well suited for studies of positional substituent effects on aromatic rings, as well as additivity of substituent effects (upon increasing number of substituents). The results for the methyl-substituted benzenes are reported in Paper V.

5.2.1 Benzene

Figure 5.1 shows the C1s photoelectron spectrum of benzene as presented in Paper III. Circles represent the experimental spectrum, while the solid line through the data shows a theoretically predicted profile based on a localized-hole approach (see chapter 3). The most intense vibrational lines are indicated as bars. From the figure, it is clear that the localized hole model is able to provide a good description of the data.

For the first time, a splitting of the most prominent peak in the experimental spectrum of benzene is observed. Two maxima of about equal intensity occur at 290.26 and 290.34 eV. As can be seen in Figure 5.1, this splitting is caused by strong excitation of a vibrational mode consisting of C*-C stretching and in-

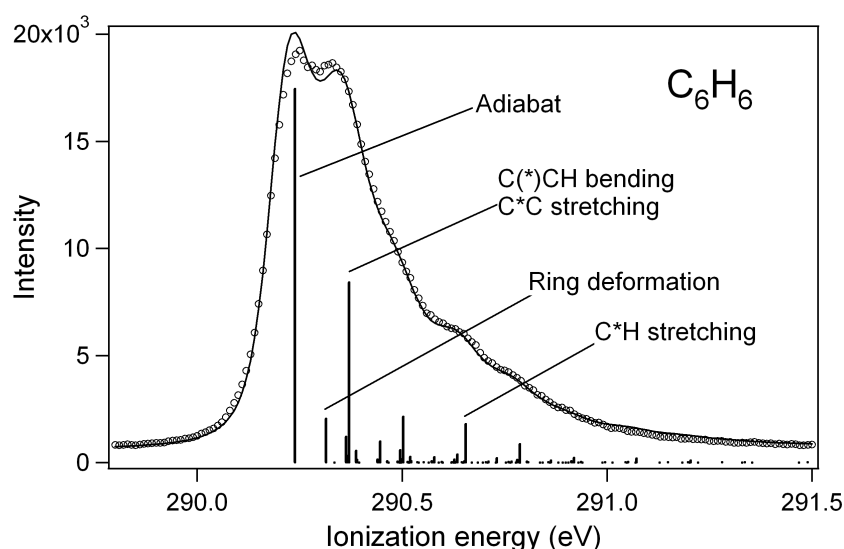


Figure 5.1: Carbon 1s photoelectron spectrum of benzene (circles) shown together with a fitting model (solid line) based on the localized-hole approximation. The most intense vibrational lines are indicated as bars. The figure is adapted from Paper III.

plane C*-C-H and C-C-H bending, with a vibrational frequency of 132 meV. Other important modes include a ring deformation mode at 76 meV and C*-H stretching at 417 meV.

5.2.2 Effects of incomplete localization of the core hole

For adjacent equivalent atoms, incomplete localization of the core hole can have a significant contribution to the C1s spectra. This was investigated thoroughly for benzene in Paper III. According to Equation 3.1 on page 19, one needs estimates for the electronic coupling integral, β , and the vibrational overlap integral, $\langle L, \nu | R, \nu \rangle$. β can be calculated from the electronic wavefunctions, and Figure 5.2 shows β plotted as a function of the C-C bond length as computed for ethyne,³⁷ ethene,⁵⁹ benzene,⁶⁰ and ethane.⁴⁷ Evidently, this parameter is determined by the distance between the symmetry-related carbon atoms. The smooth curve-fit to β suggests that in subsequent studies, one may obtain useful estimates of β through interpolation in Figure 5.2. The vibrational overlap integral for hydrocarbons is of order 0.5 for the adiabatic transition and tends to decrease as the degree of vibrational excitation increases. It can be estimated from the vibrational wavefunctions.

To examine the effect of vibronic coupling in the benzene spectrum, several

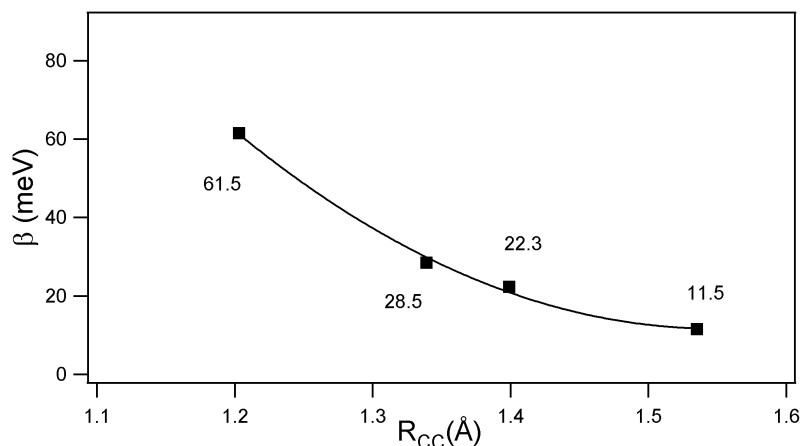


Figure 5.2: The electronic coupling integral β plotted vs. the carbon-carbon bond length in the ground state of ethyne,³⁷ ethene,⁵⁹ benzene,⁶⁰ and ethane.⁴⁷ The figure is adapted from Paper III.

models with different degrees of complexities were tested. Our most advanced model (Model III in Paper III) included calculating the vibrational overlap integrals for all vibrational lines that receive an intensity higher than 1% of that of the adiabatic peak. Of these, only vibrational levels that support vibrational overlap integrals $\langle L, \nu | R, \nu \rangle \geq 0.1$ were actually split in the fitting routine. For benzene, this implied that ten of the diabatic vibrational lines were split, while 98 remained unsplit. The fitting routine yielded a splitting pattern of 16,32,16 meV for the adiabatic peak, and the resulting fit is shown in Figure 5.3. It is clear that the experimental spectrum is very well reproduced, even in small details. Compared to the fit based on the localized-hole approximation, Figure 5.1, the improvement is substantial both in terms of reduced χ^2 and the visual appearance. The drop in χ^2 is 36%. We also tested a simpler model (Model II in Paper III) in which only the adiabatic peak is split. Actually, the resulting fit from the latter, simpler model is virtually indistinguishable from that obtained with our most elaborate model, Figure 5.3. In addition, the difference in reduced χ^2 for the two models is insignificant. Considering also that the vibrational overlap integral is expected to decrease with vibrational excitation, we contend that splitting only the adiabatic peak will probably be sufficient in most cases.

This way of taking into account vibronic coupling for equivalent adjacent carbon atoms, by splitting only the adiabatic peak, was used in fitting the spectra of both the six-membered cyclic hydrocarbons and the methyl-substituted benzenes, where applicable. In each case, including splitting of the adiabatic peak in the fitting procedure lead to a lower reduced χ^2 , although where the

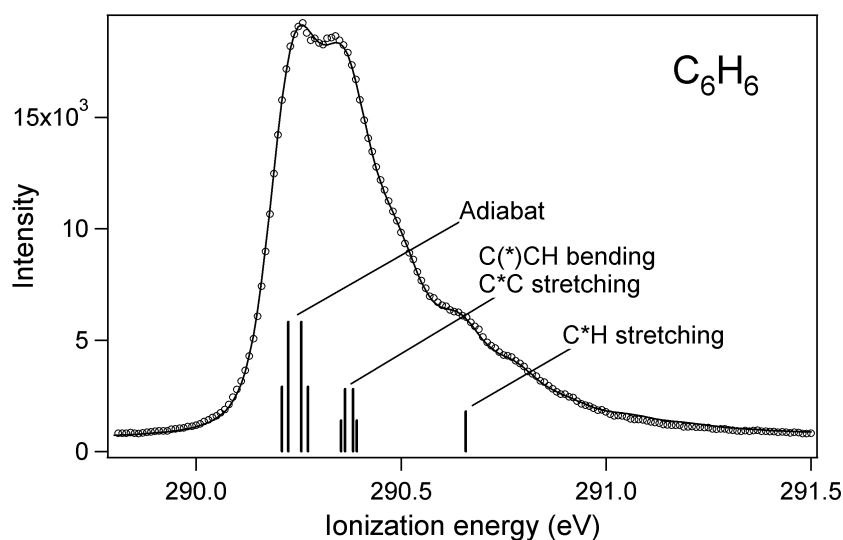


Figure 5.3: Carbon 1s photoelectron spectra of benzene including vibronic coupling for ten of the diabatic vibrational lines. The figure is adapted from Paper III.

splitting was small the improvement was small. In many cases, also the visual agreement between the experimental and theoretical spectra improved significantly. We expect that this relatively simple model of how to take into account the effects of vibronic coupling in C1s spectra, by splitting only the adiabatic peak, will work well also for other, even more complex systems involving hydrocarbons.

The C1s spectrum of d-benzene was also measured and deconvoluted, taking vibronic coupling into account by using our most elaborate model. The resulting fit to the observed spectrum was highly satisfactory. For details on the analysis of d-benzene, see Paper III.

5.2.3 Six-membered cyclic hydrocarbons

Figure 5.4 shows the C1s photoelectron spectra (circles) of cyclohexane, cyclohexene, 1,3- and 1,4-cyclohexadiene, together with the benzene spectrum, as reported in Paper IV. The overall least-squares fits are represented by the solid lines through the circles, and the theoretical vibrational profiles for each inequivalent carbon are indicated by the other lines. Vertical bars show the positions and relative intensities of the most prominent vibronic transitions. Aspects of vibronic coupling in these spectra are discussed in section 5.2.2. Inspection of this figure shows that the theoretically predicted vibrational structures agree

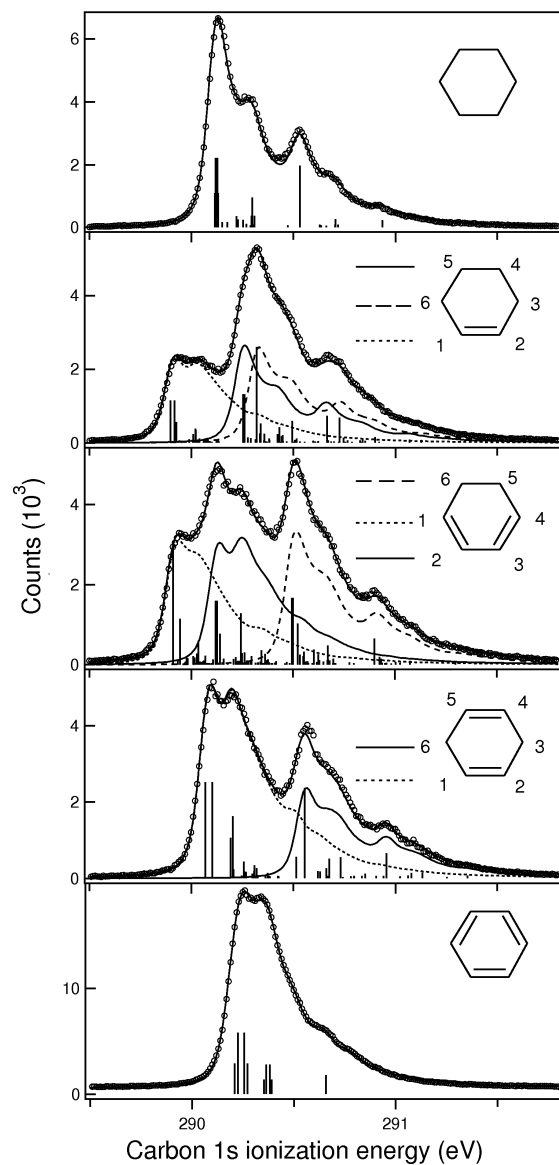


Figure 5.4: Carbon 1s photoelectron spectra of the six-membered cyclic hydrocarbons. Circles show the experimental data. The solid line through the circles show the overall least-squares fit to the data, and the other lines show the vibrational profiles for each of the inequivalent carbons. The vertical bars show the positions and relative intensities of the most prominent vibronic transitions. The figure is reprinted from Paper IV.

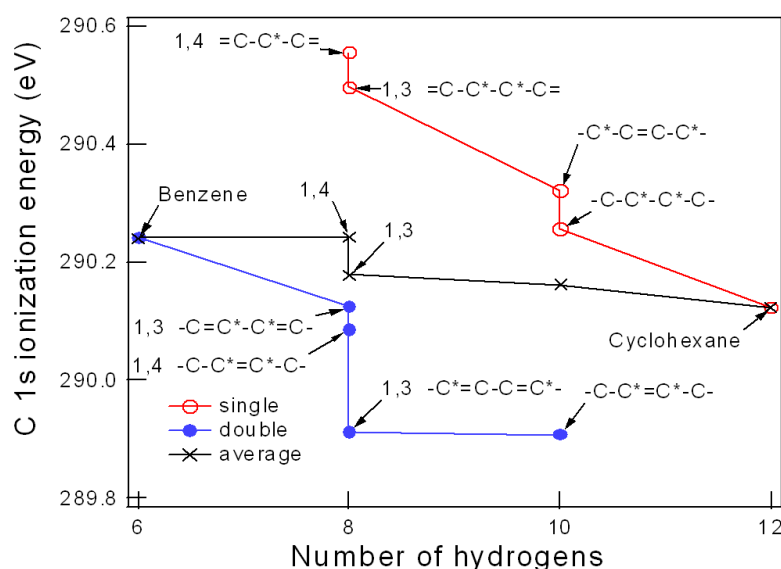


Figure 5.5: Carbon 1s ionization energies plotted against the number of hydrogens in the molecule for the six-membered cyclic hydrocarbons.

quite well with the observed structures. When comparing calculated and experimental shifts in ionization energies, we find that the theoretical predictions overestimate the experimental shifts by 12%. This is a common feature of many such calculations (see section 3.3).

The spectrum of cyclohexane exhibits the same characteristics as linear alkanes, namely strong excitation of a C*-H stretching mode and excitation of C-C-H bending modes involving the hydrogens attached to carbon atoms other than the core-ionized atom. The stretching mode gives rise to the peak in the spectrum at about 400 meV to higher ionization energy than the adiabatic peak. The bending modes are apparent as the shoulder on the main peak.

An interesting observation is that the vibrational structure of all the molecules in Figure 5.4 can be understood by considering the two extremes, cyclohexane and benzene. In cyclohexene, as an example, the double-peaked structure of benzene is apparent as a flat-topped peak at low ionization energy, while the rest of the spectrum can be seen to result from two spectra slightly displaced from each other with each resembling that of cyclohexane. Essentially the same patterns are apparent for 1,3- and 1,4-cyclohexadiene.

When it comes to ionization energies, there is a systematic trend as we go from cyclohexane to benzene, with a slight increase in the average ionization energy with decreasing number of hydrogens. This is illustrated in Figure 5.5

for the six-membered cyclic hydrocarbons. The figure also shows that carbons with double bonds have systematically lower ionization energies than do those with single bonds. From the figure, one can also note the striking difference in ionization energies (0.2 eV) between the inequivalent doubly-bonded carbons in 1,3-cyclohexadiene. This large shift is presumably due to resonance effects in the molecule, but this question has not been pursued in any detail as yet. A discussion of all shifts in ionization energies, the reasons for these shifts, and their chemical implications would be interesting and is suggested as a future project.

5.2.4 Methyl-substituted benzenes

The experimental carbon 1s spectra of the methyl-substituted benzenes (from Paper V) are shown in Figure 5.6. The circles represent the experimental data, and the black solid lines through the circles represent the sum of the least-squares fits of the theoretical vibrational profiles to the data. The other lines show the vibrational profiles for each of the inequivalent carbon atoms. As can be seen from Figure 5.6, the calculated profiles give an excellent description of the experimental data. Comparison of the theoretical and experimental ionization energies shows good agreement, except that the theoretical approach predicts shifts in ionization energies about 12% larger than observed.

5.3 Ionization energies and other chemical properties

Aromatic compounds, like benzene, are less reactive than other unsaturated molecules. The special stability for benzene is attributed to complete delocalization of the π -electrons in the ring. However, introducing substituents on the benzene ring changes the reactivity dramatically. Effects of substituents on benzene rings have been studied for many decades.⁶¹⁻⁶⁴ In Paper V, we investigated the influence of the methyl group on benzene rings, with respect to reaction rates of electrophilic substitution, proton affinities (the negative of the enthalpy of protonation), and carbon 1s ionization energies. We studied the molecules benzene, toluene, o-, m-, and p-xylene, and 1,2,4,5-tetramethylbenzene (durene). This series represents the evolution from zero to four methyl substituents on a benzene ring. These results are presented in Paper V.

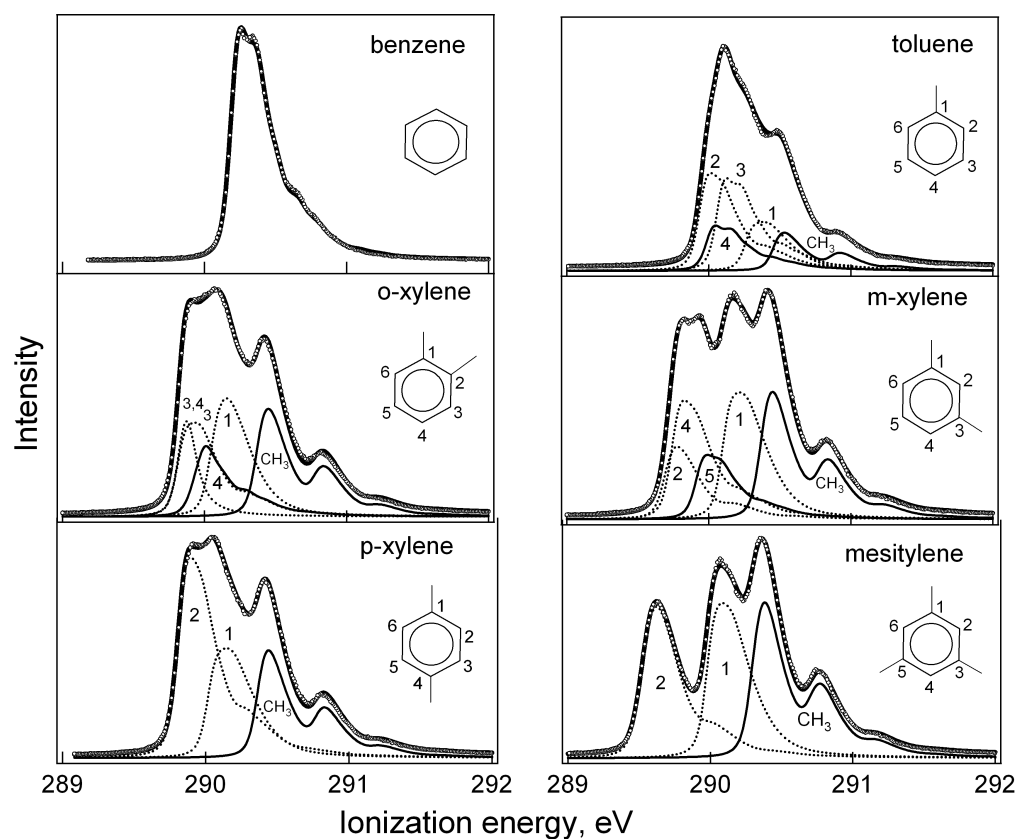


Figure 5.6: Carbon 1s photoelectron spectra of benzene and methyl-substituted benzenes. Circles show the experimental data. The solid line through the circles show the overall least-squares fit to the data, and the other lines show the vibrational profiles for each of the inequivalent carbons. The figure is adapted from Paper V.

5.3.1 Proton affinities, activation energies, and core-ionization energies

Many chemical processes involve adding a positive charge at a particular site in a molecule. Among these are core ionization, protonation and electrophilic-substitution reactions. Although the absolute energies involved in the processes are quite different, the energy changes brought about by substituents that are remote to the site of charge addition may be expected to correlate with one another. Methyl is known to be an electron-donating and ortho-para-directing substituent. In other words, the methyl group can, through hyperconjugation, donate electrons to the benzene ring, thereby stabilizing an added positive charge. The donated charge appears mostly at the ortho and para positions of the ring, while the meta position is only slightly affected by the substituent.

Two electrophilic-substitution reactions involving a protonated transition state was considered; one being the hydrogen-exchange reaction in which a tritium atom attached to one of the ring carbons is replaced by an ordinary hydrogen atom.⁶⁵ The other reaction is the desilylation reaction in which a trimethylsilyl group is replaced by a hydrogen.⁶⁶ We obtained relative activation energies, $\delta E_{act,i}$, from the reported rate constants for these reactions by using the relationship:

$$\delta E_{act,i} = -RT \ln(k_i/k_H) \quad (5.1)$$

where k_i and k_H are the rate constants for each substituted molecule and for unsubstituted benzene, respectively. In Equation 5.1, pre-exponential factors that affect the rates are ignored. The relative activation energies are plotted in Figure 5.7 versus relative gas-phase enthalpies of protonation for all the ring carbons of the methyl benzenes. The enthalpies of protonation were calculated theoretically, as described in chapter 3.^{41,42} From the figure, one can see that there is an excellent correlation between the activation energies for hydrogen-tritium exchange and the enthalpies of protonation (squares). For the desilylation reaction there are two distinct correlations, one for cases where the trimethylsilyl group is ortho to two methyl groups (solid triangles) and one for all other points (open triangles). The former correlation corresponds to situations where release of steric strain contributes significantly to the measured reaction rates, and thus, to lower activation energy. Overall, there is a good correlation between activation energies for the two solution reactions and the gas-phase enthalpies of protonation, indicating that a methyl substituent influences the energy of these types of reactions in a similar way.

In Figure 5.7, we have also plotted relative carbon 1s ionization energies versus relative enthalpy of protonation for the methyl benzenes. Correlations between proton affinities and core-ionization energies have been long known for

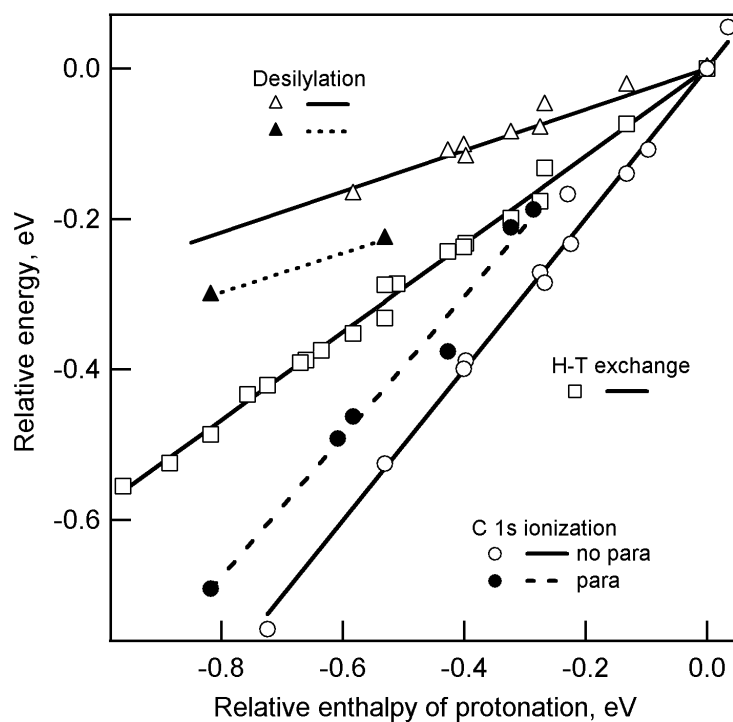


Figure 5.7: Relative energies of activation and relative carbon 1s ionization energies plotted against relative enthalpies of protonation for methyl-substituted benzenes. Triangles are for desilylation; the solid triangles are for compounds in which there are two methyl groups ortho to the trimethylsilyl group. Squares are for the hydrogen-tritium exchange reaction. Circles are for C1s ionization energies: open circles are for compounds in which there are no methyl groups para to the ionized carbon. Closed circles are for compounds in which there is a methyl group para to the ionized carbon. The lines show least-squares fits of straight lines to different sets of the data. The figure is reprinted from Paper V.

oxygen^{67,68} and nitrogen,^{67,69} but it is only recently that there have been sufficiently good data available for carbon 1s ionization energies to make such investigations possible for carbon compounds. In the figure, there are two correlation lines for the 1s ionization energies, one for cases where there is a methyl group para to the site of ionization (filled circles) and one for all other cases (open circles). Since there are two correlation lines, it is apparent that methyl substituents can have effects on the carbon 1s ionization energies that are different from their effect on the proton affinities or the rates of electrophilic substitution. This can be understood by recognizing that the π -systems for the core-ionized and the protonated species are different. At the site of protonation, there is a pair of hydrogens above and below the plane of the molecule. This leads to an extended π -orbital structure that can serve as an efficient π -electron acceptor on demand for the protonated species. For the core-ionized species, there is only one hydrogen, in the plane of the ring, and hence, no enhancement of the electron donating effect of the substituent. As a result, electron donation from the substituent is more effective with respect to protonation than it is to core ionization, giving rise to the displacement of the two lines. Comparison of the energetics of these two processes thus provides insight into this difference in electron-donation efficiency.

5.3.2 Additivity of substituent effects

The substituent effects discussed above can be summarized compactly with an additivity relationship:⁷⁰

$$\delta E_r = \sum_i n_i \alpha_{ir} + \sum_i \left(n_i(n_i - 1) \beta_{ir} + \sum_{j>i} n_i n_j \gamma_{ijr} \right)$$

where δE_r is the energy (or enthalpy) change for reaction r (ionization, protonation, or electrophilic substitution) relative to that of some reference compound (benzene in this case). The number of substituents of type i (ipso, ortho, meta, or para) is given by n_i . The coefficients α , β , and γ are characteristic of the substituent, its position, and the reaction. The first term in this expression represents the linear additive effect of the substituents, and in most treatments of additivity, this is the only term considered. The second term represents interactions between the substituents that lead to departure from additivity. In practice, these quadratic terms are small and often insignificant. Least-squares fitting was used to determine the coefficients for the effect of a methyl group on the carbon 1s ionization energies, the calculated enthalpies of protonation, and the activation energies for the two electrophilic substitution reactions in benzene. The linear coefficients are shown in Table 5.2. The values of all of the

Table 5.2: Linear additivity coefficients, α_{ir} , for the effect of methyl substituents on the 1s ionization energies, enthalpies of protonation, and activation energies of substituted benzenes (in eV). Uncertainties in the last digit are shown in parentheses. Where no value is shown, the coefficient is not statistically significant.

	Ionization	Protonation	Hydrogen exchange	Desilylation
α_{ipso}	0.046(5)	0.036(2)		
α_{ortho}	-0.264(3)	-0.279(2)	-0.174(2)	-0.084(3)
α_{meta}	-0.143(3)	-0.132(1)	-0.068(2)	-0.026(3)
α_{para}	-0.226(5)	-0.321(3)	-0.193(3)	-0.084(3)

coefficients can be found in Table 2 in Paper V. For each of the different reactions, the value of R^2 for the least-squares fitting is greater than 0.99, showing that the additivity model gives a very accurate description of the energy shifts. It is to be noted that the quadratic coefficients are small. Even if these are omitted, the model still describes most of the results well, with an rms deviation of 18 meV for the ionization energies and 19 meV for the enthalpies of protonation. This is to be compared to 8 meV and 4 meV, respectively, when including the quadratic coefficients. This indicates that the effect of multiple substituents can, to a good approximation, be set equal to the sum of the effects of the individual substituents. In Figure 5.8, the linear coefficients for the two electrophilic reactions and for the C1s ionization energies are plotted against the linear coefficients for protonation. Included, for comparison, are linear coefficients for the fluoro substituent for C1s ionization.⁷⁰ The lines shown are straight-line fits that are constrained to go through the origin (which is the point for unsubstituted benzene). For carbon 1s ionization, only the points for meta substitution are used for determining the line. We see that the additivity coefficients for ortho, meta, and para methyl substituents are all negative, regardless of the type of reaction, reflecting the electron donating power of the methyl group. By contrast, the coefficients for fluorine are positive, reflecting the well known electron withdrawing power of the fluorine substituent. It is also clear that the points for the two electrophilic substitution reactions all fall on straight lines regardless of whether there are hyperconjugative effects (ortho and para substituents) or not (meta substituents). For the core-ionization energies, however, it is apparent that the points for ortho and para substituents fall to the left of the correlation line defined by the meta substituents. This is the same effect that has been seen in Figure 5.7, illustrated more compactly in terms of additivity coefficients.

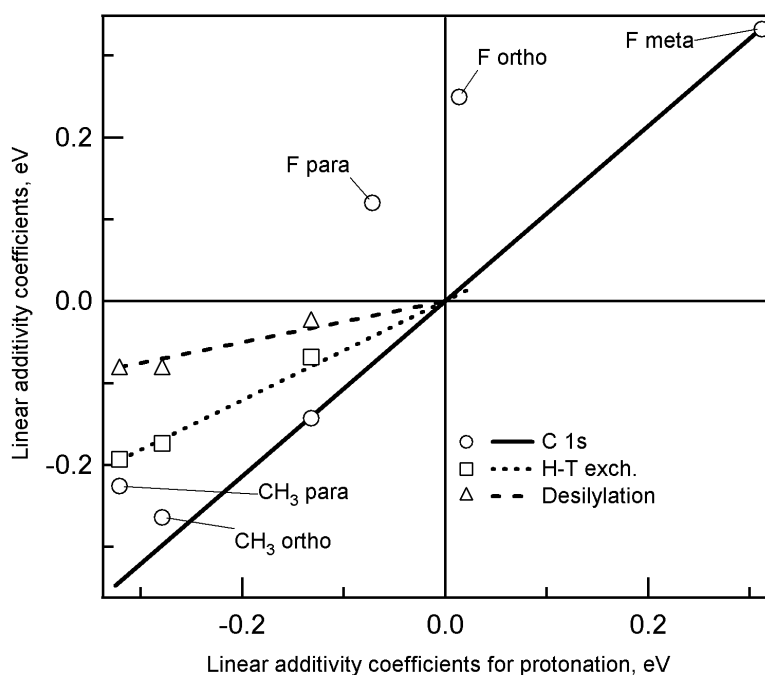


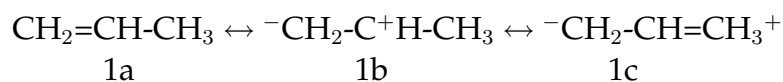
Figure 5.8: Linear additivity coefficients, α_{ir} , for desilylation (triangles), hydrogen-tritium exchange (boxes), and carbon 1s ionization (circles) plotted against the linear coefficients for the enthalpy of protonation. The figure is adapted from Paper V.

These results can also be understood in terms of Hammett σ and $\sigma+$ parameters.^{62,71} One would expect core-ionization energies to correlate with σ , since the effect of conjugation between the ionized carbon and the substituent is already included in σ . Such a correlation has been shown by Lindberg *et al.*⁶⁴ and is also found in Paper V. In the protonated species, the two hydrogens above and below the plane of the benzene ring give rise to a π -orbital structure that can conjugate with the π -orbitals on the substituent. As a result, one can expect that the enthalpies of protonation will correlate with $\sigma+$, since $\sigma+$ is defined for electrophilic-substituent reactions. This is indeed the case, as has been shown by McKelvey *et al.*⁷² and is also shown in Paper V.

5.4 Molecular reference spectra for adsorption studies

Several studies have been published recently on the reactions of unsaturated organic compounds with Group IV semiconductor surfaces, like Si and Ge.⁷³⁻⁷⁹ Attachment of organic molecules to these surfaces makes it possible to design new materials for use in Si-based device technology, for instance in microelectronics, optical materials and biosensors. X-ray photoelectron spectroscopy is a widely used tool to characterize the adsorbed state. However, the instrumental broadening in surface XPS is large, especially when conventional X-ray sources are used. This imposes a limiting factor on assignment of the inequivalent carbon atoms in the spectra. In particular, assigning saturated and unsaturated carbons seems to be problematic. In this section, some examples of adsorbed-state photoelectron spectra found in the literature will be studied, in particular with respect to assignment of singly- and doubly-bonded carbons. Parts of these results are published in Paper IV.

In gas-phase XPS, it is well known that unsaturated carbons in general have lower C1s ionization energies than do saturated ones in the same molecule.⁸⁰⁻⁸³ High-level *ab initio* calculations support this view. The reason for this can be attributed to the effect of resonance or hyperconjugation, which transfers negative charge from one carbon to another. Propene serves as a good illustration:



1c is the most important resonance form, and in this case electrons are transferred from the methyl group to the terminal CH_2 group, leading to a lower C1s ionization energy for this carbon.

However, in the literature, unsaturated carbons in photoelectron spectra of

adsorbed states are often placed at higher ionization energies than saturated ones in the same molecule. This is found for cyclopentene,^{84–86} cyclohexene,⁸⁷ 1,3-cyclohexadiene,⁸⁷ 1,4-cyclohexadiene,⁸⁷ 1,5-cyclooctadiene,⁸⁴ acetylene,⁸⁸ phenylacetylene⁸⁹ and 3-pyrroline.⁸⁵ In order to investigate this matter, we compared our gas phase ionization energies for cyclohexene, 1,3-cyclohexadiene, and 1,4-cyclohexadiene to those obtained by Tao *et al.*⁸⁷ for the same molecules physisorbed on Si(111)-7×7. Our assignment consistently places the unsaturated carbon atoms at lower ionization energy than the saturated carbons, whereas the opposite is found for the physisorbed molecules. Considering the high experimental resolution and the detailed analysis of the vibrational structure now available for gas-phase XPS, erroneous assignment of the gas-phase spectra does not seem likely. In addition, one would expect the gas-phase and physisorbed-state spectra to be similar, since a physisorbed molecule retains its identity upon adsorption. Although the molecule might be distorted in the presence of the surface, the enthalpy change involved in physisorption is not sufficient to lead to bond breaking. To investigate this discrepancy more closely, we digitized the experimental photoelectron spectra obtained by Tao *et al.* The digitized spectra were fitted with lineshapes based on the vibrational profiles and intramolecular chemical shifts as obtained for each molecule in the gas phase. The instrumental broadening parameter was optimized to approximately 1.4 eV for all three molecules, as compared to 1.2 eV in the original adsorbed-state spectra. The overall profiles were in good agreement with the experimental spectra for all the three physisorbed species. A typical example of the fits produced is shown in Figure 5.9. By comparing our fit in Figure 5.9 to the original fit in Figure 6c in ref. 87, shown as an inset in Figure 5.9, it appears that our fit is of equal or better quality, particularly at the peak maximum and at the high-energy slope. While the large instrumental broadening in this case makes it difficult to draw firm conclusions, it appears that the recorded adsorbed-state spectrum is consistent with the ionization-energy differences between saturated and unsaturated carbon atoms as observed for this molecule in the gas phase. The assignment of Tao *et al.* may therefore be incorrect.

It seems that the authors base their assignment of singly- and multiply-bonded carbons in XPS on publications in which C1s ionization energies of alkanes and alkenes are compared (refs. 90–93). In general, it is correct that alkenes have slightly higher ionization energies than alkanes. However, the relationship between alkanes and alkenes regarding which ones have the higher binding energies, is not to be confused with relative binding energies of saturated and unsaturated carbon atoms within the same molecule. As discussed above, resonance plays an important part in determining the relative binding energies within a molecule.

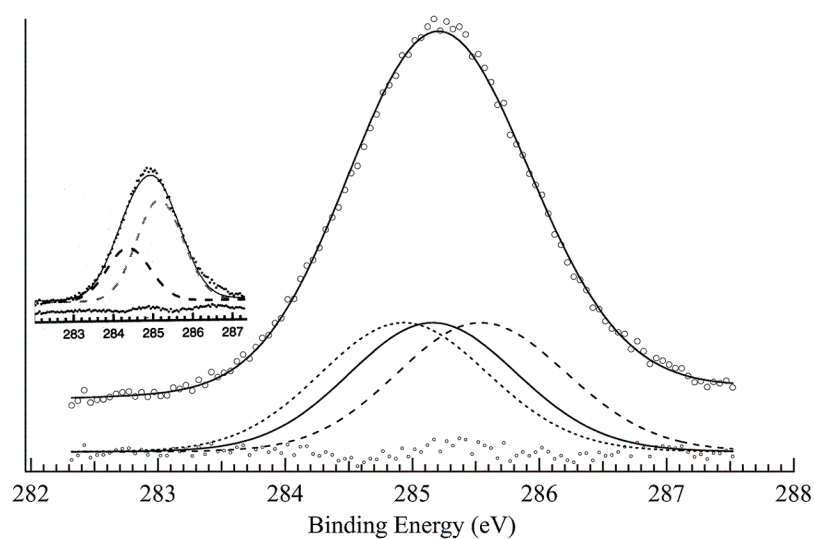


Figure 5.9: Experimental (circles) and fitted (solid line) C1s photoelectron spectrum of physisorbed 1,3-cyclohexadiene. The figure as a whole is reprinted from Paper IV. The experimental spectrum was obtained by digitizing Figure 6c in ref. 87. The fit was prepared on the basis of site-specific lineshapes (C1 and C4: dotted line, C2 and C3: solid line, C5 and C6: dashed line) as obtained in this work for the molecule in the gas phase. Inset: The original fit from Figure 6c in Tao *et al.*⁸⁷ (reprinted with permission).

Another example from the literature is a publication by Liu and Hamers.⁸⁵ The C1s photoelectron spectra of cyclopentene and 3-pyrroline chemisorbed on Si (001) were analyzed with a simple fitting procedure, in which mixed Gaussian-Lorentzian shaped peaks were used in an unrestricted curve fitting. These authors presumably base their assignment of peaks on the same assumptions as Tao *et al.*,⁸⁷ namely that unsaturated carbons have higher ionization energies than saturated ones in the same molecule. They found evidence of three peaks in both spectra: one for carbon atoms (sp^3) bonded directly to Si, one for the remaining carbons (sp^3) in the adsorbed molecule, shifted towards higher ionization energy, and finally a smaller peak at even higher ionization energy. The latter peak was attributed to alkene-like carbon atoms of a physisorbed layer. According to our experience from gas phase XPS, it is unlikely that this third peak at high ionization energy is purely from alkene-like carbons in a physisorbed layer. An origin from alkane-like carbons is more likely. Possibly there are more than three peaks in the spectra, not detected by the fitting routine. This misinterpretation of the third, smaller peak leads to the erroneous conclusion: "We observe a reproducible binding energy difference of 0.6–0.9 eV between alkane-like and alkene-like C atoms." From gas-phase XPS, the shift between singly- and doubly-bonded carbons in this type of molecule is typically of the order 0.5 eV,⁸² but with the singly-bonded carbons at the higher ionization energy. In the same publication, photoelectron spectra of adsorbed ethene and ethyne are also analyzed. The authors find, however, that the difference in C1s binding energies between ethene and ethyne is much smaller than their predicted energy shift of 0.6–0.9 eV between alkane-like and alkene-like C atoms. This finding supports our belief that the above-mentioned conclusion concerning binding-energy shifts between singly- and doubly-bonded carbons may not be correct.

These results show that rigorous analyses of gas-phase XPS measurements may be of considerable use in the analysis of photoelectron spectra of molecules adsorbed to surfaces.

Chapter 6

Conclusions

The chemistry of carbon is of special interest because of the important chemistry associated with organic molecules. The main aim of this thesis was to obtain accurate carbon 1s ionization energies for several molecules in the gas phase. Core-ionization energies correlate with various other chemical properties. A detailed study of 1s ionization energies may therefore elucidate the factors influencing related chemical processes. In the present work, carbon 1s photoelectron spectra were measured with high-resolution synchrotron radiation and state-of-the-art electron spectrometers. Advanced theoretical methods were used to prepare lineshape models for each inequivalent carbon in the molecules. The theoretical profiles were convoluted with functions to represent the instrumental and lifetime broadening and fit to the experimental data. By including calibration, highly accurate ionization energies were determined for each atom in various hydrocarbons.

Despite the high resolution of synchrotron radiation, the accuracy with which the photon energy is known is not high. Thus, for accurate measurements of ionization energies, it is necessary to include an internal standard for which the ionization energy is well known. To this end, the carbon 1s spectra of nine small molecules were measured with high accuracy. The C1s ionization energies for these molecules span most of the range of known C1s energies and provide a convenient set of potential calibration standards for future measurements.

In addition to precise knowledge about the photon energy, it is necessary to calibrate the electron spectrometer in order to obtain accurate ionization energies. A useful standard for this purpose is the xenon $N_{4,5}OO$ Auger spectrum, in combination with the 4d photoelectron spectrum. These spectra were measured with high resolution, and the Auger kinetic energies were compared with highly accurate data from optical measurements. From this, one can get information on the linearity and accuracy of the voltage supplies in the spectrometer. The xenon $N_{4,5}OO$ Auger energies given in Paper II should provide

a convenient set of calibration points for electron spectrometers at a level of accuracy that is higher than what has been available in the literature before. The quality of the two electron spectrometers used in this work, one at the ALS and one at MAX II, was assessed by this calibration procedure. Overall, the quality was found to be highly satisfactory. The results indicated no significant non-linearity and an accuracy of a few parts in 10^4 in the nominal voltages of the spectrometers.

With the resolution available with today's instrumentation, C1s spectra may reveal a complicated fine structure. In order to assign the spectra and determine ionization energies, one needs a detailed understanding of the different components of the spectra. To this end, a thorough investigation of the vibrational structure and effects of vibronic coupling in the C1s spectrum of benzene was performed. A relatively simple procedure for modeling the effects of vibronic coupling was developed, and this procedure is expected to work well also for other, more complex hydrocarbons. Due to the high resolution available, one was able, for the first time, to observe a splitting of the most prominent peak in the C1s spectrum of benzene. This splitting is due to excitation of a C*-C stretching and an in-plane C*-C-H and C-C-H bending mode.

C1s photoelectron spectra were measured for the six-membered cyclic hydrocarbons; cyclohexane, cyclohexene, 1,3-cyclohexadiene, and 1,4-cyclohexadiene. These, together with benzene, show the evolution of chemical effects with increasing number of double bonds. The experimental spectra were fit with theoretical lineshape models for each inequivalent carbon, and the various features of the spectra were unambiguously assigned to the appropriate carbon atoms in the molecules. Both adiabatic and vertical ionization energies were obtained. From these results, together with earlier studies of hydrocarbons, it is believed that the vibronic structure arising from core-ionization of hydrocarbons is well understood. This level of understanding provides an important framework for interpretation of other, more complex, spectra in which other features of chemical interest might be present. Without this framework, it would be impossible to decide whether an unexpected feature of a spectrum reflects an unexpected phenomenon or simply a lack of understanding of the vibronic excitation.

The unsaturated cyclic hydrocarbons are interesting from the perspective of functionalizing semiconducting surfaces, like silicon, by molecular attachment. It was shown in this work that high-resolution gas-phase spectra may be of considerable use in the assignment of photoelectron spectra of physisorbed molecules. As such, gas-phase XPS studies might contribute in the development of new materials for use in Si-based device technology, for instance in microelectronics.

By means of photoelectron spectroscopy and theoretical computations, a comprehensive study of the substituent effect of the methyl group on benzene rings was performed. The molecules considered were toluene, o-xylene, m-xylene, p-xylene, mesitylene, and 1,2,4,5-tetramethylbenzene. For the methyl benzenes, the shifts in ionization energies were found to correlate linearly with other chemical properties like proton affinity and relative activation energies for electrophilic substitution reactions. Deviations from these correlations provide information on the effects of conjugation for the methyl substituent. It is shown that the substituent effects of the methyl group on benzene can be described by a simple additivity relationship.

Chapter 7

Suggestions for further work

Inner-shell ionization energies may depend on both the charge distribution in the neutral state and the charge rearrangement that accompanies ionization. Quantitatively, one can write:

$$\Delta I = \Delta V - \Delta R$$

where ΔI is the ionization energy relative to some reference. V is the potential energy of a unit positive charge at the site of interest, and it depends on the charge distribution in the neutral molecule. R represents the effect of relaxation of the other charges, and depends on the ability of the ion to delocalize the added charge. Analyzing shifts in ionization energies by this relation has been done for a number of molecules.^{39,80,83} Values of ΔV can be estimated from the extended Koopmans' theorem developed by Børve and Thomas.⁹⁴ ΔI can be set equal to the experimental shifts, and from this, ΔR may be determined. The values of ΔV and ΔR may provide insight into the relative importance of initial- and final-state effects on core-ionization energies and also on other, related chemical properties. Such an analysis would be of interest for the six-membered cyclic hydrocarbons, as well as for the methyl-substituted benzenes. In particular, it might provide an explanation for the relatively large shift in ionization energy between the two doubly-bonded carbons in 1,3-cyclohexadiene. Since V is estimated by theoretical computations, one can also assess how the value of ΔV varies as calculated with different methods, basis sets, and different methods for geometry optimization. Preliminary investigations indicate that the value of ΔV is somewhat dependent on the specifications in the calculation.

In this work, proton affinities have been calculated by the method proposed by Maksić *et al.*⁴² This method has the capability of predicting proton affinities for aromatic molecules that are in good accordance with experimental evidence,

at relatively low computational costs. A more advanced method for calculation of proton affinities is Gaussian-3 (G3) theory, which provides molecular energies with a higher level of accuracy but at a higher computational cost. It would be useful to compare proton affinities from G3 theory with those from the method of Maksić *et al.*, to assess the quality of the latter, more simple approach. Theoretical proton affinities may also be compared with experimental values where available. Deviations between experimental and theoretical values might indicate rearrangement upon protonation. A preliminary study of proton affinities for the six-membered cyclic hydrocarbons show a large deviation between theoretical and experimental proton affinities for 1,3- and 1,4-cyclohexadiene. For these molecules, one might expect resonance effects to play an important part, as well as rearrangement upon protonation.

In order to corroborate assignment of adsorbed-state C1s photoelectron spectra, one may perform a more thorough analysis than what was done in this thesis. A good approach would be XPS measurements of the adsorbed species with synchrotron radiation and high-resolution electron spectrometers, thereby achieving a higher resolution than what is often reported in the literature for surface XPS. The physisorbed layer can be directly modeled by gas-phase photoelectron spectra, broadened according to the appropriate experimental resolution. However, the binding energies of the carbons in the chemisorbed layer may be different from the binding energies of the gas-phase molecules, due to chemical bonding to the surface. In ref. 95, a simple, theoretical model for simulating chemisorption by a gas-phase molecule, was used. It provided estimates of relative ionization energies of the different carbons in the chemisorbed species. This model may also be applied to the six-membered cyclic hydrocarbons.

Bibliography

- [1] H. D. Young and R. Freedman, *University Physics*, Addison-Wesley Publishing Company, Inc., USA, ninth ed., 1996.
- [2] A. Einstein, *Ann. Physik*, 1905, **17**, 132.
- [3] T. A. Carlson, *Photoelectron and Auger spectroscopy*, Plenum Press, New York, NY, 1975.
- [4] <http://www.maxlab.lu.se/> (2007).
- [5] <http://www.als.lbl.gov/> (2007).
- [6] M. Bässler, J.-O. Forsell, O. Björneholm, R. Feifel, M. Jurvansuu, S. Aksela, S. Sundin, S. L. Sorensen, R. Nyholm, A. Ausmees, and S. Svensson, *J. Electron Spectrosc. Relat. Phenom.*, 1999, **101–103**, 953.
- [7] M. Bässler, A. Ausmees, M. Jurvansuu, R. Feifel, J.-O. Forsell, P. de Tarso Fonseca, A. Kivimäki, S. Sundin, S. L. Sorensen, R. Nyholm, O. Björneholm, S. Aksela, and S. Svensson, *Nucl. Instr. and Meth. A*, 2001, **469**, 382.
- [8] N. Berrah, B. Langer, A. A. Wills, E. Kukk, J. D. Bozek, A. Farhat, and T. W. Gorczyca, *J. Electron Spectrosc. Relat. Phenom.*, 1999, **101–103**, 1.
- [9] M. G. Zahl, *Activation energies, proton affinities, and core ionization energies for chlorosubstituted ethenes*. Master's thesis, University of Bergen, 2006.
- [10] S. Aksela, A. Kivimäki, A. N. de Brito, O.-P. Sairanen, S. Svensson, and J. Väyrynen, *Rev. Sci. Instrum.*, 1994, **65**, 831.
- [11] S. Aksela, A. Kivimäki, O.-P. Sairanen, A. N. de Brito, E. Nömmiste, and S. Svensson, *Rev. Sci. Instrum.*, 1995, **66**, 1621.
- [12] L. J. Sæthre, O. Sværen, S. Svensson, S. Osborne, T. D. Thomas, J. Jauhinainen, and S. Aksela, *Phys. Rev. A*, 1997, **55**, 2748.

- [13] J. Jauhiainen, A. Ausmees, A. Kivimäki, S. J. Osborne, A. N. de Brito, S. Aksela, S. Svensson, and H. Aksela, *J. Electron Spectrosc. Relat. Phenom.*, 1994, **69**, 181.
- [14] N. Mårtensson, P. Baltzer, P. A. Brühwiler, J.-O. Forsell, A. Nilsson, A. Stenborg, and B. Wannberg, *J. Electron Spectrosc. Relat. Phenom.*, 1994, **70**, 117.
- [15] S. Svensson, J.-O. Forsell, H. Siegbahn, A. Ausmees, G. Bray, S. Södergren, S. Sundin, S. J. Osborne, S. Aksela, E. Nömmiste, J. Jauhiainen, M. Jurvan-suu, J. Karvonen, P. Barta, W. R. Salaneck, A. Evaldsson, M. Lögdlund, and A. Fahlman, *Rev. Sci. Instrum.*, 1996, **67**, 2149.
- [16] W. J. Hehre, L. Radom, P. v.R. Schleyer, and J. A. Pople, *Ab initio molecular orbital theory*, John Wiley & Sons, Inc., New York, NY, 1986.
- [17] W. Koch and M. C. Holthausen, *A chemist's guide to Density Functional Theory*, Wiley-VCH, Weinheim, Germany, 2002.
- [18] J. B. Foresman and Æ. Frisch, *Exploring Chemistry with Electronic Structure Methods*, Gaussian, Inc., Pittsburgh, PA, second ed., 1996.
- [19] C. Møller and M. S. Plesset, *Phys. Rev.*, 1934, **46**, 618.
- [20] T. Karlsten and K. J. Børve, *J. Chem. Phys.*, 2000, **112**, 7979.
- [21] C. J. Cramer, *Essentials of Computational Chemistry. Theories and Models*, John Wiley & Sons Ltd, West Sussex, England, second ed., 2004.
- [22] C. Lee, W. Yang, and R. G. Parr, *Phys. Rev. B*, 1988, **37**, 785.
- [23] P. J. Stephens, F. J. Devlin, C. F. Chabalowski, and M. J. Frisch, *J. Phys. Chem.*, 1994, **98**, 11623.
- [24] A. D. Becke, *J. Chem. Phys.*, 1993, **98**, 5648.
- [25] H. Ågren and H. J. A. Jensen, *Chem. Phys. Lett.*, 1987, **137**, 431.
- [26] H. Ågren and H. J. A. Jensen, *Chem. Phys.*, 1993, **172**, 45.
- [27] D. Nordfors, N. Mårtensson, and H. Ågren, *Phys. Rev. B*, 1988, **38**, 12922.
- [28] T. D. Thomas, L. J. Sæthre, S. Sørensen, and S. Svensson, *J. Chem. Phys.*, 1998, **109**, 1041.

- [29] Gaussian 98, Revision A.9. M. J. Frisch, G. W. Trucks, H. B. Schlegel, G. E. Scuseria, M. A. Robb, J. R. Cheeseman, V. G. Zakrzewski, J. A. Montgomery, Jr., R. E. Stratmann, J. C. Burant, S. Dapprich, J. M. Millam, A. D. Daniels, K. N. Kudin, M. C. Strain, O. Farkas, J. Tomasi, V. Barone, M. Cossi, R. Cammi, B. Mennucci, C. Pomelli, C. Adamo, S. Clifford, J. Ochterski, G. A. Petersson, P. Y. Ayala, Q. Cui, K. Morokuma, D. K. Malick, A. D. Rabuck, K. Raghavachari, J. B. Foresman, J. Cioslowski, J. V. Ortiz, A. G. Baboul, B. B. Stefanov, G. Liu, A. Liashenko, P. Piskorz, I. Komaromi, R. Gomperts, R. L. Martin, D. J. Fox, T. Keith, M. A. Al-Laham, C. Y. Peng, A. Nanayakkara, M. Challacombe, P. M. W. Gill, B. Johnson, W. Chen, M. W. Wong, J. L. Andres, C. Gonzalez, M. Head-Gordon, E. S. Replogle, and J. A. Pople; Gaussian, Inc., Pittsburgh, PA, 1998.
- [30] Gaussian 03, Revision C.02. M. J. Frisch, G. W. Trucks, H. B. Schlegel, G. E. Scuseria, M. A. Robb, J. R. Cheeseman, J. A. Montgomery, Jr., T. Vreven, K. N. Kudin, J. C. Burant, J. M. Millam, S. S. Iyengar, J. Tomasi, V. Barone, B. Mennucci, M. Cossi, G. Scalmani, N. Rega, G. A. Petersson, H. Nakatsuji, M. Hada, M. Ehara, K. Toyota, R. Fukuda, J. Hasegawa, M. Ishida, T. Nakajima, Y. Honda, O. Kitao, H. Nakai, M. Klene, X. Li, J. E. Knox, H. P. Hratchian, J. B. Cross, V. Bakken, C. Adamo, J. Jaramillo, R. Gomperts, R. E. Stratmann, O. Yazyev, A. J. Austin, R. Cammi, C. Pomelli, J. W. Ochterski, P. Y. Ayala, K. Morokuma, G. A. Voth, P. Salvador, J. J. Dannenberg, V. G. Zakrzewski, S. Dapprich, A. D. Daniels, M. C. Strain, O. Farkas, D. K. Malick, A. D. Rabuck, K. Raghavachari, J. B. Foresman, J. V. Ortiz, Q. Cui, A. G. Baboul, S. Clifford, J. Cioslowski, B. B. Stefanov, G. Liu, A. Liashenko, P. Piskorz, I. Komaromi, R. L. Martin, D. J. Fox, T. Keith, M. A. Al-Laham, C. Y. Peng, A. Nanayakkara, M. Challacombe, P. M. W. Gill, B. Johnson, W. Chen, M. W. Wong, C. Gonzalez, and J. A. Pople; Gaussian, Inc., Wallingford, CT, 2004.
- [31] g2fc. K. J. Børve; University of Bergen, 2000.
- [32] P.-Å. Malmqvist and N. Forsberg, *Chem. Phys.*, 1998, **228**, 227.
- [33] U. Gelius, E. Basilier, S. Svensson, T. Bergmark, and K. Siegbahn, *J. Electron Spectrosc. Relat. Phenom.*, 1974, **2**, 405.
- [34] T. X. Carroll, N. Berrah, J. Bozek, J. Hahne, E. Kukk, L. J. Sæthre, and T. D. Thomas, *Phys. Rev. A*, 1999, **59**, 3386.
- [35] T. Karlsen and K. J. Børve, *J. Chem. Phys.*, 2000, **112**, 7986–7991.

- [36] E. Kukk, K. Ueda, U. Hergenbahn, X.-J. Liu, G. Prumper, H. Yoshida, Y. Tamenori, C. Makochekeanwa, T. Tanaka, M. Kitajima, and H. Tanaka, *Phys. Rev. Lett.*, 2005, **95**, 133001.
- [37] K. J. Børve, L. J. Sæthre, T. D. Thomas, T. X. Carroll, N. Berrah, J. D. Bozek, and E. Kukk, *Phys. Rev. A*, 2000, **63**, 012506.
- [38] L. J. Sæthre, M. R. F. Siggel, and T. D. Thomas, *J. Electron Spectrosc. Relat. Phenom.*, 1989, **49**, 119.
- [39] L. J. Sæthre and T. D. Thomas, *J. Org. Chem.*, 1991, **56**, 3935.
- [40] R. Situmeang and T. D. Thomas, *J. Electron Spectrosc. Relat. Phenom.*, 1999, **98–99**, 105.
- [41] M. Eckert-Maksić, M. Klessinger, and Z. B. Maksić, *J. Phys. Org. Chem.*, 1995, **8**, 435.
- [42] Z. B. Maksić, B. Kovačević, and D. Kovaček, *J. Phys. Chem. A*, 1997, **101**, 7446.
- [43] T. H. Dunning, Jr., *J. Chem. Phys.*, 1971, **55**, 716.
- [44] R. Krishnan, J. S. Binkley, R. Seeger, and J. A. Pople, *J. Chem. Phys.*, 1980, **72**, 650.
- [45] T. Karlsen, K. J. Børve, L. J. Sæthre, K. Wiesner, M. Bäessler, and S. Svensson, *J. Am. Chem. Soc.*, 2002, **124**, 7866.
- [46] W. J. Stevens, H. Basch, and M. Krauss, *J. Chem. Phys.*, 1984, **81**, 6026.
- [47] T. Karlsen, L. J. Sæthre, K. J. Børve, N. Berrah, E. Kukk, J. D. Bozek, T. X. Carroll, and T. D. Thomas, *J. Phys. Chem. A*, 2001, **105**, 7700.
- [48] T. X. Carroll, J. D. Bozek, E. Kukk, V. Myrseth, L. J. Sæthre, and T. D. Thomas, *J. Electron Spectrosc. Relat. Phenom.*, 2001, **120**, 67.
- [49] P. van der Straten, R. Morgenstern, and A. Niehaus, *Z. Phys. D*, 1988, **8**, 35.
- [50] T. X. Carroll, J. A. Hahne, T. D. Thomas, L. J. Sæthre, N. Berrah, J. D. Bozek, and E. Kukk, *Phys. Rev. A*, 2000, **61**, 042503.
- [51] T. X. Carroll, K. J. Børve, L. J. Sæthre, J. D. Bozek, E. Kukk, J. A. Hahne, and T. D. Thomas, *J. Chem. Phys.*, 2002, **116**, 10221.

- [52] Spancf - <http://www.geocities.com/ekukk>. E. Kukk; Department of Physics, Materials Science, University of Turku, FIN-20014 Turku, Finland.
- [53] Igor pro 5.04; Wavemetrics, Inc., Lake Oswego, OR, 2005.
- [54] L. O. Werme, T. Bergmark, and K. Siegbahn, *Phys. Scripta*, 1972, **6**, 141.
- [55] S. Southworth, U. Becker, C. M. Truesdale, P. H. Kobrin, D. W. Lindle, S. Owaki, and D. A. Shirley, *Phys. Rev. A*, 1983, **28**, 261.
- [56] H. Aksela, S. Aksela, and H. Pulkkinen, *Phys. Rev. A*, 1984, **30**, 865.
- [57] G. Johansson, J. Hedman, A. Berndtsson, M. Klasson, and R. Nilsson, *J. Electron Spectrosc. Relat. Phenom.*, 1973, **2**, 295.
- [58] J. Nordgren, H. Ågren, C. Nordling, and K. Siegbahn, *Phys. Scripta*, 1979, **19**, 5.
- [59] K. J. Børve, unpublished material.
- [60] V. Myrseth, K. J. Børve, K. Wiesner, M. Bässler, S. Svensson, and L. J. Sæthre, *Phys. Chem. Chem. Phys.*, 2002, **4**, 5937.
- [61] F. E. Condon, *J. Am. Chem. Soc.*, 1948, **70**, 1963.
- [62] H. C. Brown and Y. Okamoto, *J. Am. Chem. Soc.*, 1958, **80**, 4979.
- [63] C. Eaborn and R. Taylor, *J. Chem. Soc.*, 1961, p. 247.
- [64] B. Lindberg, S. Svensson, P. Å. Malmquist, E. Basilier, U. Gelius, and K. Siegbahn, *Chem. Phys. Lett.*, 1976, **40**, 175.
- [65] K. E. Richards, A. L. Wilkinson, and G. J. Wright, *Austr. J. Chem.*, 1972, **25**, 2369.
- [66] C. Eaborn and R. C. Moore, *J. Chem. Soc.*, 1959, p. 3640.
- [67] R. L. Martin and D. A. Shirley, *J. Am. Chem. Soc.*, 1974, **96**, 5299.
- [68] D. Nordfors, N. Mårtensson, and H. Ågren, *J. Electron Spectrosc. Relat. Phenom.*, 1990, **53**, 129.
- [69] R. S. Brown and A. Tse, *J. Am. Chem. Soc.*, 1980, **102**, 5222.
- [70] T. X. Carroll, T. D. Thomas, H. Bergersen, K. J. Børve, and L. J. Sæthre, *J. Org. Chem.*, 2006, **71**, 1961.

- [71] L. P. Hammet, *J. Am. Chem. Soc.*, 1937, **59**, 96.
- [72] J. M. McKelvey, S. Alexandratos, J. Andrew Streiwieser, J.-L. M. Abboud, and W. J. Hehre, *J. Am. Chem. Soc.*, 1976, **98**, 244.
- [73] J. L. Armstrong and J. M. White, *J. Vac. Sci. Technol. B*, 1997, **15**, 1146.
- [74] R. Konečný and D. J. Doren, *Surf. Sci.*, 1998, **417**, 169.
- [75] F. Jolly, F. Bournel, F. Rochet, G. Dufour, F. Sirotti, and A. Taleb, *Phys. Rev. B*, 1999, **60**, 2930.
- [76] S. Letarte, A. Adnot, and D. Roy, *Surf. Sci.*, 2000, **448**, 212.
- [77] J. Eng, Jr., I. A. Hubner, J. Barriocanal, R. L. Opila, and D. J. Doren, *J. Appl. Phys.*, 2004, **95**, 1963.
- [78] M. P. Casaletto, M. Carbone, M. N. Piancastelli, K. Horn, K. Weiss, and R. Zanoni, *Surf. Sci.*, 2005, **582**, 42.
- [79] R. Gunella, M. Shimomura, F. D'Amico, T. Abukawa, and S. Kono, *Phys. Rev. B*, 2006, **73**, 235435.
- [80] L. J. Sæthre, T. D. Thomas, and S. Svensson, *J. Chem. Soc., Perkin Trans. 2*, 1997, p. 749.
- [81] L. J. Sæthre, N. Berrah, J. D. Bozek, T. X. Carroll, E. Kukk, G. L. Gard, R. Winter, and T. D. Thomas, *J. Am. Chem. Soc.*, 2001, **123**, 10729.
- [82] V. M. Oltedal, K. J. Børve, L. J. Sæthre, T. D. Thomas, J. D. Bozek, and E. Kukk, *Phys. Chem. Chem. Phys.*, 2004, **6**, 4254.
- [83] T. D. Thomas, L. J. Sæthre, K. J. Børve, M. Gundersen, and E. Kukk, *J. Phys. Chem. A*, 2005, **109**, 5085.
- [84] J. S. Hovis and R. J. Hamers, *J. Phys. Chem. B*, 1997, **101**, 9581.
- [85] H. Liu and R. J. Hamers, *Surf. Sci.*, 1998, **416**, 354.
- [86] S. W. Lee, J. Hovis, S. K. Coulter, R. J. Hamers, and C. M. Greenlief, *Surf. Sci.*, 2000, **462**, 6.
- [87] F. Tao, Z. H. Wang, and G. Q. Xu, *Surf. Sci.*, 2003, **530**, 203.
- [88] H. G. Huang, Y. H. Cai, J. Y. Huang, H. H. Tang, and G. Q. Xu, *Langmuir*, 2005, **21**, 3384.

-
- [89] F. Tao, M. H. Qiao, Z. H. Li, L. Yang, Y. J. Dai, H. G. Huang, and G. Q. Xu, *Phys. Rev. B*, 2003, **67**, 115334.
- [90] W. E. Palke and W. N. Lipscomb, *J. Am. Chem. Soc.*, 1966, **88**, 2384.
- [91] R. J. Beunker, S. D. Peyerimhoff, and J. L. Whitten, *J. Chem. Phys.*, 1976, **46**, 2029.
- [92] H. Basch and L. Snyder, *Chem. Phys. Lett.*, 1969, **3**, 333.
- [93] T. D. Thomas, *J. Chem. Phys.*, 1970, **52**, 1373.
- [94] K. J. Børve and T. D. Thomas, *J. Electron Spectrosc. Relat. Phenom.*, 2000, **107**, 155.
- [95] T. H. Andersen, M. G. Zahl, I.-H. Svenum, K. J. Børve, A. Borg, and L. J. Sæthre, *Adsorption of 1,1-dichloroethene on the Si(111)-7×7 surface*, submitted to *Surf. Sci.*, 2007.

Paper I



ELSEVIER

Journal of Electron Spectroscopy and Related Phenomena 122 (2002) 57–63

JOURNAL OF
ELECTRON SPECTROSCOPY
and Related Phenomena

www.elsevier.com/locate/elspec

Adiabatic and vertical carbon 1s ionization energies in representative small molecules

V. Myrseth^a, J.D. Bozek^b, E. Kukk^c, L.J. Sæthre^a, T.D. Thomas^{d,*}

^aDepartment of Chemistry, University of Bergen, N-5007 Bergen, Norway

^bAdvanced Light Source, Lawrence Berkeley National Laboratory, University of California, Berkeley, CA 94720, USA

^cDepartment of Physics, University of Oulu, FIN-90570 Oulu, Finland

^dDepartment of Chemistry, Oregon State University, Corvallis, OR 97331-4003, USA

Received 9 May 2001; accepted 5 July 2001

Abstract

Adiabatic and vertical carbon 1s ionization energies are reported for methane (CH₄), ethane (CH₃CH₃), ethene (CH₂CH₂), ethyne (HCCH), carbon monoxide (CO), carbon dioxide (CO₂), fluoromethane (CH₃F), trifluoromethane (CHF₃), and tetrafluoromethane (CF₄) with an absolute accuracy of about 0.03 eV. The results are in good agreement with earlier values but are measured with higher resolution and accuracy than has previously been available. © 2002 Elsevier Science B.V. All rights reserved.

Keywords: Carbon 1s core-ionization energies

1. Introduction

For over 30 years, core-ionization energies have been the subject of many experimental and theoretical investigations. The reason for this interest is that these ionization energies relate directly to properties of fundamental chemical significance such as the charge distribution in a molecule, the electron withdrawing power of substituents, and the ability of a molecule to accept or supply charge at a particular site. Of particular interest have been carbon 1s

ionization energies because of the rich and important chemistry of carbon-containing compounds.

A requirement for such measurements to be useful is that they be accurate, and in the early days of electron spectroscopy techniques were developed to provide accurate measurements. At the most basic level these involved use of characteristic X-rays whose energies were accurately known together with neon or argon as calibration gases to establish the kinetic energy scale of the analyzer [1–4]. Other approaches have measured the shift in electron kinetic energy relative to a calibrant for which the absolute ionization energy is known [5,6]. The accuracy that can be obtained is better than 0.05 eV, and measurements made at different laboratories usually agree well within this uncertainty. The limitation of using characteristic X-rays is, however,

*Corresponding author. Tel.: +1-541-737-6711; fax: +1-541-737-2062.

E-mail address: thomast@chem.orst.edu (T.D. Thomas).

the resolution, and for a molecule the measurement represents an average over the vibrational profile, or, in other terms, the vertical ionization energy.

The availability of high-brightness, high-resolution sources at third-generation synchrotrons has made it possible to resolve, at least partially, the vibrational structure for a number of small molecules. Thus, it is now possible to determine not only the vertical but also the adiabatic ionization energy. Moreover, the narrow lines and high intensity available with synchrotron radiation open the possibility of improving the absolute accuracy of the earlier measurements. With synchrotron radiation, however, the accuracy with which the photon energy is known is not high. For a given setting of the monochromator, the apparent photon energy may change from one day to the next by a large fraction of an electron volt. Also away from the photon-energy region for which the monochromator has been calibrated, the photon energy may be absolutely in error by an electron volt or more. Thus, for accurate measurements of ionization energies, it is necessary to include an internal standard for which the ionization energy is well known.

A useful standard for calibration of a carbon 1s photoelectron spectrum is the argon $2p_{3/2}$ line. Since argon is monatomic, there is no vibrational excitation and the vertical and adiabatic energies are identical. The ionization energy is known with an accuracy of about 0.02 eV; reported values range from 248.60 to 248.63 eV [1,2,7–11]. This is only 40–50 eV away from the range of carbon 1s ionization energies. We report here the results of measurements in which we have used this line to calibrate the carbon 1s photoelectron spectra for nine compounds: methane (CH_4), ethane (CH_3CH_3), ethene (CH_2CH_2), ethyne (HCCH), carbon monoxide (CO), carbon dioxide (CO_2), fluoromethane (CH_3F), trifluoromethane (CHF_3), and tetrafluoromethane (CF_4). The carbon 1s ionization energies for these molecules span most of the range of known carbon 1s energies, from about 291 to 302 eV. Since these spectra are, to one degree or another, vibrationally resolved, we have been able to determine both the adiabatic and vertical ionization energies. These energies are of interest in their own right for the chemical information that they provide and for comparison with theoretical calcula-

tions. In addition they provide potential calibration standards for future measurements.

2. Experimental procedures

The measurements were made using Beamline 10.0.1 of the Advanced Light Source of the Lawrence Berkeley National Laboratory at a photon energy of 330 eV. This beamline receives its radiation from an undulator (U10) with a 10-cm period. It is equipped with a spherical-grating monochromator that is capable of a resolving power of greater than 10^4 ; this was set to provide a resolution of 40 meV for the photoelectron measurements. Measurements of the photon absorption spectrum for the argon $2p_{3/2}$ to 4s transition and for the carbon monoxide carbon 1s to 2p transition indicated that the actual resolution of the photon beam was about 50 meV.

The electron spectra were measured with a Scienta SES-200 spectrometer [12]. This was set to have a pass energy of 40 eV, and the entrance slit of the analyzer was chosen to give an expected resolution of 40 meV. Measurements of the xenon 5s photoelectron spectrum indicated that the resolution of the analyzer under these conditions was actually about 60 meV. All measurements were made with the analyzer perpendicular to the beam direction and at an angle of 54.7° to the polarization direction.

Combining the contributions from the photon bandwidth, the spectrometer resolution, and the Doppler broadening gives an expected resolution for the carbon 1s spectra of 88 meV. Least-squares fits to the spectra (discussed below) with the resolution as one of the fitting parameters give results that are consistent with this.

The actual voltages applied to the Scienta analyzer were measured with a digital voltmeter and were found to differ slightly from the nominal voltages. Corrections of about 6 mV were made to the nominal voltages on the basis of these measurements.

The photoelectron spectra have been fit by least squares using a fitting function that includes the effects of post-collision interaction (PCI) and experimental resolution [13]. To represent the PCI effect, we have used Eq. (12) of van der Straten et al. [14], which is expected to be valid in the energy

region we have studied. This is convoluted with a Gaussian to represent the experimental resolution.

The experimental spectra and the fits for the nine molecules are shown in Fig. 1. In this figure, the circles represent the data and the solid lines indicate the least-squares fits. Specific features of the fits are discussed in the following paragraphs.

For the argon $2p_{3/2}$ spectrum there is only one peak, and the fitting is straightforward. For the molecules, however, there is vibrational structure, and each molecule presents unique challenges. For methane, carbon monoxide, and carbon dioxide, only one vibrational mode (CH or CO stretching) is excited. For the first two, the vibrational structure is sufficiently well resolved that the spectra can be fit with a progression with peak heights and positions all as free parameters. For carbon dioxide, which is

not well resolved, the energy spacing between the peaks has been fixed at 165.6 meV [15].

For ethane, two vibrational modes are excited, CH stretching and HCC bending [16–18], and the spectrum can be fit well with three peaks representing the $\nu=0, 1$ and 2 excitations of the CH stretching mode plus three more representing the $\nu=1$ bending mode in combination with each of the first three peaks. We have used two different fitting procedures for ethane. In one, all 12 parameters describing the positions and intensities are free. In the other, the positions and intensities of the (1,1) and (2,1) peaks relative to the (1,0) and (2,0) peaks are constrained to be the same as for the (0,1) peak relative to the (0,0) peak. The energies obtained from the two procedures are essentially the same. For ethene, the same set of six peaks contribute significantly to the spectrum

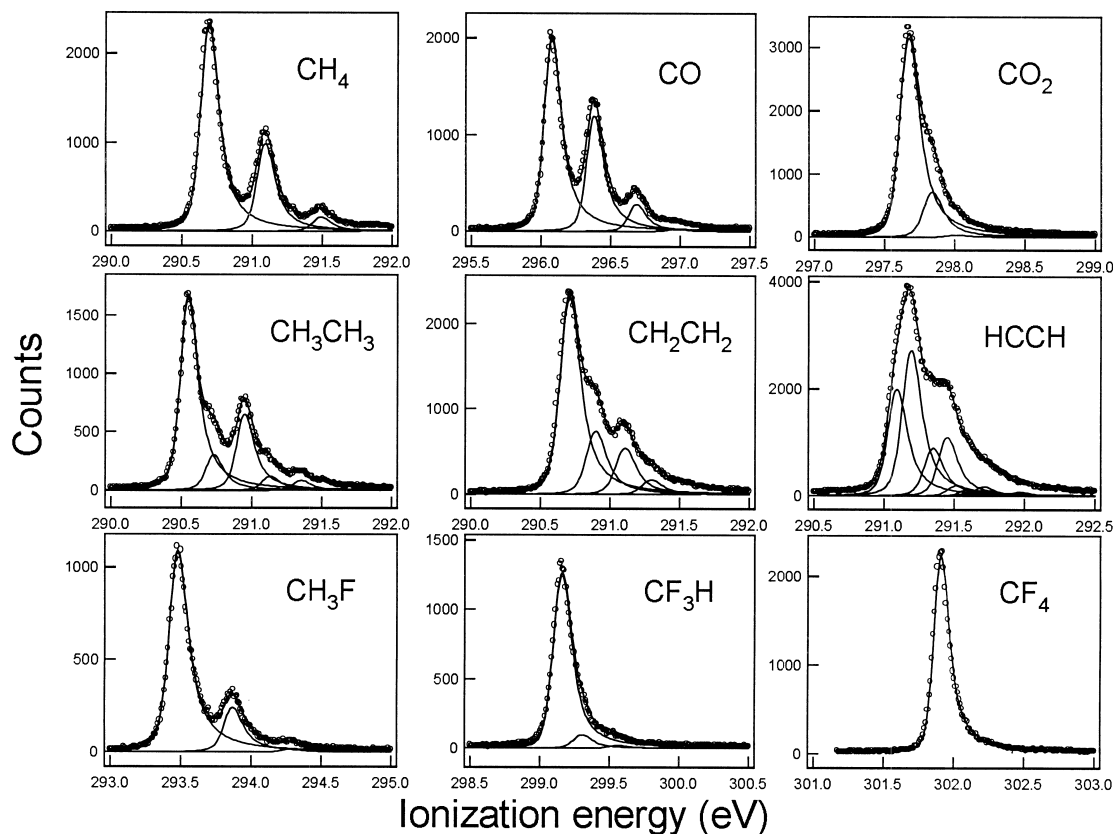


Fig. 1. Carbon 1s photoelectron spectra of the molecules studied here. The circles show the data and the lines show least-squares fits to the data.

[16,19], but in this case a completely free fit is not possible, and the peaks have been constrained in the same way as for ethane.

For ethyne, the spectrum is complicated by the significant splitting between the $^2\Sigma_g$ and $^2\Sigma_u$ states and by the prominence of CC stretching (which is almost absent in ethane and ethene). For this molecule, we have constrained the relative positions of the 11 peaks to be given by the values determined by a theoretical analysis of this spectrum [20]. The relative intensities of seven of the 11 peaks were also constrained in the same way. Comparison of the experimental spectrum with the theoretical prediction (which does not include the effect of anharmonicity) shows that too much intensity is predicted for the $\nu=2$ and 3 states of the CC stretching mode. As a result, an average vibrational energy (and, hence, the vertical ionization energy) that is based on the theoretical predictions is too high. To correct for this, we have allowed the total intensity for each of these two states to vary freely in the fit. Although this choice influences the vertical ionization energy derived from the fit, it has negligible effect on the adiabatic energy.

For tetrafluoromethane there is also only one vibrational mode expected to be excited, but the excitation is so weak that it is impossible to distinguish between vibrational excitation and a low-kinetic energy tail produced by PCI. For this molecule, we have made three fits, one assuming no vibrational excitation, one assuming that there is a $\nu=1$ peak shifted 100 meV from the main peak, but with intensity as a free parameter, and one assuming that there is a $\nu=1$ peak with free position and intensity. The effect of these different assumptions on the position of the adiabatic peak ($\nu=0$) is to shift it by only 3 meV, which is insignificant. The results of the fit assuming no vibrational excitation have been used. Trifluoromethane is, like tetrafluoromethane, somewhat ambiguous. The PCI tail obscures the weak vibrational structure, but there is some evidence for a contribution from the $\nu=1$ peak of the CH stretching mode. From the fits, the position of the adiabatic peak is almost independent of assumptions about the presence or absence of vibrational excitation. The data presented here are based on a fit in which the $\nu=1$ peak of the CH stretching mode is constrained to be displaced from

the $\nu=0$ peak by 400 meV (typical CH stretching frequency), but is unconstrained in intensity. In addition the fit allows for a weak CF stretching mode. Fluoromethane is fit with a single progression that corresponds to CH stretching.

The fitting procedure gives the nominal kinetic energy of the adiabatic peak in each molecular spectrum and of the $2p_{3/2}$ peak in the argon spectrum. These cannot be used directly to determine the ionization energies, however, since neither the absolute kinetic energy nor the absolute photon energy is known accurately. On the other hand, the difference between the kinetic energies is accurately known, and this can be combined with the known $2p_{3/2}$ ionization energy (taken to be 248.629 eV [8]). Thus, the carbon 1s ionization energy, I_C , is given by the expression:

$$I_C = 248.629 + \Delta_K + \Delta_R \quad (1)$$

where Δ_K is the difference in the measured kinetic energies (argon minus carbon) and Δ_R is the difference in the recoil energies imparted to the remaining ion. Values of the adiabatic carbon 1s ionization energies determined in this way are given in Table 1.

From the vibrational profiles that are obtained from the fits, we can also calculate the average ionization energy, which can be equated to the vertical ionization energy. These values are also given in Table 1.

3. Discussion

3.1. Comparison with other values

Previously reported values of the adiabatic ionization energies are based on X-ray photoelectron spectroscopy [21], X-ray spectroscopy [9], and electron-energy-loss spectroscopy [22]. The results of such measurements are compared in Table 1 with the results of our measurements. For four of the seven comparisons, the agreement between our results and those reported by others is within 0.02 eV. For ethene, our result agrees with that of Tronc et al. [22] nearly within the uncertainty of their measurement. For ethyne, the ionization energy is 291.179 eV for the $^2\Sigma_g$ ionic state and 291.128 eV for the average of

Table 1
Adiabatic and vertical carbon 1s ionization energies (eV) (uncertainties in the last digit are given in parentheses)

Molecule	I _C (adiabatic)			I _C (vertical)		
	This work	Other work	Ref.	This work	Other work	Ref.
Methane	290.689	290.707(3) 290.76(3)	[21] [22]	290.844	290.83(2) 290.91(5) ^a 290.85(3)	[24] [25] [33]
Ethane	290.545			290.714	290.71(2) 290.75(5) ^a 290.70(5)	[24] [25] [26]
Ethene	290.695	290.74(4)	[22]	290.823	290.70(5) ^b 290.82(5) 290.88(5)	[27] [26] [28]
Ethyne	291.128 (avg) ^c 291.179 (² Σ _g)	291.20(3)	[22]	291.249 ^c	290.85(3) 291.2(1)	[33] [27]
Carbon monoxide	296.069	296.05(3)	[22]	296.229	291.14(10) 296.24(3)	[30] [3]
Carbon dioxide	297.664	297.66(4) 297.651(10)	[22] [9]	297.699	296.28(3) 297.69(14) 297.71(5)	[33] [1] [2]
Tetrafluoromethane	301.898			301.898	297.76(4) 301.96(5) 301.96(5) 301.86(5) ^a	[33] [2] [31] [25]
Fluoromethane	293.478			293.557	301.93(3)	[33]
Trifluoromethane	299.143			299.159	293.6(1) 299.1(1) 299.24(5) ^b	[32] [32] [27]

^a 0.18 eV has been added to the results given in Ref. [25], since they used a value of 248.45 for the argon 2p_{3/2} ionization energy rather than the value of 248.629 used here.

^b The ionization energies from Ref. [27] are given relative to that in tetrafluoromethane. We have obtained absolute values by combining these with our value for tetrafluoromethane. The quoted uncertainties include those given in Ref. [27] as well as the uncertainty in our value for tetrafluoromethane.

^c Unweighted average for the ²Σ_g and ²Σ_u states.

the ²Σ_g and ²Σ_u states. The value given by Tronc et al. [22] of (291.20 eV) agrees with our value for the ²Σ_g ionic state within the uncertainty they have given. Their value is based on an extrapolation of the Rydberg series, and it is not clear which state is reached by this extrapolation. For methane, the value given by Tronc et al. [22] differs from both our value and that given by Asplund [21] by twice the uncertainty that they have indicated.

The adiabatic ionization energies we have measured are also consistent with a set of measurements that we have made at the Advanced Light Source using a different procedure [23]. In these experiments we have measured the carbon 1s photoelectron spectra of the first six compounds listed in Table 1 simultaneously with the spectrum of tetrafluoro-

methane. The measurements give the difference between the ionization energies of these compounds and that of tetrafluoromethane. The differences are consistent with the values of the ionization energies listed in Table 1 to within 0.02 eV.

Previous measurements of vertical ionization energies come primarily from X-ray photoelectron spectroscopy. In some cases, only shifts between the ionization energy of interest and that of a reference compound have been measured. Selected values are listed in Table 1 for comparison with our results [1–3,24–33]. For the most part, the agreement between our results and those reported previously is quite good. The average deviation between our vertical ionization energies and the earlier values is –0.01 eV, indicating that any systematic difference

between our measurements and the older ones is small. The root-mean-square difference between our results and the earlier ones is 0.05 eV, which is the same as the average of the uncertainties quoted by the earlier workers.

3.2. Uncertainty of the measurements

The general agreement between our results and those reported earlier indicates that the accuracy of the measurements is quite good. However, not only do our measurements depend on the accuracy with which the argon $2p_{3/2}$ ionization energy is known, but so also do many of the other measurements that have been reported. Thus, the uncertainty in our measurements is at least as great as the uncertainty in the argon ionization energy. The uncertainty quoted for this by Nordgren et al. [8] is 0.01 eV. However, the range of values that have been reported for this quantity is about 0.03 eV [1,2,7–11]. It seems more conservative to assign an uncertainty of 0.02 eV. In addition to this, there is a contribution from other systematic as well as random errors. Comparison of the values given in Table 1 with ionization-energy differences that we have measured [23] suggests that this should be about 0.02 eV — see the second paragraph of Section 3.1. Combining these uncertainties leads to an overall uncertainty in the absolute ionization energies of 0.03 eV. The relative uncertainty between one ionization energy and another is less than this, but how much less we cannot say. As a result, we give the values in Table 1 to three decimal places to allow for the possibility that the uncertainty in the relative numbers is in the third place.

Acknowledgements

VM and LJS gratefully acknowledge the Research Council of Norway for financial support. TDT acknowledges support by the National Science Foundation under Grant No. CHE-9727471. EK, JDB and the Advanced Light Source acknowledge support from the Director, Office of Basic Energy Sciences, of the US Department of Energy under Contract No. DE-AC03-76SF00098. The experimental work was carried out using the Atomic and Molecular facility funded by DOE, Office of Sci-

ence, 1996 facility initiative, BES, Chemical Sciences.

References

- [1] G. Johansson, J. Hedman, A. Berndtsson, M. Klasson, R. Nilsson, *J. Electron Spectrosc. Relat. Phenom.* 2 (1973) 295.
- [2] T.D. Thomas, R.W. Shaw Jr., *J. Electron Spectrosc. Relat. Phenom.* 5 (1974) 1081.
- [3] S.R. Smith, T.D. Thomas, *J. Electron Spectrosc. Relat. Phenom.* 8 (1976) 45.
- [4] L.J. Sæthre, T.D. Thomas, L. Ungier, *J. Electron Spectrosc. Relat. Phenom.* 33 (1984) 381.
- [5] B.E. Mills, R.L. Martin, D.A. Shirley, *J. Am. Chem. Soc.* 98 (1976) 2380.
- [6] S.R. Smith, T.D. Thomas, *J. Am. Chem. Soc.* 100 (1978) 5459.
- [7] G.C. King, M. Tronc, F.H. Read, R.C. Bradford, *J. Phys. B: At. Mol. Phys.* 10 (1977) 2479.
- [8] J. Nordgren, H. Ågren, C. Nordling, K. Siegbahn, *Phys. Scripta* 19 (1979) 5.
- [9] L. Pettersson, J. Nordgren, L. Selander, C. Nordling, K. Siegbahn, H. Ågren, *J. Electron Spectrosc. Relat. Phenom.* 27 (1982) 29; J. Nordgren, L. Selander, L. Pettersson, C. Nordling, K. Siegbahn, H. Ågren, *J. Chem. Phys.* 76 (1982) 3928.
- [10] M. Coville, T.D. Thomas, *J. Electron Spectrosc. Relat. Phenom.* 71 (1995) 21.
- [11] R. Situmeang, T.D. Thomas, *J. Electron Spectrosc. Relat. Phenom.* 98–99 (1999) 105.
- [12] N. Berrah, B. Langer, A.A. Wills, E. Kukk, J.D. Bozek, A. Farhat, T.W. Gorczyca, *J. Electron Spectrosc. Relat. Phenom.* 101–103 (1999) 1.
- [13] Curve fitting macro package SPANCF. <http://www.geocities.com/ekukk>
- [14] P. van der Straten, R. Morgenstern, A. Niehaus, *Z. Phys. D* 8 (1988) 35.
- [15] T.X. Carroll, J. Hahne, T.D. Thomas, L.J. Sæthre, N. Berrah, J. Bozek, E. Kukk, *Phys. Rev. A* 61 (2000) 042503-1.
- [16] T.D. Thomas, L.J. Sæthre, S.L. Sorensen, S. Svensson, *J. Chem. Phys.* 109 (1998) 1041.
- [17] E.E. Rennie, H.M. Köppe, B. Kempgens, U. Hergenbahn, A. Kivimäki, K. Maier, M. Neeb, A. Rüdell, A.M. Bradshaw, *J. Phys. B: At. Mol. Opt. Phys.* 32 (1999) 2691.
- [18] T. Karlsen, L.J. Sæthre, K.J. Børve, N. Berrah, E. Kukk, J.D. Bozek, T.X. Carroll, T.D. Thomas, *J. Phys. Chem. A* 2001 (in press).
- [19] J. Bozek, T.X. Carroll, J. Hahne, L.J. Sæthre, J. True, T.D. Thomas, *Phys. Rev. A* 57 (1998) 157.
- [20] K.J. Børve, L.J. Sæthre, T.D. Thomas, T.X. Carroll, N. Berrah, J.D. Bozek, E. Kukk, *Phys. Rev. A* 63 (2001) 012506.
- [21] L. Asplund, U. Gelius, S. Hedman, K. Helenelund, K. Siegbahn, P.E.M. Siegbahn, *J. Phys. B: At. Mol. Phys.* 18 (1985) 1569.

- [22] M. Tronc, G.C. King, F.H. Read, *J. Phys. B: At. Mol. Phys.* 12 (1979) 137.
- [23] J.A. Hahne, J. True, J.D. Bozek, L.J. Sæthre, T.X. Carroll, T.D. Thomas, unpublished data.
- [24] J.J. Pireaux, S. Svensson, E. Basilier, P.-Å. Malmqvist, U. Gelius, R. Caudano, K. Siegbahn, *Phys. Rev. A* 14 (1976) 2133.
- [25] W.B. Perry, W.L. Jolly, *Inorg. Chem.* 13 (1974) 1211.
- [26] L.J. Sæthre, M.R.F. Siggel, T.D. Thomas, *J. Electron Spectrosc. Relat. Phenom.* 49 (1989) 119.
- [27] D.W. Davis, PhD thesis, University of California, Berkeley, Lawrence Berkeley Laboratory Report No. LBL-1900, 1973.
- [28] A. Berndtsson, E. Basilier, U. Gelius, J. Hedman, M. Klasson, R. Nilsson, C. Nordling, S. Svensson, *Phys. Scripta* 12 (1975) 235.
- [29] T.D. Thomas, *J. Chem. Phys.* 52 (1970) 1373.
- [30] R.G. Cavell, *J. Electron Spectrosc. Relat. Phenom.* 6 (1975) 281.
- [31] W.J. Griffiths, S. Svensson, A.N. deBrito, N. Correia, C.J. Reid, M.L. Langford, F.M. Harris, C.M. Liegener, H. Ågren, *Chem. Phys.* 173 (1993) 109.
- [32] T.D. Thomas, *J. Am. Chem. Soc.* 92 (1970) 4184.
- [33] J.A. Hahne, J. True, T.D. Thomas, unpublished data.

Paper II



ELSEVIER

Journal of Electron Spectroscopy and Related Phenomena 125 (2002) 127–132

JOURNAL OF
ELECTRON SPECTROSCOPY
and Related Phenomena

www.elsevier.com/locate/elspec

Xenon $N_{4,5}OO$ Auger spectrum—a useful calibration source

T.X. Carroll^a, J.D. Bozek^b, E. Kukk^c, V. Myrseth^d, L.J. Sæthre^d, T.D. Thomas^{e,*},
Karoline Wiesner^f

^aKeuka College, Keuka Park, New York, NY 14478, USA

^bAdvanced Light Source, Lawrence Berkeley National Laboratory, University of California, Berkeley, CA 94720, USA

^cDepartment of Physics, University of Oulu, Oulu FIN-90570, Finland

^dDepartment of Chemistry, University of Bergen, N-5007 Bergen, Norway

^eDepartment of Chemistry, Oregon State University, Corvallis, OR 97331-4003, USA

^fDepartment of Physics, Uppsala University, S-75121 Uppsala, Sweden

Received 19 March 2002; accepted 22 April 2002

Abstract

In the xenon $N_{4,5}OO$ Auger spectrum there are 19 prominent lines ranging in kinetic energy from 8 to 36 eV that provide a convenient set of standards for calibrating electron spectrometers. Combining optical data with recent measurements of this spectrum gives energies for these lines that are absolutely accurate to 11 meV. For most lines the relative accuracy is better than 1 meV; for a few it is about 3 meV. The spin–orbit splitting of the xenon 4d lines is determined to be 1979.0 ± 0.5 meV. © 2002 Elsevier Science B.V. All rights reserved.

Keywords: Auger; Photoelectron; Spin–orbit; Calibration; Xenon 4d

1. Introduction

Electron kinetic-energy spectra are typically obtained by measuring the counting rate of the electrons detected in the spectrometer as a function of a voltage applied to the spectrometer. Ideally the kinetic energy is linearly related to this voltage with unit slope. In the real world, however, it is possible (and even likely) that the slope is not exactly one, that the scale is not exactly linear, and that there is an offset between the true and apparent kinetic energy scales. In typical systems the offset can be

greater than 1 eV. Thus, calibration of the spectrometer requires a knowledge of the absolute voltage, the slope, and the linearity of the scan. For this purpose, it is useful to have convenient standards spanning a range of kinetic energies by which these quantities can be measured.

A useful standard for this purpose is the xenon $N_{4,5}OO$ Auger spectrum, which has 19 prominent lines ranging in kinetic energy from 8 to 36 eV. This spectrum is excited with good intensity with photons whose energy is above the $4d_{3/2}$ threshold (69.5 eV). The relative energies of some of these lines are known with high accuracy from optical measurements. The absolute energies can be determined by combining the optical energies with the 4d ionization energies. With this information, the energy scale can

*Corresponding author. Tel.: +1-541-737-6711; fax: +1-541-737-2062.

E-mail address: thomast@chem.orst.edu (T.D. Thomas).

be calibrated and the peak energies for which optical data are not available can be measured.

Results of such measurements have been given by Werme et al. [1], Aksela et al. [2], and Southworth et al. [3]. In each case, however, there is room for improvement in the results presented. For the first two, the calibration was based on only two points in the optical scale and the results are quoted only to the nearest 0.01 eV. In the analysis made by Werme et al., it is not apparent that curve fitting was used to determine the peak positions. For the work of Aksela et al. an extensive fitting procedure was used, but the resolution was not so good as was obtained by Werme et al. or by others more recently [4]. The results given by Southworth et al. have a large uncertainty—0.05 eV.

It is useful, therefore, to reexamine this question. We present here the results of measurements of this spectrum and of the calibration of the spectrum using optical data. As a result of this analysis, we are able to produce a set of 22 Auger energies with an absolute accuracy of about 11 meV and with a relative accuracy in most cases of better than 1 meV.

2. Experimental procedures

Xenon $N_{4,5}OO$ spectra were measured in three separate experiments, two at the Advanced Light Source (ALS) using beamline 10.0.1 and one at the MAX II synchrotron using beamline I411. In one experiment at the ALS (referred to as ALS1) spectra were measured at eight photon energies from 93 to 108 eV. In these the electron kinetic energy spectrum covered the range from 18 to 42 eV, and included the 4d photoelectron peaks. In the other two experiments the electron kinetic energy spectrum ranged from about 4 to 40 eV. In one of these (ALS2) the photon energy was 96 eV, and the spectrum includes the 4d photoelectron peaks. In the other (MAX II), the photon energy was 110 eV, and the photoelectron peaks were beyond the scan range. In each case, measurements were made using Scienta SES-200 analyzers, with slits and pass energies chosen to give a resolution of 35 to 40 meV. The three experiments were well separated in time and involved three different voltage supplies for the analyzers.

The spectra have been fit by least squares to Voigt

functions, with intensity, position, Gaussian width, and Lorentzian width as free parameters. All of the Auger peaks were constrained to have the same Gaussian and Lorentzian widths. A linear, sloping background was assumed. Several fits were made, some to an entire spectrum (using as many as 72 peaks) and some to selected portions of the spectrum. For one of the spectra, in which the photoelectron kinetic energies are less than some of the Auger energies, the effects of post-collision interaction were included using Eq. (12) from van der Straten et al. [5]. The results obtained including post-collision interaction are essentially the same as those obtained with Voigt-function fits.

3. Calibration

The calibration of the Auger spectrum is based on the use of the first and second ionization energies of xenon (I_1 and I_2) and the energies, E_{ex} , of the various states of Xe^{2+} . The energy of a state in Xe^{2+} (relative to the ground state of xenon) is given by the relationship

$$E(Xe^{2+}) = I_1 + I_2 + E_{ex} \quad (1)$$

These are combined with the xenon $4d_{5/2}$ ionization energy, $I(4d_{5/2})$, to give the energies, K , of the N_5OO Auger lines through the relationship

$$K = I(4d_{5/2}) - E(Xe^{2+}) \quad (2)$$

The energies for the N_4OO Auger lines can be obtained either in a similar way from the reported value of the $4d_{3/2}$ ionization energy or from the Auger spectrum using the spin-orbit splitting as one of the fitting parameters. Here we have used the second alternative. The various energies, which have been taken from published literature [6–10], are summarized in Table 1.

The line positions, V , obtained from the least-squares fitting have been fit with the relationship

$$V = V_0 + (K + n \times SO)V_1 \quad (3)$$

where $n=0$ for N_5OO lines and 1 for N_4OO lines, and V_0 and V_1 are fitting parameters representing the offset and slope, respectively. SO is the spin-orbit splitting and is also a fitting parameter. Some fits

Table 1
Energies used in calculating the xenon $N_{4,5}OO$ Auger energies.
Uncertainties in the last digit are given in parentheses

	cm^{-1}	eV^a	Ref.
I_1	97 834.4	12.1299	[6]
I_2	169 175(30)	20.975(4)	[7]
$I(4d_{5/2})$		67.548(11)	[8,9]
$5s^25p^4\ ^3P_2$	0	0	
$5s^25p^4\ ^3P_1$	9794.6	1.2144	[7]
$5s^25p^4\ ^3P_0$	8130.7	1.0081	[7]
$5s^25p^4\ ^1D_2$	17 099.0	2.1200	[7]
$5s^25p^4\ ^1S_0$	36 102.9	4.4762	[7]
$5s5p^5\ ^3P_2$	98 263	12.1831	[6]
$5s5p^5\ ^3P_1$	103 569	12.8409	[6]
$5s5p^5\ ^1P_1$	119 026.28	14.7574	[6]
$5s^25p^35d^1 (J = 1)^b$	154 639.61	19.1729	[6]
$5s^95p^6\ ^1S_0$	210 857.55	26.1430	[10]

^a Values in cm^{-1} have been converted to electron volts by dividing by 8065.544.

^b In Ref. [6] this state is designated $5s^25p^36s$. The notation here is that given in Ref. [2].

were made using an additional, quadratic, term, but these showed that such a term is not statistically significant. Once the least-squares values of the parameters have been obtained, the process can be reversed to give experimental values of the kinetic energies. These can be compared with the original values of K to assess the quality of the procedure, or, where no optical values of K are available, they provide new estimates of these quantities.

4. Results

The spectrum measured at MAX II is shown in Fig. 1. The peaks have been numbered using the numbering scheme given by Werme et al. [1]. Because the photon energy was 110 eV, the 4d photoelectron peaks are to be found at energies only slightly higher than shown here and the photoelectron shakeup peaks are found approximately in the middle of the Auger spectrum. The strongest of these are in a region where there are only weak Auger lines, but weaker shakeup peaks are found throughout the low-energy portion of the spectrum. As will be seen below, these can complicate the fitting of the peaks.

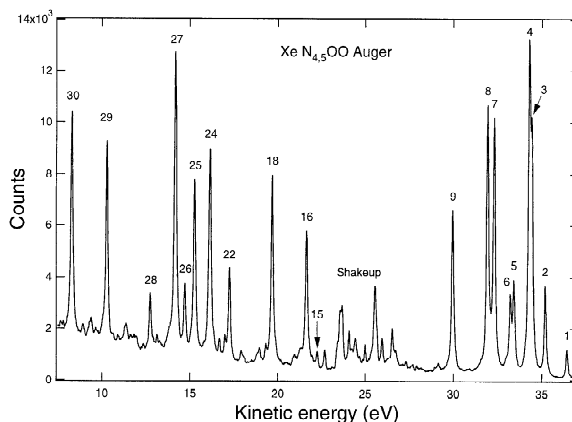


Fig. 1. The xenon $N_{4,5}OO$ Auger spectrum measured at a photon energy of 110 eV.

4.1. Spin-orbit splitting

A number of values for the spin-orbit splitting of the xenon 4d level have been reported [8,9,11–13]. These are summarized in Table 2, together with the values we have derived from our data using the procedure outlined above. Also included in this table are two values we have derived from the data of Werme et al. [1] and Aksela et al. [2] using the same procedure, as well as a value we have obtained from

Table 2
Xenon 4d spin-orbit splitting

Method	Value (meV)	Ref.
Photon absorption	1977(10)	[8]
Auger	1985(4)	^a
XPS	1980(10)	[11]
Electron energy loss	1989(3)	[9]
Auger	1971(7)	^b
XPS	1979(7)	[12]
XPS	1982(2)	[13]
XPS	1977(1)	This work, ALS1 ^c
Auger	1978(1)	This work, ALS1 ^c
Auger	1980(2)	This work, ALS2
Auger	1978(2)	This work, MAX II
Weighted average	1979.0(5)	

Uncertainties in the last decimal place are given in parentheses.

^a The data of Ref. [1] have been analyzed by us to give this value.

^b The data of Ref. [2] have been analyzed by us to give this value.

^c Average of eight measurements.

fitting the xenon 4d photoelectron peaks from eight spectra taken at different photon energies. For our results and for those derived from the data of Werme et al. and Aksela et al. the quoted uncertainties are those obtained from the statistics of the fitting procedures. The weighted average of these measurements gives a spin–orbit splitting of 1979.0 ± 0.5 meV.

4.2. Auger energies

Energies for 22 xenon $N_{4,5}OO$ Auger lines are listed in Table 3. There are three categories of energies: N_5OO energies derived directly from the data of Table 1, N_4OO energies derived from the data in Table 1 plus the value of the spin–orbit splitting mentioned above, and $N_{4,5}OO$ energies that we have derived from our measurements. As in Fig. 1, the energies are numbered according to the numbering scheme given by Werme et al. The absolute uncertainty in all of these numbers is determined primarily by the uncertainty in the $4d_{5/2}$ ionization energy, 10 meV [8], giving an overall absolute uncertainty of 11 meV. Any changes in this ionization energy or its uncertainty will cause corresponding changes in these numbers. The relative

Table 3
Xenon $N_{4,5}OO$ Auger kinetic energies (eV)

Number ^a	Energy	Method	Number ^a	Energy	Method
1	36.422	b	15	22.260	c
2	35.208	b	16	21.665	b
3	34.443	c	18	19.686	c
4	34.302	b	22	17.249	b
5	33.435	c	24	16.146(3)	d
6	33.229	c	25	15.270	c
7	32.323	c	26	14.703(3)	d
8	31.946	b	27	14.169(3)	d
9	29.967	c	28	12.741(3)	d
13	24.239	b	29	10.279	b
14	23.581	b	30	8.300	c

The absolute uncertainty is 11 eV. The relative uncertainties are 1 meV or less, except where indicated by a value in parentheses, which is the uncertainty in the last decimal place.

^a The numbering system is that used by Werme et al. [1].

^b From data given in Table 1 plus the experimentally determined value of the spin–orbit splitting, 1979 meV.

^c From data given in Table 1.

^d Determined from the measured Auger spectrum.

uncertainties are much less than this, being less than 1 meV for the first two categories of energies and about 3 meV for the energies determined from our measurements.

A comparison of our measured Auger energies and those based on the data in Table 1 (plus the spin–orbit splitting, where appropriate) is illustrated in Fig. 2. Here we have plotted the difference between the measured and the reference Auger energies versus the kinetic energy. We see that, for the most part, the two sets of data agree within a few meV. There are, however, two places, peaks 15 and 16, where there are much larger discrepancies, and it is useful to consider the source of these. They illustrate the difficulty of obtaining accurate information on line position in the case of a weak peak or of even a prominent peak if it is surrounded by a number of small peaks. The spectra in the regions of these peaks are plotted in Fig. 3 for both the MAX II data and the ALS data. These differ in that the ALS spectrum was measured at a photon energy of 96 eV and shakeup peaks do not contribute in this region of the spectrum. The MAX II spectrum was measured

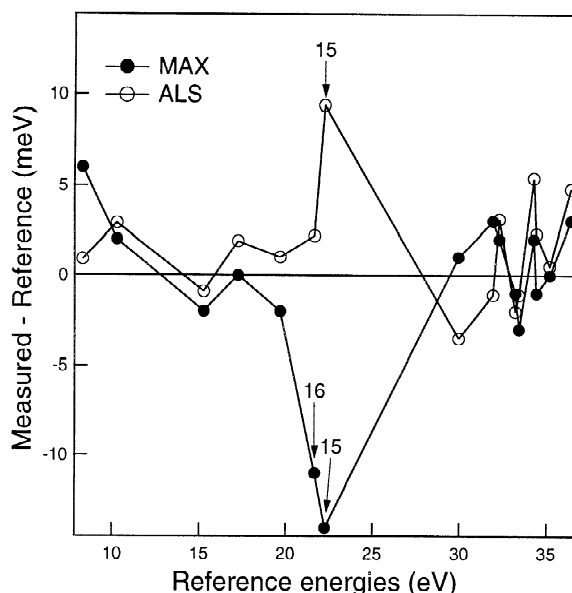


Fig. 2. Difference between the kinetic energies derived from the Auger spectra and those derived from optical data. The open circles (ALS) were measured at a photon energy of 97 eV and the closed circles (MAX II) were measured at 110 eV.

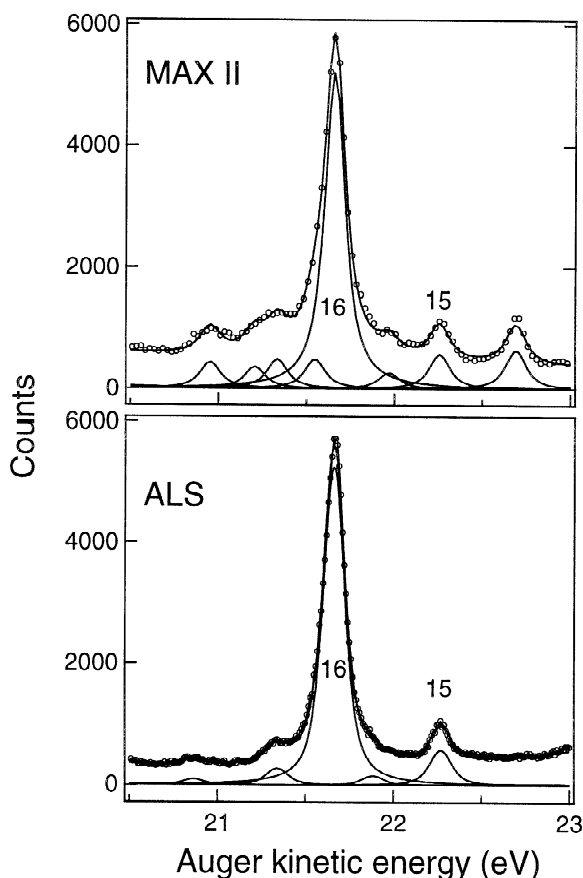


Fig. 3. Expanded view of the xenon $N_{4,5}OO$ Auger spectrum for two different experiments in the kinetic energy region 20 to 23 eV. Additional contributions to the MAX II data from shakeup are apparent.

at a photon energy of 110 eV, and, as can be seen in Fig. 1, shakeup makes a significant contribution in this region. Our experience with fitting this portion of the spectrum indicates that the derived peak positions are sensitive to inclusion of all of the small peaks. Because peak 15 is so weak, we have not used it in our calibration procedure.

Including the data for peak 16, the root-mean-square (rms) deviation of the energies we have measured from those derived from the data in Table 1 is 4 meV for the MAX II data and 2 meV for the ALS data. From these and from other results we have obtained in fitting the data, we conclude that this fitting procedure makes it possible to determine

the peak positions with a precision of about 3 meV, as indicated above. Comparable analyses of the data given by Werme et al. and by Aksela et al. give rms deviations of 8 and 13 meV, respectively.

5. Discussion

Emerging from these results is some insight into the quality of the analyzers used in this work. From the fits and from inspection of Fig. 2, we can conclude that there is no significant nonlinearity in the voltage supplies. As for the slope, the values of V_1 in Eq. (3), which reflects the relationship between the nominal voltage increments and the true voltage increments, are 1.00017(6) for the ALS data and 1.00072(12) for the MAX II data, indicating an accuracy of a few parts in 10^4 in the nominal voltages.

As can be seen from Fig. 1, our choice of a photon energy for the MAX II experiment, 110 eV, leads to significant shakeup structure in the region between 25 and 30 eV as well as to smaller peaks at lower energies. A better choice would be a photon energy greater than 130 eV, which would shift the major shakeup contributions out of the range of the Auger kinetic energies.

The relatively weak peaks 26 and 28 present a problem. These appear to be a spin-orbit doublet, but the spacing between them is only 1962 meV, which is 17 meV lower than the average spin-orbit splitting that we have observed. A similar effect is seen in the results reported by Werme et al. and Aksela et al. In view of the problems mentioned above in fitting weak peaks in the neighborhood of either strong peaks or a large number of even weaker peaks, it seems likely that this discrepancy is merely an artifact of the fitting process.

The energies given in Table 3 should provide a convenient set of calibration points for electron spectrometers at a level of accuracy that is higher than what has been available heretofore.

Acknowledgements

TXC and TDT acknowledge support by the National Science Foundation under grant No. CHE-

9727471. EK and JDB acknowledge support from the Divisions of Chemical and Material Sciences, Office of Energy Research, of the U.S. Department of Energy. LJS and VM thank the Research Council of Norway (NFR) and KW thanks the Swedish Natural Science Research Council (NFR) and the Swedish Foundation for Strategic Research for support.

References

- [1] L.O. Werme, T. Bergmark, K. Siegbahn, *Phys. Scripta* 6 (1972) 141.
- [2] H. Aksela, S. Aksela, H. Pulkkinen, *Phys. Rev. A* 30 (1984) 865.
- [3] S. Southworth, U. Becker, C.M. Truesdale, P.H. Kobra, D.W. Lindle, S. Owaki, D.A. Shirley, *Phys. Rev. A* 28 (1983) 261.
- [4] J. Jauhiainen, A. Ausmess, A. Kivimäki, S.J. Osborne, A. Naves de Brito, S. Aksela, S. Svensson, H. Aksela, *J. Electron Spectrosc. Relat. Phenom.* 69 (1994) 181.
- [5] P. van der Straten, R. Morgenstern, A. Niehaus, *Z. Phys. D* 8 (1988) 35.
- [6] C.E. Moore, *Atomic Energy Levels*, Vol. III, U.S. Government Printing Office, Washington, DC, 1971, NSRDS-NBS 35.
- [7] J.E. Hansen, W. Persson, *Phys. Scripta* 25 (1982) 487.
- [8] K. Codling, R.P. Madden, *Phys. Rev. Lett.* 12 (1964) 106.
- [9] G.C. King, M. Tronc, F.H. Read, R.C. Bradford, *J. Phys. B* 10 (1977) 2479.
- [10] J.E. Hansen, F.G. Meijer, M. Outred, W. Persson, H.O. Di Rocco, *Phys. Scripta* 27 (1983) 254.
- [11] U. Gelius, *J. Electron Spectrosc. Relat. Phenom.* 5 (1974) 985.
- [12] B.W. Yates, K.H. Tan, L.L. Coatsworth, G.M. Bancroft, *Phys. Rev. A* 31 (1985) 1529.
- [13] A. Ausmess, S.J. Osborne, R. Moberg, S. Svensson, S. Aksela, O.-P. Sairanen, A. Kivimäki, A. Naves de Brito, E. Nömmiste, J. Jauhiainen, H. Aksela, *Phys. Rev. A* 51 (1995) 855.

Paper III

Vibrational structure and vibronic coupling in the carbon 1s photoelectron spectra of benzene and deuterobenzene

V. Myrseth,^a K. J. Børve,^{*a} K. Wiesner,^b M. Bässler,^{bc} S. Svensson^b and L. J. Sæthre^a

^a Department of Chemistry, University of Bergen, Allégaten 41, NO-5007 Bergen, Norway.

E-mail: knut.borve@kj.uib.no

^b Department of Physics, Uppsala University, Box 530, SE-751 21 Uppsala, Sweden

^c MAX-lab, Box 118, SE-221 00 Lund, Sweden

Received 20th August 2002, Accepted 17th October 2002

First published as an Advance Article on the web 5th November 2002

Vibrationally resolved C1s photoelectron spectra of benzene and d₆-benzene have been recorded using monochromated synchrotron radiation at photon energies of 330 eV. The spectrum of normal benzene displays considerable vibrational structure. Particularly noteworthy is the strong excitation of a combined CCH-bending and CC-stretching mode which splits the main peak into two well-defined maxima. In d₆-benzene, the vibrational energy levels are less well separated and the vibrational structure is reduced to strong asymmetry of the main peak and a broad tail extending toward higher ionization energy. The recorded spectra are analyzed using first-principle and curve-fitting procedures. A theoretical model that allows for incomplete localization of the core hole, results in very good fits to the experimental spectra of both benzene and d₆-benzene.

I. Introduction

In the early days of electron spectroscopy it was generally believed that core photoionization was accompanied by no or very little excitation of vibrations.¹ The resolution at that time was insufficient to resolve vibrational fine structure, but the main reason for this misunderstanding was the lack of real insight in the electronic relaxation process following the creation of a core hole. In *e.g.* ref. 1 it is argued that core orbitals are “non-bonding” and therefore one should not expect vibrational substructure in the core photoelectron lines. However, the creation of a core hole leads to interatomic electronic relaxation which changes both the equilibrium geometry and the force constants. Accordingly, the ionization event is accompanied by relaxation of the nuclear framework of the molecule. Vibrational fine structure in a core photoelectron spectrum was first observed for methane in 1973,^{2,3} and the C1s main peak was resolved into at least three vibrational lines a decade later.^{4,5}

Today, dedicated third-generation synchrotrons make it possible to resolve vibrational fine structures in core-level photoelectron spectra of many molecules. A thorough analysis of the information obtained from such investigations is a prerequisite for obtaining accurate adiabatic binding energies and lifetimes of the core-ionized states, besides providing information on the structure and bonding of the excited state. Diatomic molecules possess only a single normal mode and the vibrational analysis of spectra becomes relatively straightforward. In polyatomic molecules many modes may get excited and the spectra tend to become more complex. Theoretical calculations are often needed in order to perform a reliable analysis. Theory^{6,7} and computer codes capable of simulating complex vibrational fine structure in core photoelectron spectra (thousands of vibrational lines can be handled) are available.⁸ The steps involved are the calculation of normal vibrational modes of the neutral ground state as well as those of ionic states, followed by evaluation of Franck-Condon factors in the harmonic approximation. By this

procedure one can determine accurately the adiabatic binding energy, *i. e.* the energy required to form the ion in its vibrational ground state (all $\nu = 0$).^{9–11} Knowledge of the vibrational envelope may also be used to compute average vibrational energies in the core-ionized species, thus providing a route to vertical ionization energies.

However, as was first observed in the case of the very highly resolved C1s photoelectron spectrum of acetylene (C₂H₂),¹² a procedure based on separable electronic and vibrational degrees of motion may be inadequate. Acetylene contains two equivalent carbon atoms, and in the ground state, the atomic core orbitals combine into molecular orbitals of *gerade* and *ungerade* symmetry, respectively, with a corresponding splitting of the C1s level. In core-ionized acetylene, however, shortening of the C–H bond on one side of the molecule as compared to the other, makes it energetically favorable to localize the core hole to the same side. Hence, the adiabatic electronic wave functions change notably with displacement along the asymmetric C–H stretching coordinate. This is the hallmark of vibronic coupling, and signals breakdown of the Born–Oppenheimer approximation. Cederbaum and coworkers, in a very early work¹³ and also more recently,^{14,15} describe how vibronic coupling acts as a mechanism for localizing the core hole. Rather than starting out from adiabatic electronic hole-state functions, which are proper eigenfunctions of the electronic Hamiltonian, one may anticipate the vibronically induced tendency toward localized hole states. Each localized-hole (diabatic) electronic state defines its own potential energy surface with associated normal coordinates and vibrational states. Any tendency toward delocalization of the core hole may be described as coupling of diabatic vibronic states, by the electronic Hamiltonian. In most cases, the energetic consequence of this coupling is negligible: meaning that the coupling between the core hole and the nuclear motion is sufficiently strong to localize the core hole and thus to erase the molecular splitting pattern. In acetylene, however, because of the very short carbon–carbon distance, the overlap between the degenerate atomic core orbitals is

sufficiently large to afford a notable splitting between the electronically-coupled diabatic vibronic states. This may be characterized as a case of incomplete or partial localization of the core hole, and vibronic coupling theory must be used when constructing the vibrational envelope of the photoelectron lines.

In this contribution, high-resolution C1s photoelectron spectra of benzene and d_6 -benzene (C_6D_6) are presented and analyzed in terms of vibrational excitations as well as vibronic interaction in the ionized state. Benzene contains six equivalent carbon atoms, and in the ground state, the atomic core orbitals combine into delocalized molecular orbitals, with a corresponding splitting of the C1s level into four sublevels. Since the overlap between core orbitals on neighboring carbon atoms is small, the resulting energy differences between the molecular core levels in benzene are also rather small, at 19, 38, and 19 meV. In the ionized state, the nuclear motion tends to localize the core hole and thus to erase the molecular splitting pattern. A primary goal of this study is to establish to what extent incomplete localization of the core hole makes a contribution to the fine structure of the C1s spectra of benzene and d_6 -benzene.

II. Experimental

The measurements were performed at beam line I411¹⁶ at the MAX II facility in Lund, Sweden. This beamline incorporates an undulator and a plane grating monochromator of the SX700 type, in addition to an experimental chamber for photoelectron spectroscopy equipped with a Scienta hemispherical SES-200 electron analyzer.¹⁷ The experiments were performed at the magic angle (54.7° between the polarization plane of the photons and the direction from the gas cell toward the detector) in order to minimize the effects of any spatial anisotropy in the photoelectron intensity. The monochromator slit was set to 5 μm and the pass energy of the electron analyzer was 20 eV, giving an experimental energy resolution of about 65 meV including contributions from Doppler broadening.

C1s photoelectron spectra were recorded at a photon energy of 330 eV, *i.e.* approximately 39 eV above the carbon 1s threshold. At this energy the influence from post-collision interaction (PCI) on the line shape is small but not negligible. Data acquisitions were made as a series of short runs, with the data from each run being inspected and the energy scale adjusted to account for small drifts in energy. Then the data were combined to give a summed spectrum. The binding-energy scale was calibrated using as energy reference the C1s spectrum of CO_2 , which was recorded simultaneously with the sample. A reference value of 297.664 ± 0.030 eV was used for the adiabatic core level binding energy of CO_2 .¹⁸

Benzene (99.8%), d_6 -benzene (isotopic purity 99.5 atom%) and carbon dioxide (99.995%) were obtained from commercial sources and used without further purification.

III. Theoretical and computational models

A. Franck–Condon profiles in the localized hole approximation

In order to describe the vibrational structure, density functional theory (DFT) calculations were carried out for the neutral as well as for the core-ionized molecules, providing accurate geometries, normal modes and harmonic vibrational frequencies for these species. The electronic structure calculations employed the B3LYP functional¹⁹ as implemented in the Gaussian-98 set of quantum chemical programs.²⁰

Carbon and hydrogen were described by triple- ζ bases augmented by a single set of polarization functions.^{21,22} The C1s-ionized molecules were described in the localized-hole approximation, and the core of the ionized atom was

represented by Stevens and coworkers' effective core potential (ECP),²³ scaled to account for only one electron in the 1s shell.²⁴ The valence shell of the core-ionized carbon was described by the nitrogen analogue to the carbon basis, albeit with all exponents scaled by 0.9293 as obtained by minimizing the energy of core-ionized methane.

The harmonic frequencies obtained by this procedure are expected to be higher than the observed frequencies. As an empirical correction for this failure, we use the known frequencies²⁵ for the ground-state of the molecule and scale the frequencies for the ionic state by the ratios of observed-to-calculated frequencies for the neutral state. The frequency of the C*–H stretching mode in the ionized molecule was scaled additionally by a factor of 0.97. The calculated Franck–Condon intensities are extremely sensitive to changes in bond lengths and bond angles. At the level of theory used here, the bond shrinkage upon core ionization is exaggerated by 0.2 pm in ethylene.²⁶ To account for this, the optimized C*–H bond length was adjusted accordingly.

Franck–Condon factors were computed in the full harmonic approximation,⁶ and also in a simplified approach⁷ based on a one-to-one mapping between initial- and final-state normal modes. Only negligible differences were found between the two sets of intensities, and the vibrational profiles used in the fits were based on the latter.

B. Vibronic coupling theory

Accounts of vibronic coupling in core-ionized ethyne and ethane have been presented elsewhere.^{12,27} Here, only essential elements of vibronic coupling theory as it applies to the present system are outlined. We start out from a model for the ionized molecule in which the core hole is localized to carbon atom C_{n^*} . The associated electronic wave function $|\Phi_{n^*}\rangle$ varies (in most cases) only slowly with distortions of the nuclear framework and constitutes an approximate diabatic state. From the associated potential energy surface the equilibrium geometry as well as vibrational normal modes and harmonic frequencies may be determined. Each vibrational state is defined in terms of quantum numbers of all the vibrational modes. The corresponding wave function and energy will be denoted by $|\nu_{n^*}\rangle$ and ε_{ν} , respectively. Approximate diabatic vibronic states may then be constructed as product functions: $|\Phi_{n^*}\rangle|\nu_{n^*}\rangle$.

The diabatic electronic states thus defined are not proper eigenstates of the electronic Hamiltonian (\hat{H}_e), since they are subject to the constraint of a localized core hole. They may still be used as basis for a matrix representation of \hat{H}_e , and eigenvectors of this matrix would then describe adiabatic electronic states in terms of linear combinations of the localized-hole states. However, rather than finding adiabatic electronic states, we seek molecular eigenstates, *i.e.* eigenstates of the full molecular Hamiltonian, $\hat{H} = \hat{T}_N + \hat{H}_e$, where \hat{T}_N is the nuclear kinetic-energy operator. To this end one may form a matrix representation of \hat{H} in the basis of the diabatic vibronic states defined above. This is a major undertaking for the present system, and the problem may be made more tractable by realizing that coupling of diabatic vibronic states will be most effective in the presence of degeneracy. The diabatic vibronic states form six-dimensional degenerate subsets, characterized by the same vibrational state albeit pertaining to each of the six possible locations of the core hole: $\{|\Phi_{n^*}\rangle|\nu_{n^*}\rangle\}$, $n = 1 \dots 6$. Hence, we approximate the full Hamiltonian by the block-diagonal matrix obtained by including off-diagonal integrals only within each of the six-dimensional degenerate subsets just described. Each submatrix describes the set of vibronic states that may be traced to a particular diabatic vibrational level ν . This approximation is equivalent to first-order degenerate perturbation theory, except that accidental degeneracy is disregarded. Any integrals between diabatic

states having core holes that are further apart than nearest neighbors are vanishingly small. For a pair of normalized diabatic states with neighboring core holes, we introduce the electronic overlap integral $\sigma = \langle \Phi_{1^*} | \Phi_{2^*} \rangle$ and the electronic coupling integral

$$\beta = \langle \Phi_{1^*} | \hat{H}_c | \Phi_{2^*} \rangle - \sigma \langle \Phi_{1^*} | \hat{H}_c | \Phi_{1^*} \rangle \quad (3.1)$$

Keeping only coupling terms that are linear in σ and β , the diagonal elements of the 6-by-6 Hamiltonian matrix labeled by ν , all become equal to ϵ_ν . The non-zero off-diagonal elements are all given by $(\beta + \sigma\epsilon_\nu) \langle \nu_{1^*} | \nu_{2^*} \rangle$, again keeping only terms that are linear in σ and β . The overlap matrix is congruent with the Hamiltonian, with diagonal elements equal to unity and the remaining non-vanishing elements given by $\sigma \langle \nu_{1^*} | \nu_{2^*} \rangle$. Thus, the secular determinant becomes similar to what is obtained for the valence π orbitals of benzene in Hückel theory,²⁸ except that the “ x ” parameter becomes

$$x = \frac{\epsilon_\nu - E}{[(\epsilon_\nu - E)\sigma + \beta] \langle \nu_{1^*} | \nu_{2^*} \rangle} \quad (3.2)$$

The resulting vibronic energy levels associated with a given (diabatic) vibrational energy, are then given by

$$E = \epsilon_\nu + x\beta \langle \nu_{1^*} | \nu_{2^*} \rangle, \quad x = -2, -1, -1, +1, +1, +2 \quad (3.3)$$

The magnitude of the splitting of each diabatic vibrational level is thus determined by the electronic coupling integral β , which is common to all vibrational levels, and a vibrational overlap integral specific to each (diabatic) vibrational state. Note that the indices of the vibrational wave functions refer to the atom that is core ionized, while ν is used as a compound index for the vibrational state.

The resulting splitting pattern is illustrated in Fig. 1, where the two central levels are shown to be doubly degenerate. In the XPS spectrum, the total intensity of the six vibronic levels originating from a single diabatic vibrational level is given by the Franck–Condon factor appropriate to an ion with a localized hole. However, this intensity is now distributed in a 1 : 2 : 2 : 1 pattern according to the remaining degeneracy. This implies that the computational models described in the preceding section form a useful starting point for the present refinement. Moreover, the vibrational overlap integrals in eqn. (3.3) are evaluated using the same algorithms as described for the ordinary Franck–Condon factors.⁶

In order to get quantitative results from eqn. (3.3), an estimate is needed of the electronic coupling integral β . To this end, a set of dedicated calculations, in which the core hole was explicitly included, were carried out using the MOLCAS suite of programs.²⁹ The electronic coupling integral between a pair of states having the core hole localized to two neighboring carbon atoms was estimated in a restricted active space state-interaction (RASSI) calculation.³⁰ The orbitals were optimized at the restricted active-space self-consistent field (RASSCF) level of theory, with four electrons distributed in all possible ways over two bonding and two antibonding π orbitals. The molecular geometry was the average of the two localized core-hole geometries and atomic natural orbitals (ANO) were used as follows:³¹ H:[3s,2p], C:[5s,3p,2d], and

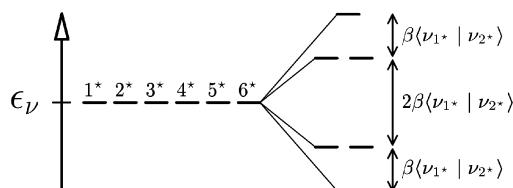


Fig. 1 A schematic representation of how each six-fold degenerate diabatic vibronic level in C1s-ionized benzene is split according to eqn. (3.3).

for core-ionized carbon, C*:[7s,5p,3d]. These calculations gave $\beta = 22$ meV.

C. Fitting models

The spectra were fit using theoretically calculated vibrational profiles, in which the energy spacing and relative intensities of vibrational lines were obtained from DFT calculations. The lineshape function takes into account lifetime broadening and post-collision interaction (PCI) as described by van der Straten *et al.*,³² while instrumental resolution is accounted for through subsequent convolution by a Gaussian function of fixed width as described in the Experimental section. The Gaussian width was fixed to 65 meV based on separate investigations of the instrumental resolution. The Lorentzian width was taken to be the same for all vibrational peaks and set to 100 meV, based on the lifetimes observed for C1s holes in other hydrocarbons.³³ The free parameters in the fits are then a constant background and the intensity and energy position of the adiabatic peak (all $\nu = 0$). A versatile IGOR PRO curve fitting routine³⁴ was used for optimization.

Three modifications of the model outlined here were used to examine the spectra for effects of incomplete localization of the core hole. These are described in the Results section.

IV. Results and discussion

In Fig. 2 the experimental C1s photoelectron spectrum of normal benzene is shown (circles) along with results from a theoretical analysis of the vibrational structure (solid line). For the first time, one can observe a splitting of the most prominent peak in the experimental spectrum of benzene. Two maxima of about equal intensity occur at 290.26 and 290.34 eV, of which the one at highest energy is caused by strong vibrational excitation. Additionally, there are clear shoulders seen at around 290.6 eV and 290.8 eV.

The bars in the diagram represent a theoretical model that assumes full localization of the core hole. The relevant normal modes of core-ionized benzene are described in Table 1. Also included in the table are the harmonic frequencies, Franck–Condon factors pertaining to vertical excitation from the vibrational ground state in the neutral molecule, and the overlap integrals $\langle \nu_{1^*} | \nu_{2^*} \rangle$ occurring in eqn. 3.3. Only modes that transform according to A_1 in C_{2v} symmetry are included in the table. However, their ancestry to modes that display the full D_{6h} symmetry of the ground state is also indicated. The presence of singly-excited modes that differ from A_{1g} symmetry

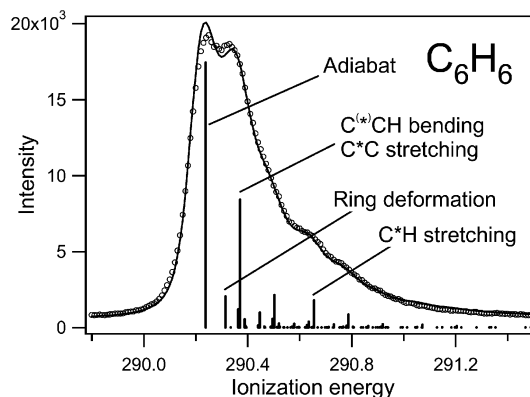


Fig. 2 The experimental C1s spectrum of benzene (circles) shown together with a fitting model (solid line) based on the localized-hole approximation. The most intense vibrational lines are indicated as bars.

Table 1 Computed vibrational frequencies in order of increasing energy, Franck–Condon factors and vibrational overlap integrals for the most important states in the C1s spectrum of normal benzene

Assignment ^a	Type ^b	ω/meV^c	Intensity ^d	$\langle \nu_1^* \nu_2^* \rangle^e$
Adiabat	—	—	1.000	0.59
ν_{18} (E_{2g})	Ring def, CC*C b	76	0.117	0.13
ν_2 (A_{1g})	Ring s	125	0.069	0.55
ν_6 (B_{1u})	Ring def	129	0.018	0.54
ν_{14} (E_{1u})	C*C s, C*CH, CCH b	132	0.482	0.36
ν_{17} (E_{2g})	C*CH, CCH b	150	0.031	0.27
$\nu_{18} + \nu_{14}$		208	0.056	0.08
$\nu_2 + \nu_{14}$		257	0.033	0.34
$2\nu_{14}$		264	0.123	0.22
$\nu_{14} + \nu_{17}$		282	0.015	0.15
$\nu_{18} + 2\nu_{14}$		340	0.014	0.05
$3\nu_{14}$		396	0.022	0.13
ν_{12} (E_{1u})	C*H s	417	0.103	0.07
$\nu_{18} + \nu_{12}$		493	0.012	0.02
$\nu_{14} + \nu_{12}$		549	0.050	0.04
$2\nu_{14} + \nu_{12}$		681	0.013	0.03
$2\nu_{12}$		834	0.011	0.01

^a Nomenclature from ground-state benzene.²⁵ The D_{6h} ancestry is indicated within parentheses. ^b Deformation (def), stretch (s), bend (b) ^c Final state vibrational harmonic frequency. ^d Franck–Condon factor, renormalized to unity for the adiabatic line. Only states receiving a relative intensity $\geq 1\%$ are included. ^e Vibrational overlap integral appearing in eqn. (3.3).

are indicative of core-hole localization. This includes modes of E_{2g} , E_{1u} and B_{1u} symmetry which would have been symmetry forbidden in D_{6h} yet transform according to A_1 in C_{2v} .

As can be seen from Table 1, the Franck–Condon profile is built up mainly from only six normal modes, thus simplifying the assignment. The most striking observation from Table 1 and Fig. 2 is that the intense vibrational peak observed in the spectrum at a binding energy of 290.37 eV, can be attributed to the ν_{14} vibrational mode in Shimanouchi's notation.²⁵ The calculations show that this mode contains C*–C stretching and in-plane C*CH and CCH bending, C* denoting the core-ionized atom. Upon core ionization, the C*–C bonds shorten by 0.029 Å while the corresponding change is -2.5° in the C*CH angles. These geometry changes add constructively when projected onto mode ν_{14} and give rise to the high Franck–Condon factor. Other large geometry changes include $+2.5^\circ$ in the CC*C angle and a shortening of the C*–H bond by 0.055 Å. The bond contraction leads to excitation of the C*–H stretching mode, which has a frequency of 417 meV. This is indeed observed in the C1s spectrum as a shoulder at around 290.6 eV. The intensity of this shoulder is roughly in accordance with the building-block model of hydrocarbon vibrations.^{35,36} In this model, the intensity of the C*–H mode in any hydrocarbon is proportional to the number of hydrogen atoms attached to the ionized carbon. In agreement with this, we find the intensity of the structure around 290.6 eV to be comparable to what is seen *e.g.* in the C1s photoelectron spectrum of trichloromethane.³⁷ In addition to the modes already mentioned, ring deformation modes are also excited upon C1s ionization.

Benzene was recently studied by Rennie *et al.*,³⁸ who analyzed the spectrum in terms of two vibrational progressions. The resulting fit gave a high-frequency mode at 386 meV, and a second mode at a significantly lower frequency. While the high-frequency mode was correctly ascribed to C*–H stretching, its frequency is much lower than computed in the present work (417 meV). Moreover, based on our results, it appears likely that their second, low-frequency progression assumes intensity that belongs to the strongly excited ν_{14} mode as well as to the ring stretching mode ν_2 which is close in energy. These differences may be ascribed to the model used

in ref. 38, where only two vibrational progressions were fitted to a fairly featureless multi-mode structure. As very recently anticipated in ref. 39, the two modes assumed by Rennie *et al.* in their empirical analysis of the spectrum take on the role of effective vibrations with limited interpretability.

Up to this point, our analysis has been made in terms of a localized-hole model of core-ionized benzene. However, the possibility of incomplete vibronic coupling in core-ionization spectra has recently been examined for several small hydrocarbons,^{12,27} and the question is of interest also for benzene. Admittedly, Fig. 2 shows that the localized model is able to provide a good theoretical description of the spectrum. Nevertheless, closer scrutiny of the doubly-split main peak reveals details that are not reproduced by the theory at this stage. In order to examine this point, we evoke the more elaborate theory of vibronic coupling as presented in section III.B. In addition to eqn. (3.3), which defines our most advanced model (Model III), we define two simpler models which can be applied to larger organic systems. In Model I, the vibrational integral appearing in eqn. (3.3) is put equal to a common constant independent of the vibrational state of the molecule. Effectively, this implies that the spectral profile obtained from the localized-hole model is repeated four times. The four replica have relative intensities and energies of 1 : 2 : 2 : 1 and $-2B$, $-B$, B and $2B$, respectively. B is left to be optimized in a fit to the observed spectrum. In Model II, the vibrational integral appearing in eqn. (3.3) is taken equal to the Kronecker function $\delta_{\nu,0}$, effectively splitting only the adiabatic peak in the spectrum. This model is based on the expectation that the higher each mode is excited, the smaller the vibrational overlap integrals become. This follows from the localized character of the modes that obtain significant Franck–Condon intensity.

Using the reduced chi-squared (χ^2) value as a measure of goodness-of-fit, we find that all of the three modified models I–III do much better than the fully localized model. The drop in χ^2 is significant and ranges from 32% for Model I to 35% and 36% for Models II and III, respectively. For Model I, the splitting parameter B optimizes to 23 meV, but the χ^2 function is very flat in this region and suffers only a very small increase if B is set to 16 meV (see below). However, the visual appearance of the main peak is not much improved compared to Fig. 2.

The fit based on Model II, with only the adiabatic peak undergoing any splitting, leads to substantial improvement both in terms of reduced χ^2 value and the visual appearance of the two most intense maxima at 290.26 eV and 290.34 eV. The energy split between the two lowest lines of the quartet making up the adiabatic peak, was optimized to 15.8 meV. The resulting fit to the experimental spectrum is virtually indistinguishable from that obtained with Model III. The latter is shown in Fig. 3.

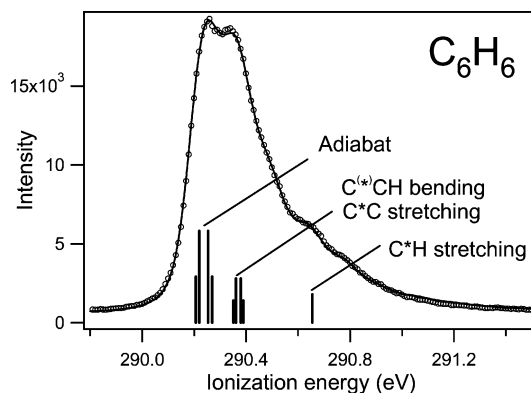


Fig. 3 The experimental C1s spectrum of benzene shown together with a fit based on Model III.

Our most elaborate model, Model III was based on theoretical estimates of the effect of hole delocalization on each vibrational line. The vibrational overlap integrals appearing in eqn. (3.3) were calculated for all vibrational lines that receive an intensity higher than 1% of that of the adiabatic peak. Of these, only vibrational levels that support vibrational overlap integrals $\langle \nu_1^* | \nu_2^* \rangle \geq 0.1$ were actually split in the fitting procedure. For benzene, this implies that ten of the diabatic vibrational lines were split, while 98 lines remain unsplit. The common electronic coupling integral β occurring in eqn. (3.3), was optimized in a fit to the experimental C1s spectrum of benzene. The resulting value of 27 meV agrees well with the 22 meV that we find from *ab initio* calculations, and lends credibility to our findings. For the adiabatic peak, the optimized value of β translates into a splitting pattern of 16, 32, 16 meV. The result of the analysis using Model III is presented in Fig. 3. We can conclude that the spectrum is very well reproduced even in small details.

The good agreement between the various ways of taking account of incomplete hole localization may be understood in two different ways. One interpretation is that what matters is to split the adiabatic line, since this is the only region where the localized-hole model is notably off. The lower intensity of the vibrationally excited states then makes it less important whether and how splitting is accounted for elsewhere. The second interpretation takes this point one step further: May the success of Models I–III be caused by either the instrumental (Gaussian) or the lifetime (Lorentzian) linewidths being originally underestimated? These two parameters are strongly correlated, and it is not feasible to determine them simultaneously in a fit to the observed spectrum. However, we tested this point within the localized-hole model, first by keeping the Gaussian width constant at $\Gamma_G = 65$ meV and optimizing Γ_L , and second by reversing the status of the two parameters, with Γ_L fixed at 100 meV.

The test fits gave optimized values of $\Gamma_L = 108$ meV ($\chi^2 = 6.70$, down by 16%) and $\Gamma_G = 84$ meV ($\chi^2 = 5.35$, down by 33%), respectively. Compared to previously determined lifetime widths in hydrocarbons, which range from 95 meV to 106 meV among saturated and unsaturated hydrocarbons (CH₄, C₂H₆, C₂H₂),³³ a Lorentzian width of $\Gamma_L = 108$ meV must be regarded as high but not entirely unrealistic for C1s in benzene. However, optimization of Γ_L gave notably less reduction in the goodness-of-fit parameter than did optimization of Γ_G , showing that the missing broadening effect is much closer in shape to a Gaussian profile than to a Lorentzian profile. This is in agreement with the pattern shown in Fig. 1, since the largest splitting occurs between the two strong, central components. However, an instrumental broadening of $\Gamma_G = 84$ meV disagrees strongly both with characterization studies which we have performed and also theoretical parameters for beam line I411 under the conditions of our experiments. Hence, we believe that the presence of an additional broadening effect due to incomplete localization of the core hole is positively present in the C1s spectrum of benzene.

For d₆-benzene, only a single, asymmetric peak is observed in the experimental C1s photoelectron spectrum (Fig. 4). The calculations suggest that two normal modes dominate the vibrational structure of the spectrum, one being a combined C*–C stretching and CCD and C*CD bending mode with a vibrational energy of 103 meV, while the other mode involves ring stretching at a fundamental frequency of 120 meV. These two modes cause the asymmetry near the top of the main peak in the experimental spectrum. Incomplete localization of the core hole was taken into account in terms of our best Model III. Using the same selection criteria as for normal benzene, 16 lines underwent splitting while 218 vibrational lines were included unsplit. Details of the Franck–Condon analysis of the vibrational structure are given in Table 2. Optimization of β reproduced the value obtained for normal benzene within

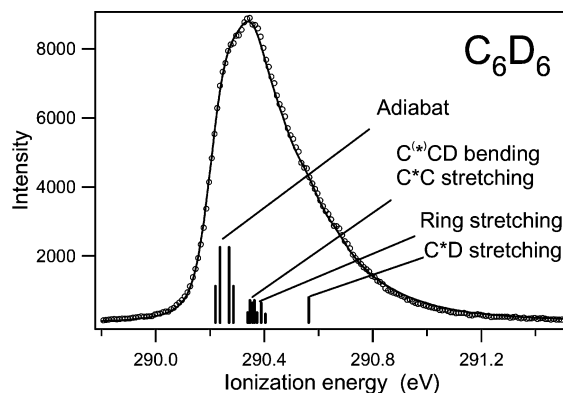


Fig. 4 Experimental (circles) and theoretical C1s core photoelectron spectrum of d₆-benzene. The solid line is a simulation based on Model III, as described in the text.

1 meV. The resulting fit to the observed spectrum is highly satisfactory, see Fig. 4.

In Fig. 5 the electronic coupling integral is plotted as a function of the C–C bond length as computed for acetylene, ethylene, benzene and ethane. Evidently, this parameter is determined by the distance between the symmetry-related carbon atoms. The same conclusion was reached by Gunnellin *et al.*,⁴⁰ based on X-ray emission studies and an analysis in terms of adiabatic states, as well as by Thomas *et al.*,⁷ who applied Landau–Zener theory to this issue. The smooth

Table 2 Computed vibrational frequencies, Franck–Condon factors and vibrational overlap integrals for the most important states present in the C1s spectrum of d₆-benzene

Assignment ^a	Type ^b	ω/meV^c	Intensity ^d	$\langle \nu_1^* \nu_2^* \rangle^e$
Adiat	—	—	1.000	0.52
ν_{18} (E _{2g})	Ring def	73	0.144	0.08
ν_{14} (E _{1u})	C*C s, C*CD, CCD b	103	0.319	0.27
ν_{17} (E _{2g})	C*CD, CCD b	110	0.068	0.20
ν_2 (A _{1g})	Ring s	120	0.285	0.50
ν_6 (B _{1u})	Ring def	124	0.036	0.46
$2\nu_{18}$		145	0.011	0.02
ν_{13} (E _{1u})	Ring s	167	0.041	0.26
$\nu_{18} + \nu_{14}$		175	0.046	0.04
$\nu_{18} + \nu_2$		192	0.041	0.08
$2\nu_{14}$		206	0.054	0.13
$\nu_{14} + \nu_{17}$		213	0.022	0.05
$\nu_{14} + \nu_2$		222	0.091	0.25
$\nu_{14} + \nu_6$		227	0.012	0.24
$\nu_{17} + \nu_2$		230	0.019	0.19
$2\nu_2$		239	0.044	0.47
$\nu_2 + \nu_6$		244	0.010	0.40
$\nu_{14} + \nu_{13}$		270	0.013	0.13
$\nu_2 + \nu_{13}$		287	0.012	0.25
$\nu_{18} + \nu_{14} + \nu_2$		295	0.013	0.04
ν_{15} (E _{2g})	C*D s	310	0.118	0.08
$2\nu_{14} + \nu_2$		325	0.015	0.13
$\nu_{14} + 2\nu_2$		342	0.014	0.24
$\nu_{18} + \nu_{15}$		383	0.017	0.01
$\nu_{14} + \nu_{15}$		413	0.038	0.04
$\nu_2 + \nu_{15}$		430	0.034	0.07
$\nu_{14} + \nu_2 + \nu_{15}$		533	0.011	0.04
$2\nu_{15}$		621	0.014	0.01

^a Nomenclature from ground-state d₆-benzene.²⁵ The D_{6h} ancestry is indicated within parentheses. ^b Deformation (def), stretch (s), bend (b) ^c Final state vibrational harmonic frequency. ^d Franck–Condon factor, renormalized to unity for the adiabatic line. Only states receiving a relative intensity $\geq 1\%$ are included. ^e Vibrational overlap integral appearing in eqn. (3.3).

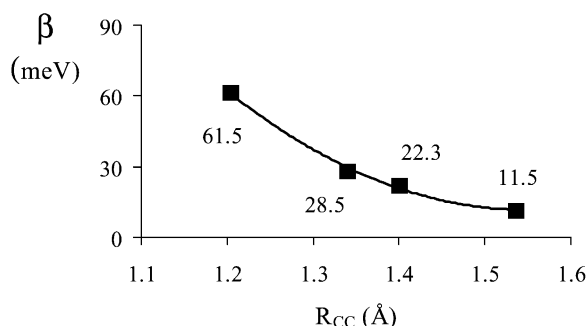


Fig. 5 The electronic coupling integral β plotted vs. the carbon-carbon bond length in the ground state of acetylene,¹² ethylene,²⁶ benzene (this work) and ethane.²⁷ In all cases, β has been computed as outlined in section III.B.

evolution of β suggests that in subsequent studies, one may obtain useful estimates of β through interpolation in Fig. 5.

Based on our best fitting models presented here, we obtain adiabatic C1s ionization energies in normal and d_6 -benzene as 290.241(30) eV and 290.226(30) meV. The shift in ionization energies between these two compounds is consistent with the small difference in zero-point vibrational energies between C_6H_6 and C_6D_6 , computed theoretically to 15 meV. Based on the vibrational profiles, an average vibrational excitation energy of 136(30) meV was computed for both core-ionized normal and d_6 -benzene. These values give 290.377(40) eV and 290.362(40) eV, for the vertical ionization energies. The former compares well with the value of 290.38 eV obtained by Holmes and Thomas using conventional X-rays.^{41,42} The uncertainty in the shift between two ionization energies is less than indicated for the absolute ionization energies, which is why we give the values to three decimal places.

V. Conclusions

High-resolution synchrotron-radiation-based electron spectroscopy has been used to obtain vibrationally resolved C1s photoelectron spectra for benzene and d_6 -benzene in the gas phase. The vibrational structures have been analyzed in terms of normal modes. The vibrational structures in the spectra are dominated by C^*-C stretching and CCH(D) and $C^*CH(D)$ bending, with important additional contributions also from $C^*-H(D)$ stretching and various ring stretching and deformation modes. Fitting models based on vibronic coupling theory indicate that the adiabatic peak consists of four lines that are split by 63 meV from the center of the first to the center of the fourth of these. This splitting may be understood as due to incomplete localization of the core hole.

Acknowledgements

Support from the Swedish Natural Science Research Council (NFR), the Swedish Foundation for Strategic Research (SSF), the Swedish Research Council for the Engineering Sciences (TFR) and the Swedish Foundation for International Cooperation in Research and Higher Education (STINT) is gratefully acknowledged. KJB and LJS thank the Research Council of Norway for support through the Programme for Supercomputing. VM thanks the Research Council of Norway for a PhD scholarship. The collaboration of the staff of MAX-lab is gratefully acknowledged.

References

- 1 K. Siegbahn, C. Nordling, G. Johansson, J. Hedman, P. F. Hedén, K. Hamrin, U. Gelius, T. Bergmark, L. O. Werme, R.

- Manne, and Y. Baer, *ESCA Applied to Free Molecules*, North-Holland Publishing Company, Amsterdam, 1971.
- 2 U. Gelius, E. Basilier, S. Svensson, T. Bergmark and K. Siegbahn, *J. Electron Spectrosc. Relat. Phenom.*, 1973, **2**, 405.
- 3 U. Gelius, S. Svensson, H. Siegbahn, E. Basilier, Å. Faxälv and K. Siegbahn, *Chem. Phys. Lett.*, 1974, **28**, 1.
- 4 K. Siegbahn in *Atomic Physics*, ed. I. Lindgren, A. Rosén, and S. Svanberg, Plenum Press, New York, 1983, vol. 8, p. 243.
- 5 L. Asplund, U. Gelius, S. Hedman, K. Helenelund, K. Siegbahn and P. E. M. Siegbahn, *J. Phys. B: At. Mol. Phys.*, 1985, **18**, 1569.
- 6 P.-Å. Malmqvist and N. Forsberg, *Chem. Phys.*, 1998, **228**, 227.
- 7 T. D. Thomas, L. J. Sæthre, S. L. Sorensen and S. Svensson, *J. Chem. Phys.*, 1998, **109**, 1041.
- 8 K. J. Børve, *g2fc*, University of Bergen, 2000.
- 9 L. J. Sæthre, N. Berrah, J. D. Bozek, K. J. Børve, T. X. Carroll, E. Kukk, G. L. Gard, R. Winters and T. D. Thomas, *J. Am. Chem. Soc.*, 2001, **123**, 10 729.
- 10 A. Giertz, K. J. Børve, M. Bässler, K. Wiesner, S. Svensson, L. Karlsson and L. J. Sæthre, *Chem. Phys.*, 2002, **277**, 83.
- 11 T. Karlson, K. J. Børve, L. J. Sæthre, K. Wiesner, M. Bässler and S. Svensson, *J. Am. Chem. Soc.*, 2002, **124**, 7866.
- 12 K. J. Børve, L. J. Sæthre, T. D. Thomas, T. X. Carroll, N. Berrah, J. D. Bozek and E. Kukk, *Phys. Rev. A*, 2001, **63**, 012 506.
- 13 W. Domcke and L. S. Cederbaum, *Chem. Phys.*, 1977, **25**, 189.
- 14 L. S. Cederbaum, *J. Chem. Phys.*, 1995, **103**, 562.
- 15 N. V. Dobrodey, H. Köppel and L. S. Cederbaum, *Phys. Rev. A*, 1999, **60**, 1988.
- 16 M. Bässler, A. Ausmees, M. Jurvansuu, R. Feifel, J.-O. Forsell, P. Fonseca, A. Kivimäki, S. Sundin, S. L. Sorensen, R. Nyholm, O. Björneholm, S. Aksela and S. Svensson, *Nucl. Instrum. Methods Phys. Res., Sect. A*, 2001, **469**, 382.
- 17 N. Mårtensson, P. Baltzer, P. A. Brühwiler, J.-O. Forsell, A. Nilsson, A. Stenborg and B. Wannberg, *J. Electron Spectrosc. Relat. Phenom.*, 1994, **70**, 117.
- 18 V. Myrseth, J. D. Bozek, E. Kukk, L. J. Sæthre and T. D. Thomas, *J. Electron Spectrosc. Relat. Phenom.*, 2002, **122**, 57.
- 19 P. J. Stevens, F. J. Devlin, C. F. Chabrowski and M. J. Frisch, *J. Phys. Chem.*, 1994, **98**, 11 623.
- 20 Gaussian 98. M. J. Frisch, G. W. Trucks, H. B. Schlegel, G. E. Scuseria, M. A. Robb, J. R. Cheeseman, V. G. Zakrzewski, J. A. Montgomery, Jr., R. E. Stratmann, J. C. Burant, S. Dapprich, J. M. Millam, A. D. Daniels, K. N. Kudin, M. C. Strain, O. Farkas, J. Tomasi, V. Barone, M. Cossi, R. Cammi, B. Mennucci, C. Pomelli, C. Adamo, S. Clifford, J. Ochterski, G. A. Petersson, P. Y. Ayala, Q. Cui, K. Morokuma, D. K. Malick, A. D. Rabuck, K. Raghavachari, J. B. Foresman, J. Cioslowski, J. V. Ortiz, A. G. Baboul, B. B. Stefanov, G. Liu, A. Liashenko, P. Piskorz, I. Komaromi, R. Gomperts, R. L. Martin, D. J. Fox, T. Keith, M. A. Al-Laham, C. Y. Peng, A. Nanayakkara, M. Challacombe, P. M. W. Gill, B. Johnson, W. Chen, M. W. Wong, J. L. Andres, C. Gonzalez, M. Head-Gordon, E. S. Replogle, and J. A. Pople; *Gaussian 98, Revision A.9*, Gaussian Inc., Pittsburgh, PA, 1998.
- 21 T. H. Dunning, Jr., *J. Chem. Phys.*, 1971, **55**, 716.
- 22 K. Raghavachari, J. S. Binkley, R. Seeger and J. A. Pople, *J. Chem. Phys.*, 1980, **72**, 650.
- 23 W. J. Stevens, H. Basch and M. Krauss, *J. Chem. Phys.*, 1984, **81**, 6026.
- 24 T. Karlson and K. J. Børve, *J. Chem. Phys.*, 2000, **112**, 7979.
- 25 T. Shimanouchi in *NIST Chemistry WebBook, NIST Standard Reference Database*, ed. W. G. Mallard and P. J. Linstrom, National Institute of Standards and Technology, Gaithersburg, MD, February 2000, vol. 69, <http://webbook.nist.gov/>.
- 26 K. J. Børve, unpublished material.
- 27 T. Karlson, L. J. Sæthre, K. J. Børve, N. Berrah, E. Kukk, J. D. Bozek, T. X. Carroll and T. D. Thomas, *J. Phys. Chem. A*, 2001, **105**, 7700.
- 28 J. N. Murrell, S. F. A. Kettle, and J. M. Tedder, *The Chemical Bond*, John Wiley, New York, 2nd edn., 1992, p. 181.
- 29 K. Andersson, M. R. A. Blomberg, M. P. Fülcher, G. Karlström, R. Lindh, P.-Å. Malmqvist, P. Neogrády, J. Olsen, B. O. Roos, A. J. Sadlej, M. Schütz, L. Seijo, L. Serrano-Andrés, P. E. M. Siegbahn, and P.-O. Widmark, *Molcas 4*, Lund University, Lund, Sweden, 1997.
- 30 P.-Å. Malmqvist and B. O. Roos, *Chem. Phys. Lett.*, 1989, **155**, 189.
- 31 K. Pierloot, B. Dumez, P.-O. Widmark and B. O. Roos, *Theor. Chim. Acta*, 1995, **90**, 87.
- 32 P. van der Straten, R. Morgenstern and A. Niehaus, *Z. Phys. D.*, 1988, **8**, 35.

- 33 T. X. Carroll, K. J. Børve, L. J. Sæthre, J. D. Bozek, E. Kukk, J. A. Hahne and T. D. Thomas, *J. Chem. Phys.*, 2002, **116**, 10 221.
- 34 E. Kukk, *SPANCF*, University of Oulu, Finland, 2000, <http://www.geocities.com/ekukk/>.
- 35 L. J. Sæthre, O. Svaeren, S. Svensson, S. Osborne, T. D. Thomas, J. Jauhiainen and S. Aksela, *Phys. Rev. A*, 1997, **55**, 2748.
- 36 S. J. Osborne, S. Sundin, A. Ausmees, S. Svensson, L. Sæthre, O. Svaeren, S. Sorensen, J. Vegh, J. Karvonen, S. Aksela and A. Kikas, *J. Chem. Phys.*, 1997, **106**, 1661.
- 37 S. Sundin, L. J. Sæthre, A. Ausmees, S. Sorensen and S. Svensson, *J. Chem. Phys.*, 1999, **110**, 5806.
- 38 E. E. Rennie, B. Kempgens, H. M. Köppe, U. Hergenahn, J. Feldhaus, B. S. Itchkawitz, A. L. D. Kilcoyne, A. Kivimäki, K. Maier, M. N. Piancastelli, M. Polcik, A. Rüdél and A. M. Bradshaw, *J. Chem. Phys.*, 2000, **113**, 7362.
- 39 E. E. Rennie, U. Hergenahn, O. Kugeler, A. Rüdél, S. Marburger and A. M. Bradshaw, *J. Chem. Phys.*, 2002, **117**, 6524.
- 40 K. Gunnelin, P. Glans, J.-E. Rubensson, C. Sæthe, J. Nordgren, Y. Li, F. Gel'mukhanov and H. Ågren, *Phys. Rev. Lett.*, 1999, **83**, 1315.
- 41 S. A. Holmes and T. D. Thomas, *J. Am. Chem. Soc.*, 1975, **97**, 2337.
- 42 There is an obvious disagreement between the C1s ionization energy that may be deduced from Fig. 4 in ref. 38 and the literature values for benzene. See W. L. Jolly, K. D. Bomben and C. J. Eyermann, *At. Data Nucl. Data Tables*, 1984, **31**, 433.

Paper IV

Carbon 1s photoelectron spectroscopy of six-membered cyclic hydrocarbons

V. M. Oltedal,^a K. J. Børve,^{*a} L. J. Sæthre,^{*a} T. D. Thomas,^{*b} J. D. Bozek^c and E. Kukk^d

^a Department of Chemistry, University of Bergen, Bergen, NO-5007, Norway.

E-mail: knut.borve@kj.uib.no

^b Department of Chemistry, Oregon State University, Corvallis, Oregon, 97330, USA

^c Advanced Light Source, Lawrence Berkeley National Laboratory, University of California, Berkeley, California, 94720, USA

^d Department of Physical Sciences, University of Oulu, Oulu, FIN-90014, Finland

Received 5th April 2004, Accepted 16th June 2004

First published as an Advance Article on the web 9th July 2004

The carbon 1s photoelectron spectra of cyclohexane, cyclohexene, 1,3-cyclohexadiene, and 1,4-cyclohexadiene have been measured. These have been analyzed in terms of a theoretical model of the vibronic structure that includes the effects of the changes in equilibrium geometry that accompany core ionization as well as those of vibronic coupling in the core-ionized molecule. This theoretical approach gives an excellent description of the vibronic structure and makes it possible to identify the contributions of the inequivalent carbon atoms to the spectra. The carbon 1s ionization energies are reported and used in the analysis of photoelectron spectra of adsorbed molecules.

1. Introduction

For more than 30 years, inner-shell photoelectron spectroscopy has been a source of important chemical information. Core-ionization energies provide a local probe of molecular charge distributions and of the ease with which a molecule can accept or donate charge at a particular site. These properties correlate with and provide insight into other, more familiar, chemical properties such as acidity, basicity, proton affinity, and reactivity.

Until recently, however, the investigation of the carbon 1s photoelectron spectra of hydrocarbons (or, the hydrocarbon portion of molecules containing a heteroatom) has been hampered by lack of resolution. Carbon atoms with quite distinct chemical properties may have carbon 1s ionization energies that differ by less than 1 eV, whereas historically the available resolution has been inferior. In addition, the vibrational excitation that accompanies core ionization in a molecule adds a complexity to the spectra that has made analysis difficult.

The availability of third-generation synchrotrons coupled with high-resolution electron spectrometers has made a striking difference in this situation. It is now possible to measure carbon 1s photoelectron spectra with a resolution of about half the natural line width (~ 100 meV) associated with the finite lifetime of each vibronic core-hole state. The result is that recently measured carbon 1s spectra in hydrocarbons show a richness of chemical effects and vibrational structure.

Understanding the chemical effects that are present in these spectra requires an understanding of the vibronic structure. This comes about from the changes in equilibrium geometry that accompany core ionization and in some cases from vibronic coupling involving the core orbitals of equivalent adjacent atoms. As a result, along with the advances in experimental capabilities, there have been corresponding developments in the theoretical methods for calculating this structure.

During the last few years, these studies have evolved from investigation of one- and two-carbon hydrocarbons, where the vibrational structure and chemical effects are simple, to studies

of more complex molecules such as propyne,¹ linear alkanes,² benzene,³ furan,⁴ thiophene,⁵ butan-2-ol,⁶ and alanine.⁷ Here we present results on the six-carbon cyclic hydrocarbons, cyclohexane, cyclohexene, 1,3-cyclohexadiene, and 1,4-cyclohexadiene. These, together with previously published results for benzene,³ show the evolution of chemical effects from a saturated molecule through the unsaturated molecules to benzene, in which resonance plays an important role. Comparison of the observed spectra with those calculated theoretically shows that a sufficiently high level of theory has been developed to give a good account of the vibrational excitation and vibronic coupling associated with core ionization.

The unsaturated cyclic hydrocarbons are interesting from the perspective of functionalizing silicon surfaces by molecular attachment.^{8–11} While photoelectron spectroscopy is a technique for characterizing the bonding of these adsorbates, assignment of carbon 1s spectra is less than straightforward at the resolution realized in these studies. For the physisorbed molecules, spectral assignment is based on stoichiometry and general expectations regarding the relative binding energies in alkanes and alkenes.⁸ One of the aims of the present study is to provide molecular reference spectra for the study of physisorbed and chemisorbed molecules.

2. Methods

2.1. Experimental procedures and analysis methods

Measurements of carbon 1s photoelectron spectra were made at beamline 10.0.1 of the Advanced Light Source using a Scienta SES-200 electron spectrometer¹² to record the data; details of the procedures are given elsewhere.^{13,14} The photon energy was 330 eV, 39 to 40 eV above the carbon 1s thresholds. The experimental resolution, including the contributions from the photon monochromator, the electron-energy analyzer, and Doppler broadening, was expected to be 60 meV on the basis of the monochromator slits and the settings of the electron spectrometer and is assumed to be Gaussian. Calibration of the carbon 1s ionization energies was based on measurements

of a mixture of the sample of interest with CF₄. The carbon 1s ionization energy of CF₄ is taken to be 301.898 eV.¹⁵ Fitting of the CF₄ spectra with the Gaussian resolution as a free parameter indicated a resolution of about 45 meV, rather less than expected. As a result, we have analyzed the data twice, once with the assumption that the resolution is 60 meV and once with the assumption that the resolution is 45 meV. Except as noted in Section 3.1.2 the differences in the results obtained by these two approaches are negligible. The fitting results presented here are those obtained using a resolution of 45 meV.

The experimental spectra have been fit by least squares using line shapes that take into account the experimental broadening, the combined effects of the lifetime of the core-hole state and the interaction between the outgoing Auger and photoelectrons (post-collision interaction, or PCI), and the vibrational excitation.¹⁶ The Lorentzian linewidth, which reflects the core-hole lifetime, was held fixed at 100 meV, in keeping with results found in other measurements.¹⁷ The effect of PCI has been described using eqn. (12) from van der Straten *et al.*,¹⁸ which is expected to be valid under the conditions of our measurements.

The effects of vibrational excitation and vibronic coupling have been determined from first principles theoretical calculations described below (Section 2.2). For each inequivalent carbon atom the vibrational profile has been calculated. This has been convoluted with the profile reflecting the effects of resolution, lifetime, and PCI, as described above, and vibronic coupling, as described below (Section 3.1.2). The data are then fit with these overall profiles, with the position and height for each profile as fitting parameters. In addition a flat background is a fitting parameter.

2.2. Theoretical

Using the Gaussian set of programs¹⁹ we have calculated the geometries, energies, harmonic vibrational frequencies, and normal modes for the ground-state and core-ionized molecules. The calculations have been carried out with the B3LYP method, using a triple- ζ basis set. For the core-ionized molecules the core of the ionized carbon atom was represented by an effective core potential (ECP). See ref. 2 for details of the basis set and the effective core potential. From these calculations it is possible to obtain predicted relative (but not absolute) ionization energies for all of the carbon atoms.

Vibrational frequencies calculated in this way are typically higher than those observed experimentally. In keeping with our experience with other molecules²⁰ we have scaled all frequencies by 0.99 except for that of the CH stretching modes for the hydrogens attached to the core-ionized carbon. In this case the scaling factor was 0.95 for sp³ hybridization and 0.96 for sp² hybridization. In addition, the present level of theory exaggerates the contraction of the CH bonds that takes place upon core ionization. Comparison with very accurate calculations for methane,²¹ ethane,²⁰ and ethene²² indicates that this excess contraction is about 0.3 pm for hydrogen attached to an sp³ carbon and 0.2 pm for hydrogen attached to an sp² carbon, and, therefore, for the purpose of calculating Franck–Condon factors, the CH bond lengths at the core-ionized carbons have been lengthened accordingly.

The Franck–Condon factors needed to predict the vibrational profiles have been calculated by the g2fc program, which reads the output file of Gaussian and produces a vibrational profile for input into the fitting routine. Details of this procedure are given in the Appendix.

In all of these molecules, there are equivalent carbon atoms: Six in cyclohexane, three pairs of two in cyclohexene and 1,3-cyclohexadiene, and four of one kind and two of another in 1,4-cyclohexadiene. In a molecular orbital description of the molecules, the carbon 1s orbitals combine into bonding and antibonding combinations to give delocalized orbitals, with splittings proportional to the electronic coupling integral β .³

When core-ionization takes place, vibronic coupling in the core-ionized molecule can modify this picture. In the limit that β is very small, vibronic coupling leads to a picture in which the core hole can be viewed as completely localized on one of the carbon atoms.²³ For the molecules considered here, β is small enough that the holes can be considered localized, but not so small that its effect on the spectrum can be ignored.

When β is small, we can use first-order perturbation theory.^{20,24} Taking a molecule with two equivalent atoms as an example, each vibronic level is subject to a splitting equal to $2\beta\langle L, \nu | R, \nu \rangle$, where the quantity in brackets is an overlap integral between the vibrational wavefunctions when the core hole is localized on the left atom and those when it is localized on the right atom. The set of quantum numbers, ν , describes the vibrational excitation. For hydrocarbons $\langle L, 0 | R, 0 \rangle$ is of order 0.5 and tends to decrease as the degree of vibrational excitation increases. The electronic integral β depends strongly on the distance between the carbon atoms and is about 10 meV for adjacent single-bonded carbon atoms and about 30 meV for adjacent double-bonded carbon atoms;³ it may be ignored for nonadjacent atoms. As a practical matter, the splitting of the vibronic levels has significant effects only on the peaks in the spectra that correspond to the adiabatic transition (*i.e.* between vibrational ground states, $\nu' = 0 \leftarrow \nu = 0$),^{3,20} and we have confined our consideration of these effects to this peak in each case.

The coupling integral β can in principle be evaluated directly from the wavefunctions. We have, instead, obtained approximate values of β from the energies of the carbon 1s orbitals as given by the Gaussian calculations. To a reasonable approximation, β is related to the elements of the Hamiltonian matrix by the matrix formed from the eigenvectors that describe the molecular orbitals in terms of atomic orbitals.

3. Results and discussion

The carbon 1s photoelectron spectra for the four cyclic hydrocarbons that we have studied as well as that of benzene³ are illustrated in Fig. 1. In this figure the experimental data are represented by the open circles. The overall least-squares fits are illustrated by the solid lines through the circles, and the vibrational profiles for each inequivalent carbon atom are indicated by the other lines. Vertical bars show the positions and relative intensities of the most prominent vibronic transitions. (It is to be noted that the maxima of the spectra are shifted by the effects of PCI from the positions of the vertical bars to higher ionization energies by 18 meV.)

Inspection of this figure indicates that the theoretically predicted vibrational structures agree quite well with the observed structures. It is to be noted that each type of carbon atom produces a unique vibrational profile, and this uniqueness makes it possible to assign unambiguously the various features of the spectrum to the appropriate carbon atoms in the molecule. Even for cyclohexene, where the profiles for the inequivalent single-bonded carbon atoms are similar, the assignments are clear. Using the reverse assignment in the fit leads to a higher value of χ^2 and to an intensity ratio for the two carbons that differs significantly from the stoichiometric value of 1.

The adiabatic carbon 1s ionization energies that have been derived from these measurements as well as that of benzene³ are given in Table 1. It is to be noted that these energies are rather independent of the details of the fitting procedure. Using different levels of approximation concerning the vibrational structure leads to changes in these energies of only a few meV. On the basis of other measurements of such ionization energies,¹⁵ we estimate the absolute uncertainty in these results to be 0.04 eV (including the uncertainty in the ionization energy of the reference compound CF₄) and the relative uncertainty to be no more than 0.02 eV.

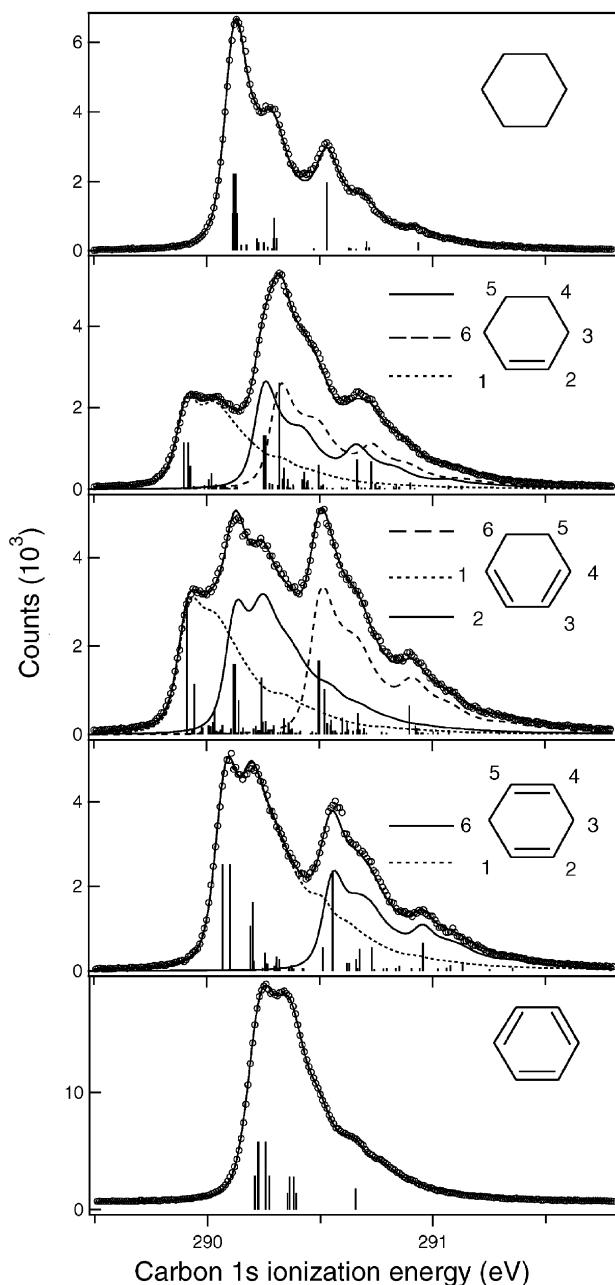
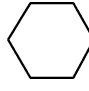
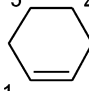
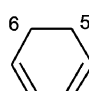
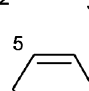
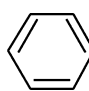


Fig. 1 Carbon 1s photoelectron spectra of cyclic six-carbon hydrocarbons measured at a photon energy of 330 eV. Open circles show the experimental data. The solid lines through the data show the overall least-squares fits to the data, and the other lines show the vibrational profiles for each of the inequivalent carbons. The vertical bars show the positions and relative intensities of the most prominent vibronic transitions.

3.1. Vibrational structure and vibronic coupling

There are two components to the structure that is apparent in the photoelectron spectra. One, which we can refer to as vibrational excitation, arises from the changes in equilibrium geometry. This can be adequately described using a model in which the core hole is considered to be localized on a single carbon. As noted in Section 2.2, in the limit of weak electronic coupling between the core orbitals of the carbon atoms, this is a good approximation. The second component affecting the spectrum arises because this approximation is not perfect, and additional structure may arise. To use a convenient, but oversimplified notation, we can refer to this as the effect of vibronic coupling. The contribution from each of these components is discussed in the following paragraphs.

Table 1 Measured adiabatic C 1s ionization energies in eV

Compound ^a	Carbon ^b	Ionization energy	ΔI_{expt}	ΔI_{calc}
		290.123	0.0	0.0
	1,2	289.908	-0.215	-0.214
	4,5	290.257	0.134	0.143
	3,6	290.321	0.198	0.203
	1,4	289.912	-0.211	-0.209
	2,3	290.124	0.001	0.001
	5,6	290.497	0.374	0.409
	1,2,4,5	290.086	-0.037	0.001
	3,6	290.556	0.433	0.458
		290.241	0.118	0.126

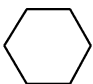
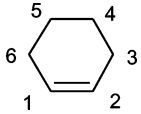
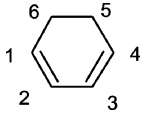
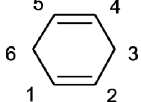
^a From the top: Cyclohexane, cyclohexene, 1,3-cyclohexadiene, 1,4-cyclohexadiene and benzene. ^b Positional numbers identify the ionized carbons.

3.1.1. Vibrational structure. The vibrational structure seen in Fig. 1 can be understood by considering the two extremes, cyclohexane and benzene. The spectrum of cyclohexane is essentially the same as that of ethane²⁰ and other linear alkanes.² These are characterized by strong excitation of a localized CH stretching mode involving the CH bond attached to the core-ionized carbon and by CCH bending modes involving the hydrogens attached to carbon atoms other than the core-ionized atom. The contribution of the stretching mode is apparent in the peak at an ionization energy about 400 meV higher in ionization energy than the main peak of the spectrum. The bending modes are apparent as the shoulder on the main peak and also as a shoulder on each of the peaks corresponding to CH stretching. For benzene, at the other extreme, CH stretching plays a smaller role since there are only half as many hydrogens as on cyclohexane. However, CCH bending modes as well as ring deformation modes are more important in benzene, giving rise to the observed double-peak structure.

The other spectra can be understood as resulting from combinations of these two pictures. In cyclohexene, the double-peaked structure of benzene is apparent as a flat-topped peak at low ionization energy, while the rest of the spectrum can be seen to result from two spectra slightly displaced from each other with each resembling that of cyclohexane. A similar pattern is seen for 1,4-cyclohexadiene, except that here the splitting of the -C=C- peak at low ionization energy is more apparent, and ring excitation modes contribute to the -C- spectrum at high ionization energy. Essentially the same patterns are apparent for 1,3-cyclohexadiene.

3.1.2. Vibronic coupling. In keeping with the discussion in Section 2.2, each of the vibronic lines in the spectrum should be split into two or more lines, with the splitting proportional to $2\beta\langle L, \mathbf{v}|R, \mathbf{v}\rangle$. In the analysis of the benzene spectrum, Myrseth *et al.*³ showed that the agreement between experiment and theory was significantly improved by including this effect. In general, however, the vibrational overlap integral, $\langle L, \mathbf{v}|R, \mathbf{v}\rangle$, is expected to decrease with vibrational excitation.

Table 2 Splitting of the adiabatic vibrational peaks due to vibronic coupling, meV

Compound ^a	Carbon ^b	Calculated	Experimental ^c
		8	0 to 14
	1,2 4,5 3,6	19 7 0	33 to 45
	1,4 2,3 5,6	0 9 6.5	
	1,2,4,5 3,6	33 0	26 to 39

^a From the top, the compounds are: Cyclohexane, cyclohexene, 1,3-cyclohexadiene, and 1,4-cyclohexadiene. ^b Positional numbers identify the ionized carbons. ^c The lower (upper) value is obtained assuming an instrumental resolution of 60 meV (45 meV).

Thus, this splitting is expected not to be important for high-lying vibrational states. Investigating this possibility, Myrseth *et al.* found that including this splitting only for the adiabatic state ($v' = 0 \leftarrow v = 0$) gave agreement between experiment and theory that was almost as good as that obtained by considering the theoretically calculated splitting for all vibrational states.

For the ground state of each core-ionized species the electronic coupling integral β has been estimated as outlined above, the vibrational overlap integral $\langle L, v|R, v \rangle$ has been calculated, and the theoretically predicted adiabatic peak has been split accordingly. In most cases, this involves splitting the peak into two peaks of equal intensity with a splitting equal to $2\beta\langle L, v|R, v \rangle$. For cyclohexane, where there are six equivalent carbons, the splitting pattern is like that of benzene with four peaks with intensity ratios of 1:2:2:1 and an energy splitting pattern of $\beta\langle L, v|R, v \rangle/2\beta\langle L, v|R, v \rangle/\beta\langle L, v|R, v \rangle$. The calculated values of $2\beta\langle L, v|R, v \rangle$ are indicated in Table 2. The least-squares fits shown in Fig. 1 have been calculated using these values.

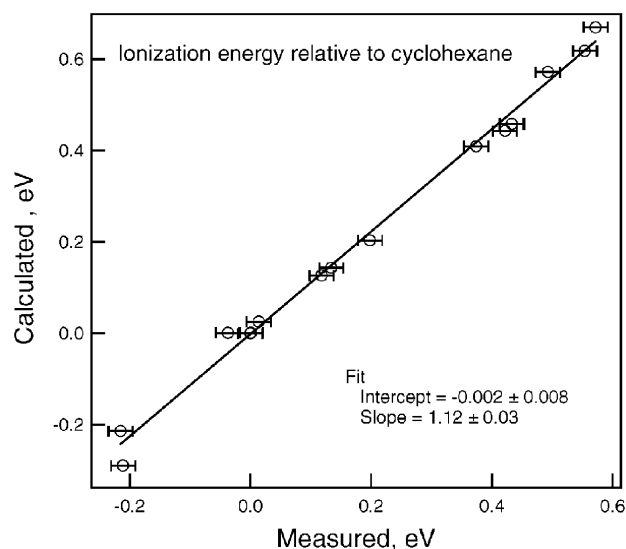
In each case, including the splitting in the fitting procedure leads to a lower value of χ^2 , although where the splitting is small, the improvement is small. For cyclohexane, where the spectrum is simple, and for the $-\text{C}=\text{C}-$ carbons of cyclohexene and the $=\text{C}-\text{C}=\text{C}$ carbons of 1,4-cyclohexadiene, where the splitting is relatively large, we have also determined experimental values of the splitting by finding the splitting that gives a minimum in χ^2 . Since introducing such a splitting has approximately the same effect on the predicted spectrum as increasing the experimental broadening, the derived splitting and the assumed resolution are strongly correlated. To show this effect, we list in Table 2 the range of splittings determined using assumed resolutions of 45 and 60 meV. For cyclohexane and 1,4-cyclohexadiene, this range brackets the value from theory, indicating that this theoretical approach gives a reasonable description of this effect. For cyclohexene, however, the experimentally derived splitting is significantly greater than predicted. The cause of this discrepancy is not known, although we note that it is consistent with a failure of the theoretical model to predict the correct intensities for the low-energy vibrational modes.

3.2. Ionization energies

There is a systematic variation of ionization energies as we go from cyclohexane to benzene, with a slight increase in the average ionization energy through this series. In closer detail, the carbons with double bonds have systematically lower ionization energies than do those with single bonds. For each of these categories, single- and double-bonded carbon, the increase in ionization energy with decreasing total number of hydrogens is more pronounced than is the corresponding increase for the average ionization energy. These results show the power of high-resolution photoelectron spectroscopy. With the lower resolution that was previously available one would have observed only the average behavior, and the differences between these molecules would not have been apparent.

We defer a discussion of the shifts in ionization energy, the reasons for these shifts, and their chemical implications to a subsequent publication. For the present, we consider the results of theoretical calculations of the ionization energies. The method we have described in Section 2.2 provides relative ionization energies and these are listed in Table 1, relative to the carbon 1s ionization energy in cyclohexane. The calculated and experimental shifts in ionization energy are compared in Fig. 2, where the calculated shifts in ionization energy are plotted against the experimental values. Also included in this figure are results for ethene,¹⁵ ethane,¹⁵ and propene.²⁵ The solid line represents a least-squares fit of a straight line to the points. Inspection of Fig. 2 shows that the theoretical calculations reproduce all of the features of the experimental results well. The average absolute deviation between the theoretical and experimental shifts is 0.03 eV and the root-mean-square (rms) deviation is 0.04 eV. This comparison corroborates the assignments of measured ionization energies to specific carbon atoms that we have made on the basis of the vibrational structure. There are no systematic differences in the agreement between double- and single-bonded carbon atoms. However, the theoretical predictions systematically overestimate the shifts by 12%. This is a common feature of many such calculations;²⁶⁻²⁸ the trends are predicted correctly, but the slopes are either too high or too low (depending on the details of the basis sets and methods used).

If we consider only the deviations from the least-squares line in Fig. 2, the average absolute deviation of the points from the line is 0.019 eV and the root-mean-square deviation is 0.024 eV. The last number sets an upper limit on the relative uncertainty of our measurements since it must reflect the inaccuracies of both the measurements and the calculations. Since there is no reason to

**Fig. 2** Calculated versus measured shifts in carbon 1s ionization energies.

expect these to be correlated with one another, we can conclude that the error for either is less than 0.024 eV.

These calculated results are to be compared with those of Chong²⁹ for hydrocarbons containing one to four carbons. In his work, the relative ionization energies of 19 compounds are predicted with an average absolute deviation of 0.08 eV and rms deviation of 0.09 eV. These figures are to be compared with the corresponding values of 0.03 and 0.04 eV mentioned above.

3.3. Molecular reference spectra for use in adsorption studies

Very recently, several studies have been published on the adsorption of cyclohexene,¹¹ 1,3-cyclohexadiene,¹¹ 1,4-cyclohexadiene,¹¹ benzene¹⁰ and also other unsaturated hydrocarbons^{8,9} on various silicon surfaces. Carbon 1s photoelectron spectroscopy is commonly used for characterizing the adsorbed states, even though spectral assignment may be a problem. The instrumental resolution is the most important limiting factor in this respect, ranging below 0.6 eV⁹ to below 1.2 eV.¹¹

In Table 3, our ionization energies are compared to those obtained by Tao *et al.*,¹¹ for physisorbed cyclohexene and cyclohexadienes. There is a large, but trivial energy shift of *ca.* 5 eV between the two data sets due to the difference in reference level. More interesting is the fact that our assignment consistently places the unsaturated carbon atoms at lower ionization energy than the saturated atoms, whereas the opposite is found for the physisorbed molecules. From what is presented above regarding the vibrational fine structure, erroneous assignment of the gas-phase spectra does not seem likely. This leaves us with two possible explanations for this discrepancy evident in Table 3: Either the assignment made by Tao *et al.*, is incorrect, or their spectra represent molecules that are perturbed beyond what is reasonable to characterize as physisorption. In order to investigate this matter more closely, we digitized the photoelectron spectra in Fig. 6 of ref. 11 and used them in fitting procedures as described in Section 2.1. As fitting functions we used lineshapes based on the vibrational profiles and intramolecular chemical shifts as obtained for each molecule in the gas phase. Hence, overall intensity and energy position and the experimental resolution were the only three free parameters in the fit. The instrumental resolution was optimized to approximately 1.4 eV for all three molecules.

A typical example of the fits produced is shown in Fig. 3. The overall profiles are in good agreement with the experimental spectra for all the three physisorbed species. By comparing our fit in Fig. 3 to the original fit in Fig. 6c in ref. 11, shown as an inset in Fig. 3, it appears that our fit is of equal or better quality, particularly at the peak maximum and at the high-energy slope. While the large instrumental broadening in this case makes it difficult to draw firm conclusions, it appears that the recorded spectrum is consistent with relative ionization energies between saturated and unsaturated carbon atoms as observed for this molecule in the gas phase. The assignment of Tao *et al.*,¹¹ may

Table 3 Comparison of vertical ionization energies (eV)

Compound	Carbon ^a	Average ionization energy	
		Gas phase ^b	Physisorbed ^c
Cyclohexene	sp ²	290.07 ^d	285.0
	sp ³	290.48 ^d	284.4
1,3-Cyclohexadiene	sp ²	290.18 ^d	285.1
	sp ³	290.69 ^d	284.4
1,4-Cyclohexadiene	sp ²	290.25 ^d	285.1
	sp ³	290.75 ^d	284.4

^a Average over ionized carbons of the given hybridization. ^b Assigned in this work. ^c Assigned in ref. 11. ^d Obtained by adding computed average vibrational energies 0.16 eV (sp²) and 0.19 eV (sp³) to the adiabatic energies.

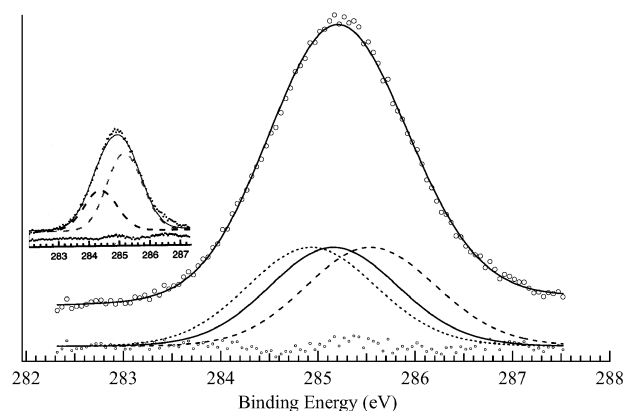


Fig. 3 Experimental (open circles) and fitted (solid line) C1s photoelectron spectrum of physisorbed 1,3-cyclohexadiene. The experimental spectrum was obtained by digitizing Fig. 6c in ref. 11. The fit was prepared on the basis of site-specific lineshapes (C1 and C4: dotted line, C2 and C3: solid line, C5 and C6: dashed line) obtained in this work for the molecule in the gas phase. Inset: The original fit from Fig. 6c in ref. 11.³⁰

therefore be incorrect, and it is not necessary to invoke a more complicated process than physisorption to explain the spectrum.

4. Conclusions

The carbon 1s photoelectron spectra of the six-carbon cyclic hydrocarbons are rich in detail arising from both vibronic structure and the chemical inequivalence of the carbon atoms. Both of these features can be well understood using the results of first-principles theoretical calculations.

Considering these results together with our earlier studies of alkanes,^{2,13,20,21} benzene,³ and alkynes,^{1,24} we can conclude that the vibronic structure arising in the core ionization of hydrocarbons is well understood. Such structure arises, in general, from the changes in equilibrium geometry that accompany core ionization. In addition, in some cases, it includes effects due to vibronic coupling.

This level of understanding provides an important framework for the interpretation of other, more complex, spectra in which other features of chemical interest might be present. Without this framework it would be impossible to decide whether an unexpected feature of a spectrum reflects an unexpected phenomenon or simply a lack of understanding of the vibronic excitation.

Rigorous analyses of gas-phase spectra may be of considerable use in the analysis of photoelectron spectra of adsorbed molecules.

Appendix: The *g2fc* program for computing Franck–Condon profiles in polyatomic molecules

In the harmonic approximation, calculation of many-dimensional Franck–Condon factors is based on the Duschinsky relation, *i.e.* an assumption of linearly related normal coordinates in the initial (1) and final (2) electronic states:

$$Q^{(2)} = JQ^{(1)} + K \quad (1.1)$$

Ref. 31 provides a detailed procedure for computing the mode-coupling matrix *J* and the displacement vector *K* from the normal mode output from the Gaussian series of programs.¹⁹ Prior to this, it is important to decide on a common Cartesian coordinate system for initial and final states. The contribution from overall translation is removed by having the origin of the coordinate system coincide with the center of mass for both the neutral and ionized molecules. With this choice, the position of atom *a* in molecular structure 1 is denoted by r_{1a} , and a preliminary orientation of molecular structure 2 is given by atomic positions $\{r_{2a}^0\}$.

The vibrational normal modes are orthogonal to rotational modes only to within terms that are linear in the distortions. A family of rigid-body rotations of structure 2 is defined through $r_{2a} = \hat{R}r_{1a}^0$, where \hat{R} is a rotational matrix. \hat{R} should be chosen such that the structural difference between 1 and 2 has a vanishing projection onto rotational modes. Using an explicit representation of the six rigid-body coordinates in terms of mass-weighted Cartesian coordinates,³² this statement translates into

$$\sum_a m_a r_{1a} \times \hat{R}r_{2a}^0 = 0 \quad (1.2)$$

Expressing \hat{R} in terms of the three Eulerian angles, one may show that eqn. (1.2) also defines the stationary condition for the mass-weighted Euclidean norm of the deviation between the two structures:

$$\sum_a m_a \|r_{1a} - \hat{R}r_{2a}^0\|^2 \quad (1.3)$$

In actual applications, we perform the rotation of structure 2 by a direct method³³ for superimposing atoms of two molecules by quaternion algebra.

Once the Duchinsky parameters have been obtained, the Franck–Condon integrals may be computed according to one of many algorithms. We have implemented the recursive algorithm by Malmqvist and Forsberg.³⁴ In practical use, we find that the diagonal, or parallel-modes, approach³⁵ works very well^{3,20} for preparing vibrational line shapes for deconvolution of core-level photoelectron spectra. In this approximation, the J matrix is replaced by the identity matrix, *i.e.* mode-mixing is neglected while differences in vibrational frequencies between the two molecular states are accounted for. In the present study, all molecules were described using both the full and the diagonal Franck–Condon approximation. Again we found that the errors introduced by the parallel-modes approximation are negligible when preparing vibrational line shapes for deconvolution of core-level photoelectron spectra. However, this holds provided that (i) the displacement vector K is computed by projection onto the final-state normal modes rather than onto those of the initial state, and (ii) the normal coordinates are resorted to optimize the diagonal of J .

An advantage of the parallel-modes approach, is that anharmonicity may be taken into account for selected modes. Earlier work on methane¹³ and ethane²⁰ shows an appreciable effect of anharmonicity in the symmetric C*–H stretching mode, where C* denotes the ionized carbon atom. Based on this, we have used Morse potentials for the symmetric C*(sp³)–H stretching modes, with $\omega_e x_e / \omega_e$ taken from methane.²¹

Acknowledgements

TDT acknowledges support by the National Science Foundation under Grant No. CHE-9727471. JDB acknowledges support from the Divisions of Chemical and Material Sciences, Office of Energy Research, of the U. S. Department of Energy. VMO, LJS, and KJB thank the Research Council of Norway (NFR) for financial support and for a grant of computer time through the Programme for Supercomputing. EK acknowledges financial support from the Research Council of the Academy of Finland.

References

- 1 L. J. Sæthre, N. Berrah, J. D. Bozek, K. J. Børve, T. X. Carroll, E. Kukuk, G. L. Gard, R. Winter and T. D. Thomas, *J. Am. Chem. Soc.*, 2001, **123**, 10729.

- 2 T. Karlsen, K. J. Børve, L. J. Sæthre, K. Wiesner, M. Bässler and S. Svensson, *J. Am. Chem. Soc.*, 2002, **124**, 7866.
- 3 V. Myrseth, K. J. Børve, K. Wiesner, M. Bässler, S. Svensson and L. J. Sæthre, *Phys. Chem. Chem. Phys.*, 2002, **4**, 5937.
- 4 E. E. Rennie, U. Hergenbahn, O. Kugeler, A. Rüdél, S. Marburger and A. M. Bradshaw, *J. Chem. Phys.*, 2002, **117**, 6524.
- 5 A. Giertz, M. Bässler, O. Bjørneholm, H. Wang, R. Feifel, C. Miron, L. Karlsson, S. Svensson, K. J. Børve and L. J. Sæthre, *J. Chem. Phys.*, 2002, **117**, 7587.
- 6 E. E. Rennie, I. Powis, U. Hergenbahn, O. Kugeler, S. Marburger and T. M. Watson, *J. Phys. Chem. A*, 2002, **106**, 12221.
- 7 I. Powis, E. E. Rennie, U. Hergenbahn, O. Kugeler and R. Bussy-Socrate, *J. Phys. Chem. A*, 2003, **107**, 25.
- 8 J. S. Hovis and R. J. Hamers, *J. Phys. Chem. B*, 1997, **101**, 9581.
- 9 H. Liu and R. J. Hamers, *Surf. Sci.*, 1998, **416**, 354.
- 10 Y. Cao, X. M. Wei, W. S. Chin, Y. H. Lai, J. F. Deng, S. L. Bernasek and G. Q. Xu, *J. Phys. Chem. B*, 1999, **103**, 5698.
- 11 F. Tao, Z. H. Wang and G. Q. Xu, *Surf. Sci.*, 2003, **530**, 203.
- 12 N. Berrah, B. Langer, A. A. Wills, E. Kukuk, J. D. Bozek, A. Farhat and T. W. Gorczyca, *J. Electron Spectrosc. Relat. Phenom.*, 1999, **101–103**, 1.
- 13 T. X. Carroll, N. Berrah, J. D. Bozek, J. Hahne, E. Kukuk, L. J. Sæthre and T. D. Thomas, *Phys. Rev. A*, 1999, **59**, 3386.
- 14 J. Bozek, T. X. Carroll, J. Hahne, L. J. Sæthre, J. True and T. D. Thomas, *Phys. Rev. A*, 1998, **57**, 157.
- 15 V. Myrseth, J. D. Bozek, E. Kukuk, L. J. Sæthre and T. D. Thomas, *J. Electron Spectrosc. Relat. Phenom.*, 2002, **122**, 57.
- 16 Curve fitting macro package spancf, <http://www.geocities.com/ekukk>.
- 17 T. X. Carroll, K. J. Børve, L. J. Sæthre, J. D. Bozek, E. Kukuk, J. A. Hahne and T. D. Thomas, *J. Chem. Phys.*, 2002, **116**, 10221.
- 18 P. van der Straten, R. Morgenstern and A. Niehaus, *Z. Phys. D*, 1988, **8**, 35.
- 19 M. J. Frisch, G. W. Trucks, H. B. Schlegel, G. E. Scuseria, M. A. Robb, J. R. Cheeseman, V. G. Zakrzewski, J. A. Montgomery, Jr., R. E. Stratmann, J. C. Burant, S. Dapprich, J. M. Millam, A. D. Daniels, K. N. Kudin, M. C. Strain, O. Farkas, J. Tomasi, V. Barone, M. Cossi, R. Cammi, B. Mennucci, C. Pomelli, C. Adamo, S. Clifford, J. Ochterski, G. A. Petersson, P. Y. Ayala, Q. Cui, K. Morokuma, D. K. Malick, A. D. Rabuck, K. Raghavachari, J. B. Foresman, J. Cioslowski, J. V. Ortiz, A. G. Baboul, B. B. Stefanov, G. Liu, A. Liashenko, P. Piskorz, I. Komaromi, R. Gomperts, R. L. Martin, D. J. Fox, T. Keith, C. Y. P. M. A. Al-Laham, A. Nanayakkara, M. Challacombe, P. M. W. Gill, B. Johnson, W. Chen, M. W. Wong, J. L. Andres, C. Gonzalez, M. Head-Gordon, E. S. Replogle and J. A. Pople, *Gaussian 98*, revision a9, Gaussian Inc., Pittsburgh, PA, 1998.
- 20 T. Karlsen, L. J. Sæthre, K. J. Børve, N. Berrah, E. Kukuk, J. D. Bozek, T. X. Carroll and T. D. Thomas, *J. Phys. Chem. A*, 2001, **105**, 7700.
- 21 T. Karlsen and K. J. Børve, *J. Chem. Phys.*, 2000, **112**, 7979.
- 22 K. J. Børve, unpublished.
- 23 W. Domcke and L. Cederbaum, *Chem. Phys.*, 1977, **25**, 189.
- 24 K. J. Børve, L. J. Sæthre, T. D. Thomas, T. X. Carroll, N. Berrah, J. D. Bozek and E. Kukuk, *Phys. Rev. A*, 2000, **63**, 12506.
- 25 T. D. Thomas, L. J. Sæthre and K. J. Børve, work in progress.
- 26 L. J. Sæthre, M. R. F. Siggel and T. D. Thomas, *J. Electron Spectrosc. Relat. Phenom.*, 1989, **49**, 119.
- 27 L. J. Sæthre and T. D. Thomas, *J. Org. Chem.*, 1991, **56**, 3935.
- 28 R. Situmeang and T. D. Thomas, *J. Electron Spectrosc. Relat. Phenom.*, 1999, **98–99**, 105.
- 29 D. P. Chong, *Chin. J. Phys. (Taipei)*, 2000, **38**, 57.
- 30 Reprinted from *Surf. Sci.*, vol. 530, F. Tao, Z. H. Wang and G. Q. Xu, Covalent binding of cyclohexene, 1,3-cyclohexadiene and 1,4-cyclohexadiene on Si(111)-7 × 7, pages 203–215, Copyright (2004), with permission from Elsevier.
- 31 P. Chen, in *Unimolecular and Bimolecular Dynamics*, ed. C. Y. Ng, T. Baer and I. Powis, John Wiley and Sons, 1994, ch. 8, p. 372.
- 32 J. E. Bright Wilson, J. C. Decius and P. C. Cross, *Dover*, 1980, chapter 2.5.
- 33 D. J. Heisterberg, unpublished results, 1990..
- 34 P.-Å. Malmqvist and N. Forsberg, *Chem. Phys.*, 1998, **228**, 227.
- 35 T. D. Thomas, L. J. Sæthre, S. L. Sorensen and S. Svensson, *J. Chem. Phys.*, 1998, **109**, 1041.

Paper V

Abstract only. Full-text not available due to publisher restrictions.

The Substituent Effect of the Methyl Group. Carbon 1s Ionization Energies, Proton Affinities, and Reactivities of the Methylbenzenes

Velaug Myrseth,[†] Leif J. Sæthre,[†] Knut J. Børve,[†] and T. Darrah Thomas*,[‡]

Department of Chemistry, UniVersity of Bergen, NO-5007 Bergen, Norway, and Department of Chemistry, Oregon State UniVersity, CorVallis, Oregon 97331-4003

t.darrah.thomas@oregonstate.edu

Abstract

High-resolution carbon 1s photoelectron spectra have been measured for methyl-substituted benzenes. By using these data together with molecular structure calculations to predict the vibrational profiles expected in the spectra, it has been possible for the first time to assign 1s ionization energies to each of the inequivalent carbon atoms in these molecules. There exist linear correlations between the ionization energies and the energy changes for other chemical processes, such as enthalpies of protonation and activation energies for hydrogen exchange and protodesilylation. There are deviations from these correlations for sites in which hyperconjugation plays a role in the process. These can be understood by recognizing that the core-ionization energies reflect primarily the Hammett parameter π whereas the other energies reflect π^+ . The ionization and reaction energies can be summarized compactly with a linear model in which the total effect of the substituents is equal to the sum of the effects of the individual substituents. A slightly better description is obtained with a quadratic model, which allows for interaction between the substituents.

<http://dx.doi.org/10.1021/jo0708902> © 2007 American Chemical Society

Published on Web 06/27/2007